DYE LASERS WITH INDUCED BRAGG GRATINGS

Iain A. McIntyre

A Thesis Submitted for the Degree of PhD
at the
University of St Andrews

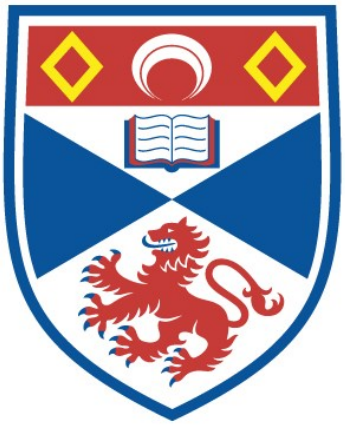

1985

Periodic Dielectric Disturbances and Novel Optics.

A thesis presented by

Ewan Donald Findlay B.Sc. M.Sc.

to the

University of St. Andrews

in application for the degree of

Doctor of Philosophy.

28 June 1994.

Declarations

I certify that E. D. Findlay has spent nine terms at research in the Physical Sciences Laboratory of St. Salvator's College, in the University of St. Andrews, under my direction, that he has fulfilled the conditions of ordinance No. 16 (St. Andrews) and that he is qualified to submit this thesis in application for the degree of Doctor of Philosophy.

A. Maitland

Research Supervisor.

I hereby certify that this thesis has been composed by me and is a record of the work done by me and has not previously been presented for a higher degree.

This research was carried out in the Physical Science Laboratory of St. Salvator's College, in the University of St. Andrews, under the supervision of Prof. A Maitland.

E. D. Findlay.

Acknowledgements

I would like to thank Prof. Arthur Maitland for his guidance throughout this work and thank Dr. Peter Hirst and Frits Akerboom for many helpful discussions. I am also grateful for the financial support of the DRA Above-Water Systems and to Dr. Bill Dawber in particular.

Thanks must also go to the climbers of St. Andrews for some memorable times on coire walls, on summits and on whisky.

To Laura

Periodic Dielectric Disturbances and Novel Optics.

Contents.

Appendix 3.

Abstract.

Several possible methods for creating permanent and temporary periodic dielectric disturbances and their application to optics have been examined.

The coupled mode theory is used to describe the travelling wave electro-optic diffractor (TWEOD) proposed by Dawber *et al* [2.1]. A basic theoretical model of the TWEOD is presented and developed to give the design parameters for the construction of a working barium titanate TWEOD operating at 10 GHz.

The coupled mode theory is also used to describe the dielectric disturbances created by pump beam interference patterns within a laser medium. Pump architectures which yield a periodic disturbance and thus create temporary diffraction gratings are analysed.

Permanent dielectric disturbances can be generated in glass heated to temperatures above the transformation point. Some possible methods for imposing both uniform and periodic dielectric disturbances on glass, which are generated by imposing stresses on the glass whilst it is at its transformation temperature are proposed. Uniformly pre-stressed glass can be used to improve the angular response of glass acousto-optic diffractors. Periodically prestressed glass forms a permanent acousto-optic diffraction grating. Acoustic standing waves may also be used to induce periodic structural change in other transparent media and on the surface of etchable substrates. Such acoustically induced structures may be used as permanent diffraction gratings and holograms.

A potential application for some of the novel devices described in this work is illustrated in the implementiation of an optical frequency division multiplexer ("optiplexer") [7.2] for video signals (3 dB Bandwidth of 6 MHz) using acousto-optic frequency shifting techniques. This is a times six improvement on the channel bandwidth of 1 MHz for the optiplexer achieved by Dawber *et al* [7.2]

Chapter 1.

Devices for Radio Frequency Spectrum Analysis.

§1.1 Radio Frequency Spectrum Analysis.

A "spectrum analyser", for the purposes of this thesis may be defined as a device, or collection of devices, capable of resolving the different frequency elements of the electro-magnetic spectrum.

The ideal spectrum analyser can, theoretically, take the entire electro-magnetic spectrum and separate all the frequency components therein without loss of information. As with most ideals, the perfect spectrum analyser is unattainable, but small sections of the total spectrum are analysable to greater or lesser degrees of resolution by practicable systems. The radio frequency ("rf") and micro-wave bands (10 MHz -100 GHz) in principle comprise such an analysable section. Spectrum analysis of rf and micro-wave is of increasing usefulness in the modern world where the electromagnetic spectrum is becoming increasingly cluttered and therefore accessing the appropriate signal, or combination of signals, is becoming an increasingly difficult task.

Solid state electronics is the obvious technology for rf spectrum analysis due to its predominance in the rest of rf processing. The electronic technique for spectrum analysis involves sampling a window in the chosen frequency range at any one time, because electronic signal detection relies on heterodyning the signal to be analysed with an internal reference signal. The introduction of range limits of the sampling window has two major implications. The most important of these is that the sampling frequency imposes itself as the frequency resolution limit. Thus the higher the resolution required the longer the spectrum analyser must dwell on a smaller "slice" of the frequency range. The second implication is that sampling of one part of the frequency range incurs loss of information that may lie outside the sampled range. Thus, for a high resolution electronic spectrum analyser we must sacrifice a large amount of potential information or build large and

cumbersome networks of filters each with its own receiver. The electronic spectrum analyser is therefore a trade-off between resolution, information loss and size.

The requirements of a compact high resolution rf spectrum analyser having no information loss can be met by acousto-optic spectrum analysers based on a simple acousto-optic device known as the Bragg cell (see figure 1.1) [1.1,1.2]. A Bragg cell consists of a piezo-electric transducer which introduces the rf signal into an acousto-optic medium as an acoustic wave which then interacts with a collimated beam of light to produce a diffraction pattern. The angle of diffraction is dependent on the value of the incoming radio frequency and the frequency of the optical radiation. Thus, when used in conjunction with lasers, photodetector arrays and the technology of integrated optics, Bragg cells provide us with a high resolution method for analysing an rf spectrum without information loss.

Acousto-optic spectrum analysers are, however, limited to operating within a given range of frequencies. Each individual Bragg cell has its own operational bandwidth which is dependent on a set of built-in design parameters ranging from the acoustic interaction depth to the impedance of the piezo-electric transducer. There is also a general limitation on the operational frequency range of Bragg cells in the form of an upper frequency limit which is due to acoustic attenuation of high frequency components in the signal [1.3].

The upper frequency limit on present acousto-optic devices is of the order of 1 GHz. Thus, acousto-optic spectrum analysers can cover the lower end of the rf spectrum (10 MHz - 1 GHz) but the analysis of signals in the range 1 - 100 GHz requires heterodyne detection and filter banks.

Optical spectrum analysis of the upper rf band (1 - 100 GHz) may be accomplished by exploiting the electro-optic effect. Using travelling wave electro-optic techniques analogous to acousto-optic spectrum analysis, it should be possible to create an electro-optic spectrum analyser. We justify our optimism for such a device by citing the existence of electro-optic

devices capable of modulating laser radiation at frequencies of the order of 60 GHz. These existing electro-optic modulators are of two basic types; standing wave switch devices [1.4,1.5,1.6] or travelling wave interferometer devices [1.7,1.8,1.9], neither of which is capable of being used for the purposes of spectrum analysis except as part of a high resolution interferometer [1.10]. Several implementations of a travelling wave electro-optic diffraction device have been suggested by Dawber et al [1.11,1.12]. These possible implementations range from a simple rf strip-line containing an electro-optic crystal, to pump current modulation of a monolithic solid state laser.

All optical devices for rf spectrum analysis share the same basic mathematical description, because they are all based on rf signal-induced dielectric changes of the interaction medium, which in turn cause diffraction. The acousto-optic, electro-optic and permanent phase gratings that shall be discussed in the following chapters can thus be described by the same set of equations and parameters.

§1.2 Design Parameters for Optical rf Spectrum Analysers.

All optical radio-frequency spectrum analysers can be described in terms of the same parameters. The two parameters involved in the design of travelling wave phase gratings are the quality factor Q and the time bandwidth product τB [1.1,1.2,1.11]. The Q factor is the more important of these design parameters in that it dictates the diffraction regime in which the device operates and applies to all types of phase grating. The Q factor is a measure of both the angle of diffraction and the resolution of the grating. The Q factor is defined in terms of the interaction length, L, the optical wave number, K, and grating wave number, k_g,

$$Q = \frac{k_g^2 L}{K} . \qquad (1.1)$$

Thus Q increases with angle of diffraction and with resolution. The regime for which $Q \leq 1$ is that in which an optical wave-front undergo multiple deflections to produce an array of equally spaced points of light given a "single" grating frequency and a monochromatic collimated optical input. The $Q \leq 1$ regime is described by the Raman Nath equations [1.13] and coincides with grating spacings of the same order as the interaction length. The regime for which $Q \gg 1$ is that in which an optical wave-front undergoes a single deflection and thus a single grating frequency results in a single diffracted spot on illumination with a collimated light source. The $Q \gg 1$ regime is known as the Bragg regime because of its close analogy to Bragg scattering in x-ray crystallography [1.14].

Obviously for the purposes of spectrum analysis it is more desirable to utilise the direct single grating frequency diffraction angle relation which occurs in the Bragg regime than the multi-angle pattern of the Raman Nath.

The time bandwidth product, τB, is defined as the product of the optical window transit time of the travelling wave grating and the device bandwidth. The transit time dictates the lowest resolvable frequency for the device and the bandwidth dictates the maximum range of frequencies over which the device is operable. Thus the value of τB for a given device approximates to the number of grating lines, N, the device creates when operating at its upper frequency limit, f_{max},

$$\tau B = \frac{D}{v} \Delta f \approx N = \frac{D}{v} f_{max}, \tag{1.2}$$

where D is the optical window size in the direction of the acoustic wave propagating with velocity v. The bandwidth, Δf, can be dictated by a combination of factors which range from transducer impedance to interaction length.

The transducer in an acousto-optic modulator acts as an electronic band pass filter and as such can produce an upper and lower frequency limit for the device. The other major

impedance effect in acousto-optic modulators is acoustic absorption within the interaction media, which increases as the square of the frequency. Chang gives a figure of ~1 $dBcm^{-1}$ for the attenuation of a surface acoustic wave with frequency 1 GHz in $LiNbO_3$ [1.6]. The acoustic absorption thus provides an upper frequency limit for all acousto-optic devices.

In electro-optic diffraction devices transducers are not required and the device impedance is determined by the choice of material and device dimensions. Thus, given the correct choice of electro-optic medium (i.e. one without an absorption band in the spectral region of interest), the value of the time bandwidth product is dictated by the device dimensions only. The interaction length, L, affects the bandwidth by way of the condition that the grating wave should not change phase significantly (i.e. by less than $\pi/4$) during the time it takes an optical wave front to interact with the grating. For the travelling wave electro-optic diffractor the interaction length also dictates the diffraction efficiency per watt of rf power in the travelling wave. Thus there is a trade off between the diffraction efficiency of the device and its upper operating frequency (i.e. bandwidth).

The optical window size, D, has an obvious effect on the time bandwidth product (1.2) and the electrical thickness only affects the impedance of the system as seen by the rf radiation.

§1.3 Coupled Mode Maxwellian Theory for Phase Diffraction Gratings.

All perturbations to the dielectric constant of a transparent medium are capable of changing the path of an electro-magnetic wave within that medium. If there is a periodicity to the dielectric perturbation, then diffraction will occur only under the correct conditions [1.15,1.16,1.17]. The foremost condition for diffraction to occur is the phase match condition, which can be written as

$$\mathbf{K}_{out} - \mathbf{K}_{in} \pm \mathbf{k}_g = 0, \tag{1.3}$$

where: $\mathbf{k}_g$ is the grating wave vector for the perturbation, or a component of the

perturbation; $\mathbf{K}_{out}$ and $\mathbf{K}_{in}$ are the output and input optical wave-vectors, respectively (Figure 1.2). In the case of travelling wave gratings, the output frequency, ω_{out}, of the optical radiation differs from the input frequency, ω_{in}, by the grating frequency, ω_g;

$$\omega_{out} - \omega_{in} \pm \omega_g = 0. \tag{1.4}$$

Equation (1.4) holds for all cases except those of standing wave gratings, which have non-zero frequency components, but have an effective frequency of zero due to the cancelling of the two travelling wave frequency components that make up the standing wave.

The theory for all cases, moving or stationary, high or low grating frequency, can be put in terms of a perturbation to the dielectric tensor within Maxwell's equations. The total dielectric tensor's elements including the acoustic or electrical perturbation can be written as

$$\varepsilon_{ij}^{(T)} = \varepsilon_{ij} + \Delta\varepsilon_{ij}\,, \tag{1.5}$$

where $\Delta\varepsilon_{ij}$ represents the perturbation*.

Maxwell's equations are

$$\nabla\times\mathbf{E} + \mu_o\partial\mathbf{H}/\partial t = 0, \tag{1.6}$$

$$\nabla\times\mathbf{H} - \varepsilon.\partial\mathbf{E}/\partial t = \mathbf{J}, \tag{1.7}$$

$$\nabla.(\varepsilon.\mathbf{E}) = \rho, \tag{1.8}$$

$$\nabla.\,\mathbf{H} = 0, \tag{1.9}$$

where the symbols have their usual meaning [1.18].

* The dielectric tensor as stated here includes ε_o and will be taken to include it unless stated otherwise.

On imposing the conditions of zero conductivity and no net charge on the medium, the familiar wave equation is obtained for the propagation of electromagnetic radiation in an otherwise general medium, by taking the curl of (1.6), noting the $\rho=0$ result from (1.8) and substituting from (1.7);-

$$\nabla^2\mathbf{E} = \varepsilon.\frac{\partial^2\mathbf{E}}{\partial t^2} \quad . \tag{1.10}$$

If the perturbation to the dielectric constant is negligible a solution for the electric field of the form

$$\mathbf{E}(\mathbf{r}) = \mathbf{E}_o(\mathbf{r})\exp[i(\omega t - \mathbf{K}.\mathbf{r})] \tag{1.11a}$$

can be obtained from equation (1.10). The solution stated in equation (1.11a) has the form of a travelling wave with wave-vector **K** and field amplitude vector $\mathbf{E}_o(\mathbf{r})$. The angular frequency, ω, in (1.11a) is related to the wave-vector, **K**, by the expression

$$\omega = \left|\sqrt{K_i^2/\mu_o\varepsilon_{ij}\,\mathbf{e}_j}\right|. \tag{1.11b}$$

The dielectric perturbation $\Delta\varepsilon_{ij}$ is now introduced. The dielectric tensor is taken to be homogeneous in the z-direction and the perturbation is taken to be in the x-direction. The total dielectric constant can thus be written as

$$\varepsilon_{ij}^{(T)}(x,y,z) = \varepsilon_{ij}(x,y) + \Delta\varepsilon_{ij}(x,y). \tag{1.12}$$

The dielectric perturbation given by (1.12) can be visualised as a super-position of sine waves travelling in the x-direction (see figure 1.3), which is a generalisation of the sinusoidal perturbation used by Kogelnik [1.15]

To obtain the coupled mode equations for two optical modes propagating within a perturbed dielectric medium the equations describing multi-mode coupling are derived first. The coupling of two modes is then treated as a special case. Thus we deviate from Kogelnik's theory [1.15] for the coupling of two modes in a general lossy dielectric medium by a plane-wave sinusoidal perturbation of arbitrary direction.

The optical wave incident on the perturbed region of dielectric is taken to be a plane wave with a wave-vector, **K**, given by

$$\mathbf{K} = |\mathbf{K}| \begin{pmatrix} \sin\theta \\ 0 \\ \cos\theta \end{pmatrix} = \begin{pmatrix} \xi \\ 0 \\ \beta \end{pmatrix}, \tag{1.13}$$

where the x and z components are re-labelled for convenience.

The unperturbed solution to the wave equation (1.10) can now be rewritten in the form

$$\mathbf{E}(\mathbf{r}) = \mathbf{E}_o(x,y)\exp[i(\omega t - \xi x - \beta z)], \tag{1.14}$$

where $\mathbf{E}_o(x,y)$ is determined by the equation

$$\left\{ \frac{\partial^2}{\partial x^2} + \frac{\partial^2}{\partial y^2} + \omega^2 \mu_o \varepsilon_{ij}(x,y) - \beta^2 \right\} E_j(x,y)\exp[-i\xi x] = 0, \tag{1.15}$$

which is equation (1.10) expanded with reference to (1.11) and the condition of dielectric homogeneity in the z-direction.

On applying the Lorentz reciprocity theorem to the solutions of (1.15) it can be shown that they form a set of orthogonal functions [1.4]. The m^{th} member of this set of functions is

denoted by the subscript m;

$$\mathbf{E}_m(\mathbf{r},t) = \mathbf{E}_m(x,y)\exp[i(\omega t - \xi_m x - \beta_m z)]. \tag{1.16}$$

An arbitrary field distribution oscillating at frequency ω can be represented by its projection onto the function space [1.19] formed by the above set of orthogonal functions

$$\mathbf{E}(\mathbf{r}) = \sum_{\text{all m}} A_m |m\rangle \exp[i(\omega t - \xi_m x - \beta_m z)], \tag{1.17a}$$

where A_m is the projector of the arbitrary field vector $\mathbf{E}_o(x,y)$ on to the basis vectors $\mathbf{E}_m(x,y)$ denoted by $|m\rangle$;

$$A_m = \langle m \mid \mathbf{E}(\mathbf{r}) \rangle . \tag{1.17b}$$

The basis vector $|m\rangle$ is normalised by taking it to be the vector $\mathbf{E}_m(x,y)$ with unit Poynting vector. Thus, the inner product of two basis vectors is given by

$$\langle n|m\rangle = \frac{2\omega\mu_o}{|\mathbf{K}|}\delta_{nm}. \tag{1.18}$$

We now return to the general case, where the perturbation of the dielectric is included and the field distribution at t=0 is arbitrary. By substituting (1.17a) into (1.10) and applying equation (1.15) to eliminate the differentials of $\mathbf{E}(x,y)$ and the unperturbed dielectric terms, the following equation is obtained;

$$\sum_{\text{all m}} \left[\frac{\partial^2 A_m}{\partial z^2} - 2i\beta_m \frac{\partial A_m}{\partial z} \right] |m\rangle \exp[i(\omega t - \xi_m x - \beta_m z)]$$

$$= -\mu_o \omega^2 \sum_{\text{all k}} \Delta\varepsilon(x,y)\, |k\rangle A_k \exp[i(\omega t - \xi_k x - \beta_k z)] . \tag{1.19}$$

In the case of a weak perturbation the value A_m will vary slowly with z. Thus the parabolic approximation [1.20]

$$\left| \beta_m \frac{\partial A_m}{\partial z} \right| \gg \left| \frac{\partial^2 A_m}{\partial z^2} \right| \tag{1.20}$$

can be employed.

Applying the approximation (1.20) to (1.19) and taking its inner product with the arbitrary mode vector |n>, an expression for the variation of the amount of radiation in the m^{th} mode with respect to distance is obtained;-

$$\frac{dA_m}{dz} = -\frac{i\omega}{4}\frac{|K_m|}{\beta_m}\sum_{\text{all } k} <m|\Delta\varepsilon(x,y)|k> A_k \exp[-i(\xi_k - \xi_m)x - i(\beta_k - \beta_m)z]. \tag{1.21}$$

To transform the general perturbation of the dielectric tensor, $\Delta\varepsilon(x,y,z)$, into a form where the phase match condition (1.3) emerges from our treatment, it is expressed as a Fourier series;

$$\Delta\varepsilon_{ij}(x,y) = \sum_{\alpha \neq 0} \Delta\varepsilon_{ij}^{(\alpha)}(x,y)\exp[i\frac{2\pi\alpha}{\Lambda}x] \ . \tag{1.22}$$

In equation (1.22) the symbol Λ denotes the fundamental wavelength of the perturbation and the $\alpha = 0$ term is omitted since it has already been included as the unperturbed dielectric term in equation (1.13). The expansion of the dielectric perturbation as a Fourier series implies that the mode coupling constant,

$$\chi_{mk} = \frac{\omega}{4} <m|\Delta\varepsilon(x,y,z)|k> \ ,$$

can also be expanded as such a series

$$\chi_{mk} = \frac{\omega}{4}\sum_{\alpha\neq 0} <m|\Delta\varepsilon^{(\alpha)}(x,y)|k> \exp[i\frac{2\pi\alpha}{\Lambda} x]$$

$$= \sum_{\alpha\neq 0} \chi^{(\alpha)}_{mk} \exp[i\frac{2\pi\alpha}{\Lambda} x] \ . \qquad (1.23)$$

By employing (1.23) equation (1.21) can be condensed into its final form;

$$\frac{dA_m}{dz} = -i\frac{|\mathbf{K}_m|}{\beta_m}\sum_{\substack{all\ k \\ \alpha\neq 0}} \chi^{(\alpha)}_{mk} A_k \exp\left[-i\left(\xi_k - \xi_m - \frac{2\pi\alpha}{\Lambda}\right)x - i(\beta_k - \beta_m)z\right], \qquad (1.24)$$

which contains all the information relating to the diffraction pattern generated by the dielectric perturbation.

The only quantity that can be obtained from (1.24) without integration is the phase match condition. Conservation of momentum dictates that the phase term in (1.24) is zero when phase matching occurs. Thus the best case coupling between modes |k> and |m> yields the non-trivial solution

$$\left(\xi_k - \xi_m - \frac{2\pi\alpha}{\Lambda}\right)x + (\beta_k - \beta_m)z = 0 \qquad (1.25)$$

which states that the components of the incident and diffracted wave-vectors are linked by a term dependent on the frequency of the dielectric perturbation. The phase match condition also dictates the angle of diffraction between the modes |k> and |m>. The simplest non-trivial case occurs when $|2\pi\alpha/\Lambda| < |k_k|, |k_m|$ and $|k_k| = |k_m|$, which occurs in the Bragg

regime. The Bragg diffraction equation (1.25) yields the familiar expression for the Bragg angle, θ_B,

$$\sin\theta_B = \frac{\alpha\lambda}{2\Lambda}, \tag{1.26a}$$

where λ is the wavelength of the optical radiation in an isotropic medium.

The other phase match condition of interest is that for Raman Nath diffraction. Equation (1.25) yields a first order Raman Nath diffraction angle, θ_{RN},

$$\tan\theta_{RN} = \frac{\alpha\lambda}{\Lambda}, \tag{1.26b}$$

which in the small angle approximation [1.20] is twice the Bragg angle, as would be expected from the two geometries.

Both the Bragg and Raman Nath diffraction regimes are of general interest, but for optical signal processing of radio frequencies Bragg diffractors are preferred since a single input rf grating frequency corresponds to a single diffraction angle, given a collimated coherent optical input.

For a description of Bragg diffraction only two interacting optical modes are required. Equation (1.25) will now be solved for the special case of two interacting modes.

The two modes are denoted by the numbers 1 and 2, the subscript 1 denoting the incident radiation and 2 denoting the diffracted radiation. The consideration of only two modes

simplifies expression (1.24) to two coupled-mode equations [1.15]

$$\frac{dA_1}{dz} = -i\frac{|\mathbf{K}_1|}{\beta_1}\chi_{12}^{(\alpha)} A_2 \exp[-i\Delta\beta z] \tag{1.27a}$$

and

$$\frac{dA_2}{dz} = -i\frac{|\mathbf{K}_2|}{\beta_2}\chi_{21}^{(-\alpha)} A_1 \exp[+i\Delta\beta z] \tag{1.27b}$$

where the phase terms $\Delta\beta$ is

$$\Delta\beta = \left(\xi_2 - \xi_1 - \frac{2\pi\alpha}{\Lambda}\right)\tan\theta + (\beta_2 - \beta_1).^{\dagger} \tag{1.27c}$$

The phase term $\Delta\beta$ (1.27c) contains both the x-component and the z-component of the wave-vectors, which are linked by the tangent of the angle of incidence of the input radiation.

The equation (1.27c) embodies the principle of conservation of momentum as seen above in equation (1.3). The equations (1.27a,b) comply with the principle of conservation of energy, and are consistent with the expression [1.4, 1.17]

$$\frac{d}{dz}\left\{|A_1|^2 + |A_2|^2\right\} = 0, \tag{1.28}$$

if and only if the coupling constants comply with the relation

$$\frac{|\mathbf{K}_2|}{\beta_2}\chi_{21}^{(-\alpha)} = \left[\frac{|\mathbf{K}_1|}{\beta_1}\chi_{12}^{(\alpha)}\right]^*. \tag{1.29}$$

---

† It is interesting to note that the equations (1.27) are of the same form as those that describe optical parametric oscillations and optical second harmonic generation [1.21,1.22,1.23,1.24,1.25,1.26].

The condition on the conjugate of the coupling constant can also be obtained from its definition (1.23) and the condition of Hermitian self-adjointness [1.19] on the dielectric perturbation.

When we apply the condition of one input optical wave and two output waves

$$A_1(0) = A_1(z=0) = 0,$$
$$A_2(0) = A_2(z=0) \neq 0 \tag{1.30}$$

along with equation (1.13) to the coupled mode equations (1.27), the following solutions are obtained;

$$A_1(z) = A_2(0).\frac{\chi_{12}}{\gamma\cos\theta}.\sin\gamma z.e^{-i\Delta\beta z/2}, \tag{1.31}$$

$$A_2(z) = A_2(0).\left[\cos\gamma z - \frac{i\Delta\beta}{2\gamma}\sin\gamma z\right].e^{i\Delta\beta z/2}, \tag{1.32}$$

where γ is given by

$$\gamma^2 = \frac{\Delta\beta^2}{4} + \frac{|\chi_{12}^{(\alpha)}|^2}{\cos^2\theta}. \tag{1.33}$$

From the results (1.31) and (1.32) the diffraction efficiency and the optimum interaction length can be obtained. The diffraction efficiency is thus given by

$$\frac{I_{out}}{I_{in}} = \frac{|\chi_{12}^{(\alpha)}|^2}{\gamma^2\cos^2\theta}\sin^2\gamma z, \tag{1.34}$$

which can be optimised to give 100% diffraction into the output mode by satisfying the phase match condition $\Delta\beta = 0$ and using the optimum grating medium thickness,

$$b_{optimum} = \frac{\pi}{2} \frac{\cos\theta}{|\chi_{12}^{(\alpha)}|} . \tag{1.35a}$$

The interaction length, L, over which the incident radiation interacts with the dielectric perturbation is thus

$$L = \frac{\pi}{2} \frac{1}{|\chi_{12}^{(\alpha)}|} . \tag{1.35b}$$

For the calculations done for the devices described in the following chapters the small angle approximation, $\cos\theta \approx 1$, holds. Thus the interaction length, L, and the grating medium thickness, b, will be taken to be equal.

The interaction length, L, can be optimised by (1.35), but it will also be constrained by other design requirements including Q and the time-bandwidth product. We now revert to a specific example to illustrate the inter-play of the diffraction efficiency with the optical angle of incidence, θ, and the change in refractive index, Δn.

In figure 1.4 the normalised diffraction efficiency is plotted against the optical angle of incidence, θ, for a $LiNbO_3$ Bragg cell operating at 500 MHz with quality factors $Q \approx 10$ and $Q \approx 50$. The angle taken up by the zeroth order of the diffraction pattern when $Q \approx 50$ is one fifth of that for $Q \approx 10$. Thus the higher the value of Q the higher the resolution of the Bragg cell.

In figure 1.5 the diffraction efficiency is plotted against the perturbation amplitude in the refractive index, Δn, when the phase matching (1.2) is satisfied, for three values of the interaction length, L. This demonstrates that the coupling from the incident radiation to the

diffracted beam is a combination of the refractive index perturbation and the interaction length. From the γ in the argument of the sinusoidal term of equation (1.34) we infer that the size of the perturbation to the refractive index can effect the distribution of the diffracted light, but in all practical cases index changes of less than 10 have a negligible effect. (In the acousto-optic and first order electro-optic effects refractive index variations of 10 are unheard of.) The only place we may expect a deviation from the diffraction patterns shown in figure 1.4 is when the grating medium is optically active as in a laser gain medium (see chapter 3).

§1.4 Conclusions.

In this chapter we have given an account of the design parameters and theory behind stationary and travelling wave phase gratings.

The design parameters Q and τB are commonly used figures of merit which originated in the description of acousto-optic diffraction gratings. Both Q and the τB are dimensionless and can be maximised at the expense of the other design parameters.

Expressions for the diffraction efficiency and the angle of diffraction have been derived using coupled mode theory for optical interaction with a dielectric, which can be applied to such diverse phenomena as the acousto-optic effect and optical parametric oscillation. The "diffraction efficiency" and the Bragg angle apply to all effects that the coupled mode theory can be applied to, and therefore to all dielectric perturbation effects, but the parameters Q and τB only apply to the grating and spectrum analysis applications of the theory.

To find out how the parameters for phase gratings interact we must examine specific grating types.

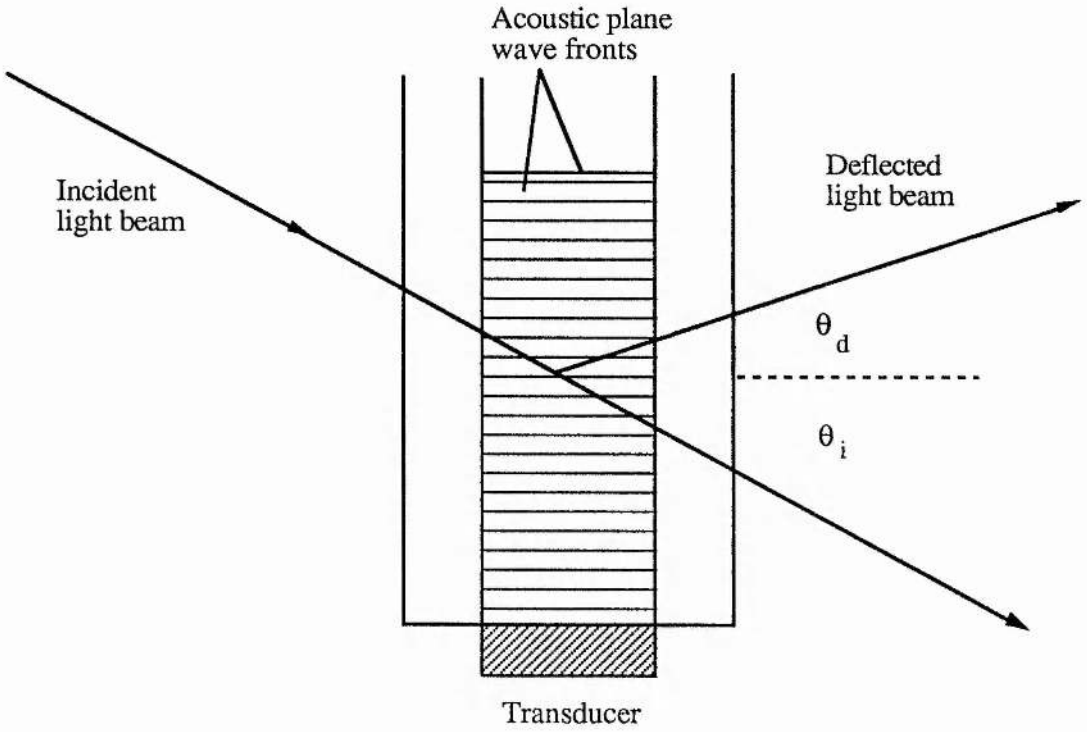

Figure 1.1. Diagram of a Bragg cell implemented in an anisotropic medium neglecting refractive effects at the dielectric boundaries.

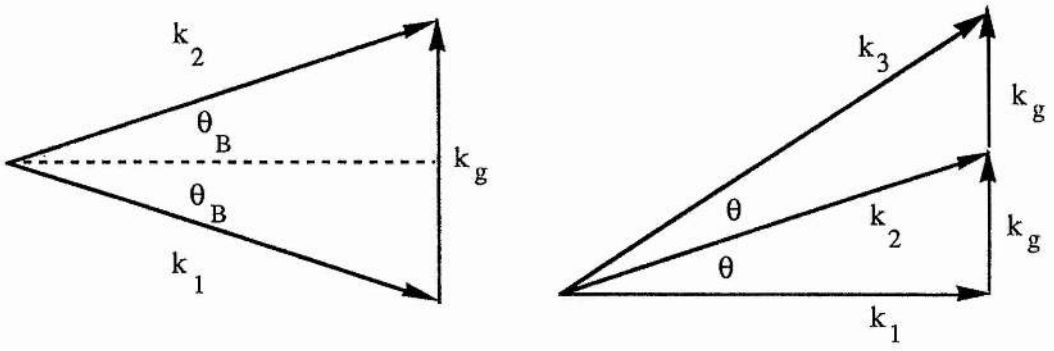

Bragg Regime. Raman Nath Regime.

Figure 1.2 (a) Phase match diagram for the case of addition of phonons, or rf-photons, to the incident light in both the Bragg and Raman Nath regimes; $\mathbf{k}_2 = \mathbf{k}_1 + \mathbf{k}_g$, $\mathbf{k}_3 = \mathbf{k}_2 + \mathbf{k}_g$.

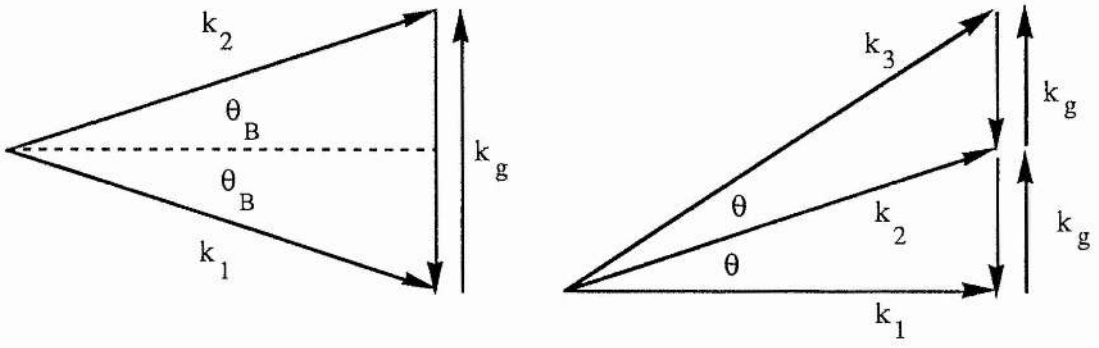

Bragg Regime. Raman Nath Regime.

Figure 1.2 (b) Phase match diagram for the case of resonant subtraction of phonons, or rf-photons, from the incident light in both the Bragg and Raman Nath regimes; $\mathbf{k}_1 = \mathbf{k}_2 - \mathbf{k}_g$, $\mathbf{k}_2 = \mathbf{k}_3 - \mathbf{k}_g$.

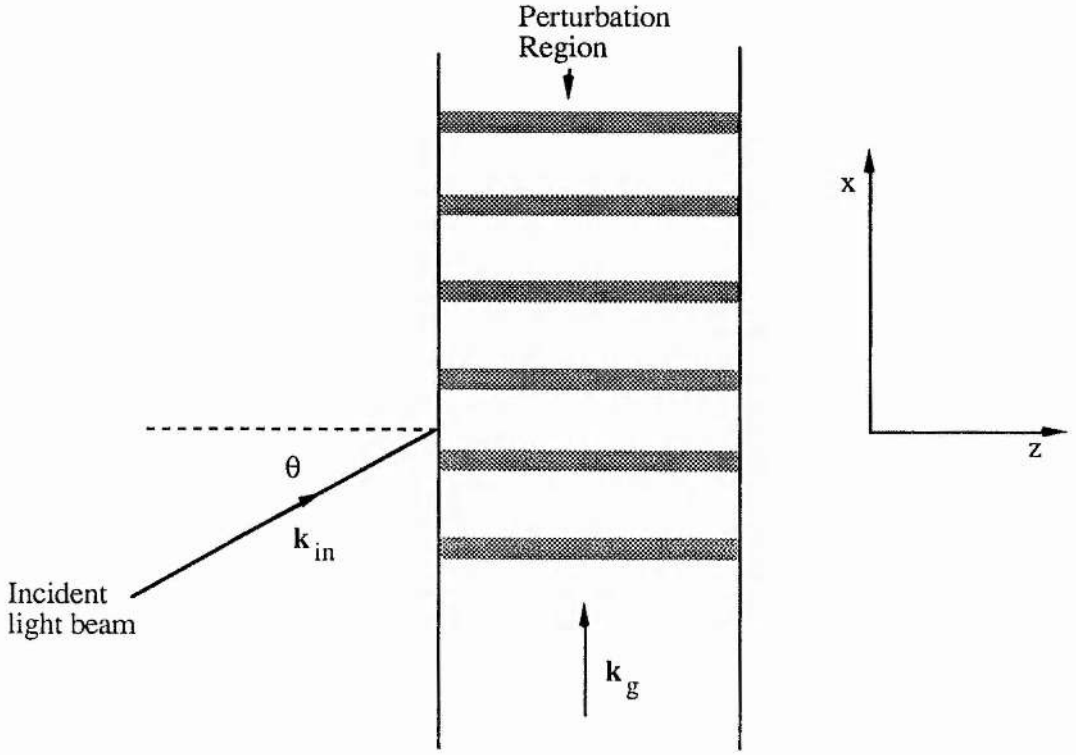

Figure 1.3. Diagram showing the directions of propagation for the incoming light and the grating wave with respect to the x and z axes.

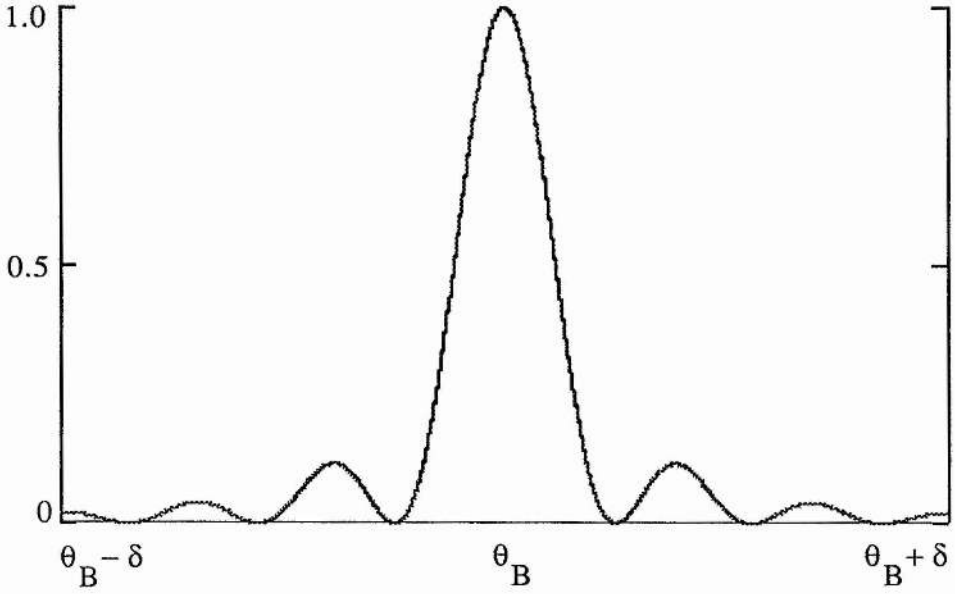

Graph (a) Normalised diffraction efficiency when Q = 10.5.

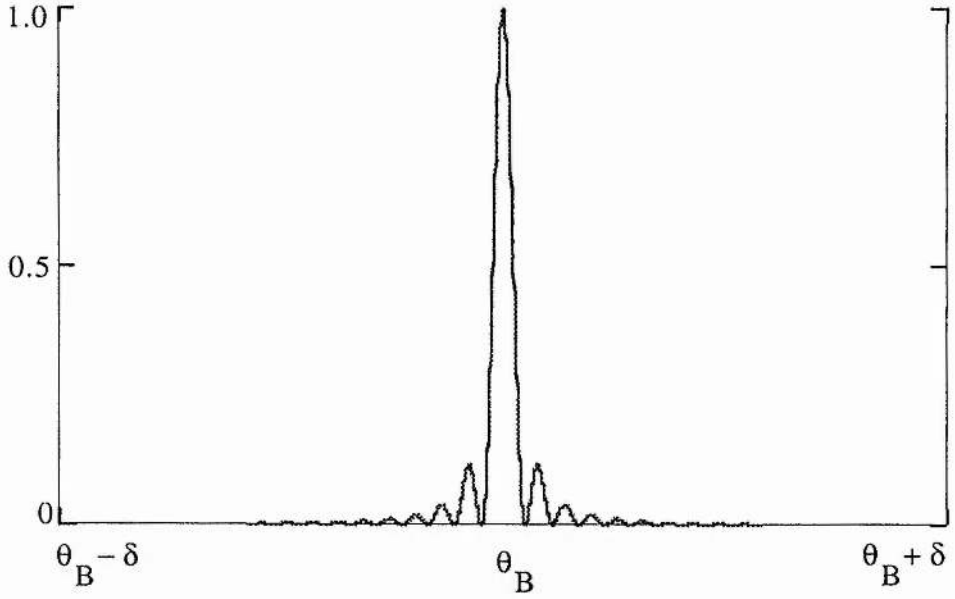

Graph (b) Normalised diffraction efficiency when Q = 52.3.

Figure 1.4. Graphs of the normalised diffraction efficiency against optical angle of incidence for a $LiNbO_3$ acousto-optic Bragg Cell Operating at 500 MHz and illuminated by a HeNe laser for two values of Q. The quantity δ is the same for both graphs and is the order of milli-radians.

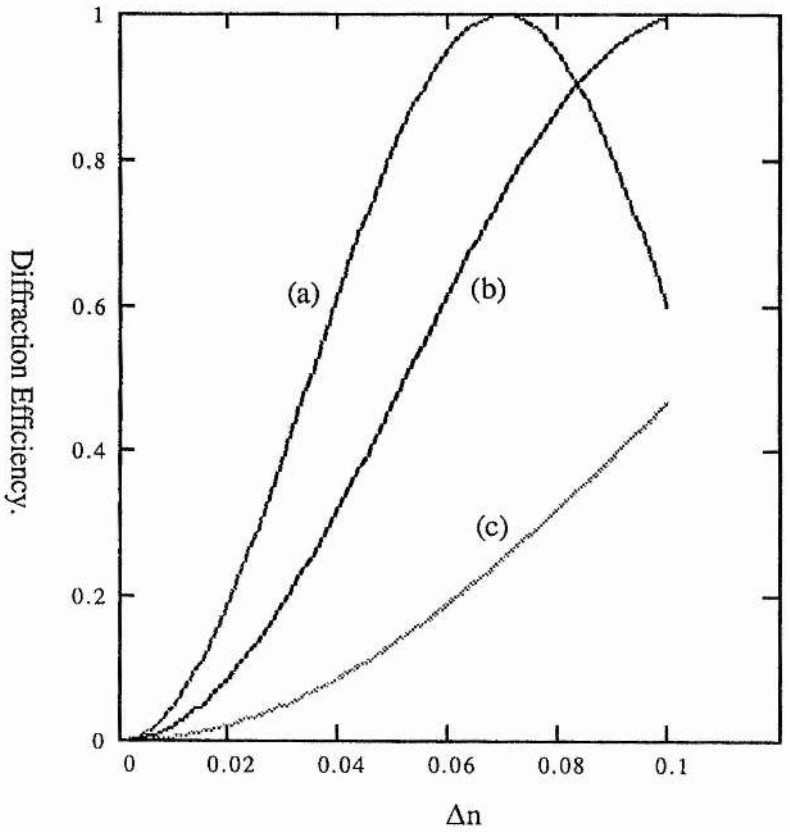

Figure 1.5. Graphs of diffraction efficiency at the Bragg angle against the refractive index perturbation depth, Δn, for three interaction lengths; (a) 15 mm, (b) 10 mm, (c) 5 mm.

§1.5 References.

[1.1] Acousto-Optic Signal Processing - Theory and Application. Ed: N J Berg and J N Lee. Marcel Dekker Inc. (New York) 1983.

[1.2] Acousto-Optic Signal Processing: Fundamentals and Application. P K Das and C M DeCusatis. Artech House (London). 1991.

[1.3] 3 GHz Bandwidth Bragg Cells. J C Poncot, P Nyeki, P H Defranould and J P Huiguard. Proc. IEEE Ultrasonics Symposium 1987. page 501-3. 1987.

[1.4] Optical Waves in Crystals. A Yariv and P Yeh. John Wiley and Sons (Int.) 1984.

[1.5] Optical Guided-Wave Gallium Arsenide Monolithic Interferometer. J P Donnelly, N L DeMeo, G A Ferrante, K B Nichols and F J O'Donnel. Appl. Phys. Lett. **45**(4) page 360-2. 1984.

[1.6] Handbook of Microwave and Optical Components (Volume 4. Fibre and Electro-Optical Components). Chang (Ed.) Wiley Interscience (New York). 1991.

[1.7] Solid State Laser Engineering. 2Ed. W. Koechner. Springer Verlag (Berlin) 1988.

[1.8] Velocity Matched Electro-Optic Phase Modulator for Wide Optical Sideband Generation. B Y Lee, T Kobayashi, A Morimoto and T Sueta. Electronics Lett.s **28** (3) page 330-2. 1992.

[1.9] Optical Intensity Modulation to 40 GHz using a Waveguide Electro-Optic Switch. S K Korotky, G Eisenstein, R S Tucker, J J Veselka and G Raybon. Appl. Phys. Lett. **50** (23) page 1631-3. 1987.

[1.10] Private communication. W N Dawber. 1993.

[1.11] Radiofrequency Analysis Using Optical Signal Processing (Ph.D. Thesis). W N Dawber. Uni. of St. Andrews, Scotland. 1991.

[1.12] Light Modulating Cells. W N Dawber, P F Hirst, A Maitland and P Sutton. UK patent 9021044.4 (file AW(R) 5520) 27 Sept 1990.

[1.13] The Diffraction of Light by Ultrasound. M V Berry. Academic Press (London). 1966.

[1.14] Solid State Physics. N W Ashcroft and N D Mermin. Holt, Rinehart and Winston (Philadelphia). 1976.

[1.15] Coupled Mode Theory for thick Hologram Gratings. H Kogelnik. Bell Syst. Tech. J. **48**(9) page 2909. 1969.

[1.16] Coupled-Wave theory of Distributive Feedback Lasers. H Kogelnik and C V Shank. J. Appl. Phys. **43**(5) page 2327. 1972.

[1.17] Coupled Mode Theory for Guided Wave Optics. A Yariv. IEEE J. Quantum Electronics **QE 9**(9) page 919. 1973.

[1.18] Electricity and Magnetism. B I Bleaney and B Bleaney. Oxford Uni. Press (Oxford). 1959.

[1.19] Group Theory in Physics Vol.1, (Appendix B) J F Cornwell. Academic Press (London). 1984.

[1.20] Advanced Engineering Mathematics. 6Ed. E Kreyszig. John Wiley and Sons (Int.). 1989.

[1.21] Concerning one possibility of amplification of light waves. S A Akhmanov and R V Knokhlov. Soviet Phys. JETP **16**, page 252. 1963.

[1.22] Interaction between light waves in a non-linear dielectric.
J A Armstrong, N Bloembergen, J Ducuing and P S Pershan.
Phys. Rev. **127**, page 1918. 1962.

[1.23] Generation of Optical Harmonics.
P A Franken, A E Hill, C W Peters and G Weinreich.
Phys. Rev. Lett.s **7** page 118. 1961.

[1.24] Tuneable Optical Parametric Oscillators. S E Harris.
Proc IEEE **57**(12) page 2096. 1969.

[1.25] Single Cavity Noncollinear Optical Parametric Oscillation. J Falk and E Murray.
Appl. Phys. Lett.s **14**(8) page 245. 1969.

[1.26] Theory of Optical Parametric Noise. D A Kleinman.
Phys. Rev. **174**(3) page 1027. 1968.

Chapter 2.

Travelling Wave Electro-Optic Diffraction in Barium Titanate.

§2.1 Introduction.

In this chapter we investigate travelling wave electro-optic diffraction devices based on the first order electro-optic effect and, in particular, a single crystal barium titanate electro-optic diffraction device† .

The motivation for developing a travelling wave electro-optic diffractor (TWEOD) [2.1] comes from the operational limits of acousto-optic spectrum analysis technology, which is of the order of 3 GHz. The presence of an upper operational limit for acousto-optic devices is due to acoustic propagation losses, which are approximately proportional to the square of the acoustic frequency [2.2]. (Lithium niobate, the most commonly used interaction medium in acousto-optic spectrum analysis, has a surface wave absorption of 1 dB/cm at 1 GHz [2.2].) There is therefore a large region of the rf spectrum (3-100 GHz) already in use for communication for which there is not a corresponding non-heterodyning method spectrum analysis.

Bragg cell spectrum analysers based on the electro-optic effect should be capable of analysing the range 1 - 100 GHz, since the electro-optic effect in its many forms has a response ranging from dc to optical frequencies [2.3].

The TWEOD can be described by the two general parameters already devised for the description of acousto-optic phase gratings, Q (1.1) and τB (1.2). For the best performance of the TWEOD, Q and τB should be maximised for the required bandwidth. Both the Q and τB of a TWEOD are proportional to the dielectric constant of the electro-optic interaction medium at the radio frequency. Thus a material with a high dielectric constant is required. Of all the common electro-optic crystals in use today, barium titanate has the highest dielectric constant at dc to radio frequencies. The dielectric constant of $BaTiO_3$ at dc is given as 4300 by Merz [2.4] and as 3000 by Dawber [2.5]. The electro-optic constant of

---

† We have recently discovered two papers in which a device similar to the TWEOD was described. The E-O grating implemented in single crystal KTN. The theoretical description of the device did not deal with parameters applicable to single processing and the device did not comply with condition (2.10).
{M G Cohen & E I Gordon. Appl. Phys. Lett. 5(9) pp.181-2. (1963). E I Gordon & M G Cohen. IEEE J Quantum. Elect. **QE-1**(5) pp.191-98. (1965)}

$BaTiO_3$ as given as 108×10^{-12} m/V by Dawber [2.5], which is high in comparison with other electro-optic crystals' values.

§2.2 General Theory for Travelling Wave Electro-Optic Diffractors.

A theory for all TWEOD devices can be derived from the general coupled mode equations given in chapter 1. In chapter 1 our treatment of phase gratings assumed only one diffracted mode and therefore is only applicable in the Bragg diffraction regime, $Q \gg 1$. The TWEOD will in general operate in the Raman Nath regime, $Q \leq 1$, where multi-mode diffraction occurs. To justify the use of the two interacting modes model to describe a TWEOD the argument used by Sapriel [2.6] for low power Raman Nath diffraction can be employed.

The diffraction efficiency per watt of rf power in $BaTiO_3$ is of the order of 0.1% as calculated using the two interacting modes model (section 2.3.4). Thus we can employ Sapriel's argument, which states that for low Q, low diffraction efficiency acousto-optic cells* , "...only the +1 and –1 orders appear, symmetrically in relation to the central beam; then when ..." the modulation strength "...increases +2 and –2 orders appear then +3 and so forth." [2.6].

In the Raman Nath regime, when the incoming optical radiation is perpendicular to the direction of rf propagation, with low grating efficiency there will be two diffracted modes of order one. In the Bragg regime when the optical beam is at θ_B (1.26) to the direction of rf propagation theoretically there will be only one mode. In both the Raman Nath and Bragg regimes for small diffraction angles the number of diffracted optical modes propagating will increase with an increase in the diffraction efficiency. In the operational

---

* Sapriel uses the parameter $\zeta = KL\delta n$, which is the product of the optical wave number, the interaction length and the refractive index modulation depth, to give a measure of the amount of light diffracted by the grating. We use our calculated value of diffraction efficiency instead.

regime of the TWEOD the efficiency is so small as to give only the first order diffracted mode or modes.

Thus, we justify the application of the single diffracted mode theory of chapter 1 to a system where $Q < 1$ and explain the possible Raman Nath correction factor of 2 that must be applied when there are two first order diffraction modes. We shall ignore the factor of 2 for the following theoretical calculations, but it will be kept in mind during experimentation.

The theory in chapter 1 is for a general dielectric perturbation and as such requires to be put into the appropriate form for the electro-optic effect before the introduction of specific $BaTiO_3$ values.

The theoretical treatment of the TWEOD starts with a restatement of the mode coupling constant given by equation (1.23),

$$\chi_{12}^{(\alpha)} = \frac{\omega}{4} \langle 1| \Delta\varepsilon^{(\alpha)}(x,y,z) |2\rangle. \tag{2.1}$$

Since the envisaged device operates at low intensities and with radio frequencies less than 100 GHz, the value for the dielectric perturbation given by the first order electro-optic effect (where the change in the dielectric constant is small compared with its original value) is used;

$$\Delta\varepsilon_{ij} = \varepsilon_o \Delta\varepsilon_r = -\varepsilon_o |\varepsilon_r|^2 r_{ijk} E_k . \tag{2.2}$$

In equation (2.2) the subscript "r" denotes the observed value for the relative dielectric constant at the optical frequency.

On putting the value of the dielectric perturbation (2.2) into equation (2.1) and using the normalisation condition (1.18) the following relation is arrived at for the coupling coefficient

$$\chi_{12}^{(\alpha)} = -\frac{\omega}{2}\left[\varepsilon_o \mu_o |\varepsilon_r|^3\right]^{1/2} r_c |\mathbf{E}|, \tag{2.3}$$

where the subscript "c" denotes that the electro-optic tensor has been contracted with respect to optical propagation modes |1> and |2> and the perturbing rf electric field amplitude vector **E**. The equation (2.3) can be written in the more accessible form

$$\chi_{12}^{(\alpha)} = -\frac{1}{2}\frac{2\pi}{\lambda_o} n^3 r_c |\mathbf{E}| , \tag{2.4}$$

where n is the refractive index as seen by the optical input beam and λ_o is the wavelength of the optical input beam in vacuum.

The resulting mode coupling efficiency given in equation (1.34) can be stated for the electro-optic case as follows

$$\frac{I_{out}}{I_{in}} = \frac{\left[\frac{\pi}{\lambda_o} n^3 r_c |\mathbf{E}|\right]^2}{\left[\frac{\Delta\beta}{2}\right]^2 + \left[\frac{\pi}{\lambda_o} n^3 r_c |\mathbf{E}|\right]^2} \times \sin^2\left[\left[\left[\frac{\Delta\beta}{2}\right]^2 + \left[\frac{\pi}{\lambda_o} n^3 r_c |\mathbf{E}|\right]^2\right]^{1/2} L\right]. \tag{2.5}$$

When the phase factor $\Delta\beta$ is zero and the efficiency is small (2.5) can be approximated to by the first term in its MacLaurin expansion [2.7] and thus we obtain the diffraction

efficiency per watt of rf power

$$\eta \approx 2\left[\frac{\pi}{\lambda_o} n^3 r_c\right]^2 \frac{\mu_o c}{\sqrt{\varepsilon_{rf}}} \frac{L^2}{A}. \tag{2.6}$$

In equation (2.6) the expression for the RMS rf power in a lossless strip line [2.8] (figure 2.1) has been substituted for the square of the electric field:

$$P = \sqrt{\frac{\varepsilon_o \varepsilon_{rf}}{\mu_o}} \frac{A}{2} |\mathbf{E}|^2, \tag{2.7}$$

where $A = a \times b$ is the cross section of the strip line perpendicular to the rf wave's direction of propagation.

The other parameters of the TWEOD can also be put into a more convenient form. The value of Q (1.1) can be written in terms of the optical wavelength λ_o and the radio frequency ν_{rf},

$$Q = \frac{2\pi\varepsilon_{rf}}{nc^2} \lambda_o L \nu_{rf}^2, \tag{2.8}$$

and the value for the time bandwidth product (1.2) can be expressed similarly;

$$\tau B = \frac{\sqrt{\varepsilon_{rf}}}{c} D\Delta f, \tag{2.9}$$

where D is the optical window size and Δf is the device bandwidth.

The bandwidth of the device is constrained by the "moving grating" condition [2.5], which states that the grating wave front should not change by more than $\pi/2$ in the time it takes for

the interrogating wave-front to cross the grating region;

$$\frac{nL}{c} < \frac{1}{4\nu_{rf}} . \tag{2.10}$$

The maximum grating frequency, ν_{max}, has an associated maximum Bragg angle, θ_{Bmax}, which can be obtained from the Bragg condition (1.26);

$$\sin\theta_{Bmax} = \frac{\lambda_o\sqrt{\varepsilon_{rf}}}{2nc}\nu_{max} = \frac{\lambda_o\sqrt{\varepsilon_{rf}}}{8n^2L} . \tag{2.11}$$

Another useful measure of a TWEOD's angular performance is the change in angle per unit change in grating frequency from a given centre ν_{rf};

$$\Delta\theta_B = \frac{\frac{\lambda_o\sqrt{\varepsilon_{rf}}}{2nc}}{\left[1 - \left[\frac{\lambda_o\sqrt{\varepsilon_{rf}}}{2nc}\nu_{rf}\right]^2\right]^{1/2}} . \tag{2.12}$$

The design parameters given in equations (2.6-12) for a TWEOD are general for all first order electro-optic travelling wave diffractors, given the condition of $Q \gg 1$ or low power operation. From the general design parameters given above, the design curves for a 'perfect' $BaTiO_3$ TWEOD are now drawn.

§2.3 Design Curves and Constants for a $BaTiO_3$ TWEOD.

In section 2.2 the general theory for a TWEOD based on a single electro-optic crystal was described. We now wish to apply the general theory to the special case of a strip line mounted $BaTiO_3$ TWEOD.

§2.3.1 The Dielectric Properties of $BaTiO_3$.

We start by stating the dielectric properties of single crystal $BaTiO_3$ and how these affect the stripline design for a TWEOD.

The electro-optic tensor for $BaTiO_3$ in its 4mm room temperature state is given as [2.3];

$$\begin{aligned} r_{113} = r_{223} &= 8\times10^{-12}\text{m/V} \\ r_{311} = r_{131} = r_{232} = r_{322} &= 108\times10^{-12}\text{m/V} \\ r_{333} &= 23\times10^{-12}\text{m/V} . \end{aligned}$$

The dielectric tensor for $BaTiO_3$ at radio frequency we use for our calculations is the same as Dawber's [2.5];

$$\begin{aligned} \varepsilon_{11} = \varepsilon_{22} &= 3000 \\ \varepsilon_{33} &= 1000 . \end{aligned}$$

The refractive indices at a wavelength of 6328Å [2.3] are

$$n_e = 2.365 \qquad n_o = 2.437.$$

Note that the values for the dielectric constant tensor elements are vague due to the nature of $BaTiO_3$ as a single uniform crystal (see Appendix 1).

The best orientation of a $BaTiO_3$ crystal for use as a TWEOD is with its z-axis along the direction of rf propagation and at right angles to the optical direction of propagation (see figure 2.1). The result of this orientation is to present the rf field with the largest dielectric constant possible whilst being able to make use of the highest of the three available electro-

optic constants, which has its maximum effect when the optical polarisation is at right angles to rf field polarisation.

Another factor that affects the performance of the $BaTiO_3$ TWEOD is the impedance encountered by the rf wave. Not only will the line impedance affect the rf power coupling efficiency, but it will also dictate the perturbation field per watt of input power. The $BaTiO_3$ crystal orientation affects the strip-line impedance of the crystal by way of the rf dielectric constant, as can be seen from the expression for the impedance of a perfect stripline,

$$Z_l = \frac{a}{b}\left[\frac{\mu_o}{\varepsilon_o \varepsilon_{rf}}\right]^{1/2}. \qquad (2.13)$$

The stripline impedance is also affected by the maximum frequency response required of the TWEOD (2.10) by way of the interaction length, L, which is equivalent to the stripline width, b. For a required impedance, the stripline separation, a, can be varied to compensate for the width, b, and thus allow us to attain high maximum frequencies.

Crystal size and impedance are therefore linked with maximum grating frequency and diffraction efficiency.

§2.3.2 Diffraction Angles in $BaTiO_3$ TWEODs.

Both the maximum angle and the angular shift per unit frequency shift are dependent on the relative dielectric constant, ε_{rf}, of $BaTiO_3$, which can have values ranging from 1420 [2.9] to 4300 [2.4] at room temperature, depending on the levels of impurity.

The values for the maximum diffraction angle θ_{Bmax} (2.11) and $\Delta\theta_B$ (2.12) for a collimated HeNe laser beam are plotted against the dielectric constant over the range of

possible values of ε_{rf} in figure 2.2.

As well as the graph in figure 2.2 the exact values for the deflection angle at 10 GHz and 50 GHz are required for a dielectric constant of $\varepsilon_{rf} = 3000$. The value for the angular deflections of a HeNe beam, taking Snell's law [2.10] into account, for the two grating frequencies are as follows;

$$\theta_{Bmax}(\nu_{rf}) = \frac{\lambda_o \sqrt{\varepsilon_{rf}}}{2c} \nu_{rf}, \tag{2.14}$$

$$\theta_{Bmax}(10\ \text{GHz}) = 0.6\ \text{mrad}, \qquad \theta_{Bmax}(50\ \text{GHz}) = 3\ \text{mrad}.$$

The values for the maximum diffraction angles given here are large enough to be detected when the incident radiation has an angle of divergence which is less than 10 μrad. For a Gaussian beam the beam divergence is given by the equation [2.3]

$$\theta_{beam} \approx \frac{\lambda_o}{\pi w_o n}, \tag{2.15}$$

which for a HeNe laser yields a beam waist radius of $w_o = 20$ mm given a divergence angle of 10 μrad.

During TWEOD experiments optical angular factors, such as the beam divergence, must be accounted for so as to avoid the diffracted beam being unresolvable. To improve the angular quality of the HeNe laser beam we intend to use a spatial filter consisting of a telescope with a high quality pin hole at its intermediate focal point. The resulting beam from such a system can be considered as a plane wave since the pin hole is an effective point source placed in the front focal plane of the second lens. Thus in our calculations we can legitimately consider the incident beam on the TWEOD crystal to be perfectly collimated.

§2.3.3 Time-Bandwidth Product and Q for $BaTiO_3$ TWEODs.

Both the time-bandwidth (2.9) and Q (2.8) for a TWEOD are dependent on the maximum grating frequency, which is in turn dictated by the interaction length, L (2.10).

Taking the dielectric constant to be 3000 and using the current $BaTiO_3$ crystal growth limit of 10 mm as the device dimension D both the time-bandwidth product, τB, and the quality factor, Q, can be plotted against the upper frequency limit, ν_{rf}, for a TWEOD (figure 2.3).

If we assume that there is no variation in dielectric constant with radio frequency we can see from the graphs in figure 2.3 that both Q and τB are linear with ν_{max} and that the values of Q for all $BaTiO_3$ TWEODs, with 1 GHz < ν_{max} < 100 GHz, are below one. Thus all our $BaTiO_3$ TWEODs will operate in the Raman Nath regime.

The values of Q and τB for the three device sizes we choose to study are as follows;

D	L	ν_{max}	Q	τB
6 mm	2.5 mm	10 GHz	0.014	10.9
7 mm	2.5 mm	10 GHz	0.014	12.8
10 mm	0.6 mm	50 GHz	0.083	91.3

The above values for τB can be compared with acousto-optic Bragg cell time bandwidths, which can be as large as 4400 [2.1], to emphasise the need for a material of larger rf dielectric constant and single crystal size than $BaTiO_3$.

§2.3.4 Diffraction Efficiency in $BaTiO_3$ TWEODs.

The value of the diffraction efficiency, η, (2.6) can be expressed in terms of the maximum grating frequency (2.10);

$$\eta = \frac{1}{2}\left[\frac{\pi}{\lambda_o} cn^3 r_c\right]^2 \frac{\mu_o}{\sqrt{\varepsilon_{rf}} na} \frac{1}{\nu_{max}}, \tag{2.16}$$

which is plotted for the frequencies ν_{max} = 1 GHz to 100 GHz in figure 2.4. From equation (2.16) the diffraction efficiencies for devices with dimensions 2.0 × 0.6 × 10.0 mm and 2.0 × 2.5 × 7.0 mm (a × b × c) operating at 50 GHz and 10 GHz, respectively, are calculated to be 0.05 % per watt and 0.2 % per watt.

The diffraction efficiency (2.16) is primarily dependent on the radio frequency electric field in the crystal and therefore on the strip line impedance (2.13) of the crystal. The electric field within the crystal is proportional to the rf input power and the impedance. Thus to increase the diffraction efficiency for a given power input one would expect to increase the impedance, but this is not the case. The impedance of a lossless strip line [2.8] is inversely proportional to the electro-optic interaction length, L, and thus diffraction efficiency per watt (2.6) can be expressed as

$$\eta = 2\left[\frac{\pi}{\lambda_o} n^3 c r_c \mu_o\right]^2 \frac{1}{Z_l \varepsilon_{rf}}, \tag{2.17}$$

which decreases with line impedance (figure 2.5).

§2.4 $BaTiO_3$ TWEOD Experiments.

§2.4.1 Introduction.

Using the above design curves we composed two basic $BaTiO_3$ TWEOD designs; one for a 50Ω strip lie and the other for 20Ω, which have operating frequencies of 50 GHz and 10 GHz respectively. Both designs assume that the dielectric constant is $\varepsilon_{rf} = 3000$.

The 50Ω / 50 GHz device was designed to work in a coaxial-stripline-coaxial rf coupling configuration and the 20Ω / 10 GHz for a simple stripline configuration. The 20Ω / 10 GHz was also used in a free space-stripline-free space configuration and for the purpose of measuring the electro-optic constant and the dielectric strength of $BaTiO_3$.

§2.4.2 Measurement of the Electro-Optic Constant for $BaTiO_3$.

To measure the electro-optic constant for our $BaTiO_3$ sample we used an interferometric technique.

The smallest of the batch of the $BaTiO_3$ crystals was sandwiched between two electrodes with its c-axis parallel to them, as for a TWEOD, and then placed in one arm of a highly stable Mach-Zehnder interferometer [2.10] (figure 2.6). The interference pattern emerging from the interferometer was recorded as a reference while the voltage across the crystal was held at zero. The voltage across the crystal was then varied and the interference pattern obtained compared with the reference pattern over a range of different optical input polarisations. The following values for the electro-optic constant were obtained:

Polarisation with respect to c-axis, ζ.	Refractive index V=0 $n(\zeta)$	r_c $\times 10^{-12}$ m/V
0°	2.365	151 ± 10
45°	2.400	116 ± 8
90°	2.437	Not Detected

where r_c was calculated using the expression

$$r_c = \left[\frac{\lambda_o}{n(\zeta)^2 L}\right]\frac{a}{V} \qquad (2.18)$$

The effective electro-optic constant along the c-axis is 39% greater than that used in calculations for the diffraction efficiency per watt η (2.6) in section 2.2.4. These results for the dc electro-optic effect in $BaTiO_3$ would result in a 93% increase in the calculated value for η (e.g. the calculated value of $\eta(20\ \Omega, 10\ GHz) = 0.2\%$ will become 0.4%). The recalculated efficiency curves using the experimentally obtained values for the electro-optic constant are plotted in figure 2.7.

§2.4.3 Dielectric Strength of $BaTiO_3$.

The dielectric strength of the $BaTiO_3$ crystal used in the dielectric constant experiment was measured by destructive testing.

The dc voltage across the crystal was increased gradually until the crystal sheared at 45° to its c-axis and the field direction. The required voltage for shearing to occur was measured to be 2 kV. The crystal dimension in the field direction was a = 5.14 mm and thus the field for catastrophic breakdown was

E (destructive) = 4 kV/cm.

On taking the maximum rf field before breakdown to be half the dc value, the maximum rf power inputs for the two crystal impedances are found to be

20 Ω _____ 900 W(RMS)

50 Ω _____ 60 W(RMS).

Note that the dielectric strength as calculated here does not take into account any local

heating effects or electrical breakdown effects, either internal or external to the crystal, that may occur at radio frequencies.

Radio frequency sources of average power in the region of 1-10 watts shall be used for the rest of the experiments.

§2.4.4 $BaTiO_3$ TWEOD with a Pulsed 3 GHz Source.

Barium titanate crystals were placed in front of a pulsed radar set in an attempt to observe rf modulation of radiation from a HeNe laser (figure 2.8). The radar set emitted pulses of centre frequency 3.05 GHz at a repetition rate of 850 Hz with a peak power of 13 kW at a pulse length of 1 μs, and was intended to combine with the frequency of the laser sidebands [2.11] of separation 237 MHz to give a signal in the detectable region below 2 GHz.

We did not observe either a diffracted spot or modulation related to travelling wave diffraction when a plain crystal was illuminated with a collimated beam of width equal to the dimension of the crystal along its axis. Neither did we observe a straight phase modulation when the crystal was placed in an interferometer of beam width less than 1 mm. The system also failed to produce a result when the crystal had silver electrodes painted on its top and bottom surfaces and was connected to the rf source by an unmatched copper coupling.

We attribute the failure to observe the modulation of both the laser centre frequency and sidebands to the small coupling efficiency of the rf into the $BaTiO_3$ crystals. If the output of the radar set is taken to uniformly fill a quadrant of a sphere and the crystal is taken to be at 1 cm from the rf output (the smallest distance before breakdown occurs) then the power that enters a crystal of zero reflectivity is 5.6% of the total output. On taking the 98%

reflectivity of $BaTiO_3$ into account, the peak power in the crystal is 26 watts and the corresponding rf travelling wave peak power is calculated to be 0.5 watts.

The design parameters for the system are as follows;

Crystal No.	Structural Additions	Dimensions c × a × b (mm)	τB	Q × 10^{-3}	Diffraction Efficiency
510(3)	None	6.90 × 6.10 × 2.76	3.84	1.42	0.035%
510(1)	Ag Electrodes	6.18 × 6.23 × 2.78	3.44	1.43	0.043%

The peak phase shifts in the optical radiation within the two crystals, given 26 watts of rf enter the crystal at peak power, are of the order of 1 mrad and therefore undetectable given the sensitivity of our apparatus.

The method given in this section for proving the principles behind the TWEOD was discontinued due to the lack of other available coupling configurations.

§2.5 Designs for $BaTiO_3$ TWEODs Operating at 10 GHz and 50 GHz.

Both the 10 GHz and 50 GHz TWEOD proof of principle designs are intended to be used with continuous wave (cw) rf sources.

The 10 GHz design consists of a 500 Ω ridged rectangular wave-guide (WG-16) with a matched transition into stripline which changes in cross-section along its length so as to adiabatically match to the impedance of the $BaTiO_3$ crystal, $Z \approx 20\ \Omega$. The stripline then couples in and out of the $BaTiO_3$ crystal before a symmetrical section couples the rf to free space (figure 2.9). The crystals for use in the 10 GHz design have the following design

parameters, given that $\varepsilon_{rf} = 3000$:

Dimensions	ν_{max}	θ_{Bmax}	τB	η
$c \times a \times b$ (mm)	GHz	μrad		%/W
$7.03 \times 6.98 \times 2.63$	11.7	676	15.0	0.06
$7.53 \times 6.63 \times 2.40$	12.8	739	17.6	0.06

Thus our design for a 10 GHz TWEOD will give a detectable deflection of an incident collimated laser beam at rf power levels of 17 W for 1% diffraction efficiency.

A coaxial-stripline-coaxial configuration was considered for the 50 GHz TWEOD (figure 2.10), but the possibility of air breakdown at the coaxial cable-crystal interface, due to the quality of the contact, made it unacceptable. A stripline implementation similar to that for the 10 GHz device is the most likely alternative.

The $BaTiO_3$ crystal for the 50 GHz TWEOD has the following dimensions

$c \times a \times b$ (mm) $\quad 10.0 \times 2.0 \times 0.6$ (mm),

which gives it a line impedance of 50 Ω. The diffraction efficiency per watt for the 50 Ω, 50 GHz $BaTiO_3$ TWEOD is 0.05% and the diffraction angle is $\theta_B(50\ \text{GHz}) = 2.9$ mrad.

On successfully completing the set of experiments on the 10 GHz TWEOD we intend to proceed to experiment with a stripline implementation of the 50 GHz TWEOD.

§2.6 Conclusions.

We conclude that a working $BaTiO_3$ TWEOD is a theoretical possibility and that the crystals we possess exhibit an electro-optic effect, which on application of a radio frequency field will form a travelling wave phase grating.

The diffraction efficiencies and angles for a $BaTiO_3$ TWEOD are small and prompt us to search for an alternative material, possibly a ceramic or a doped ferroelectric crystal.

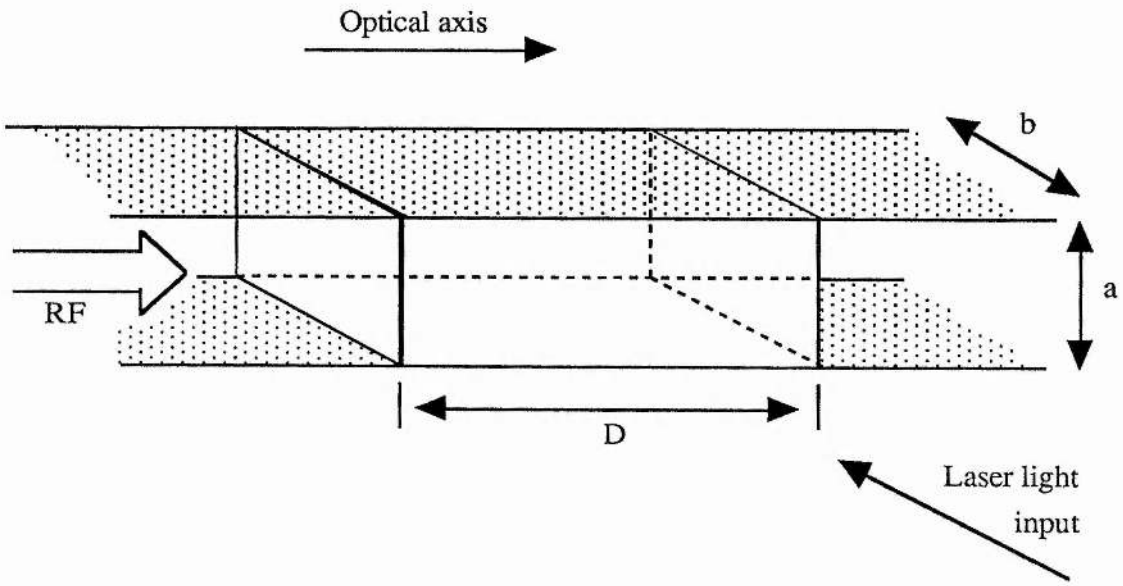

Figure 2.1. Schematic diagram of a travelling wave electro-optic diffraction device in the double stripline implementation.

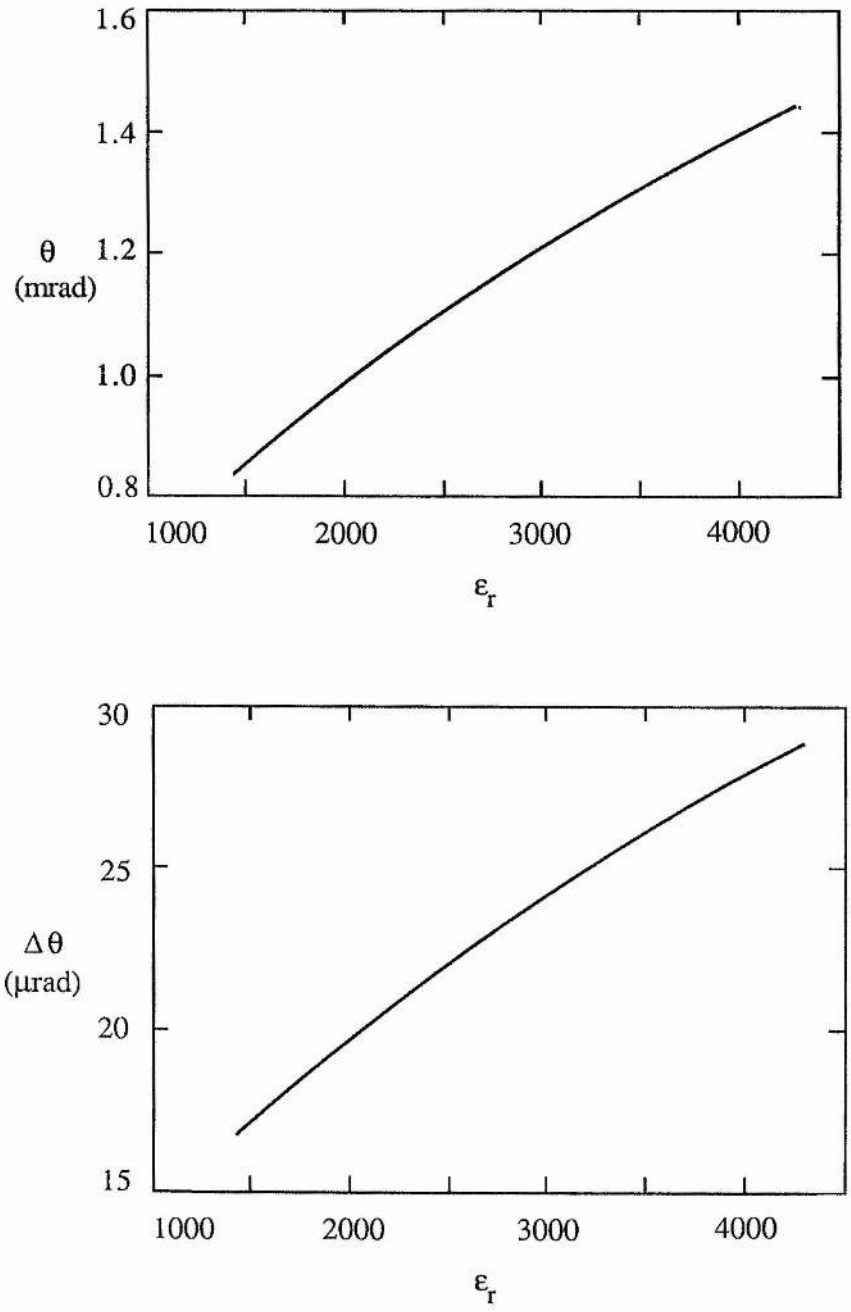

Figure 2.2. Graphs of the diffraction angle, θ, for a grating frequency of 50 GHz and the change in angle, $\Delta\theta$, for a 1 GHz shift in grating frequency from a 50 GHz centre frequency over the range of possible dielectric constants for $BaTiO_3$, ε_r. We assume that the incident radiation is a collimated HeNe laser beam.

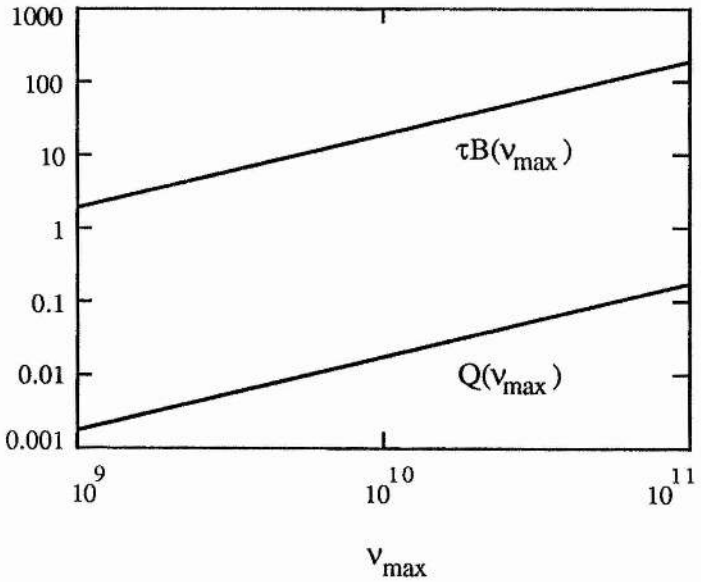

Figure 2.3. Log-log plot of Q and τB against the maximum grating frequency for a $BaTiO_3$ TWEOD illuminated by a collimated HeNe laser beam.

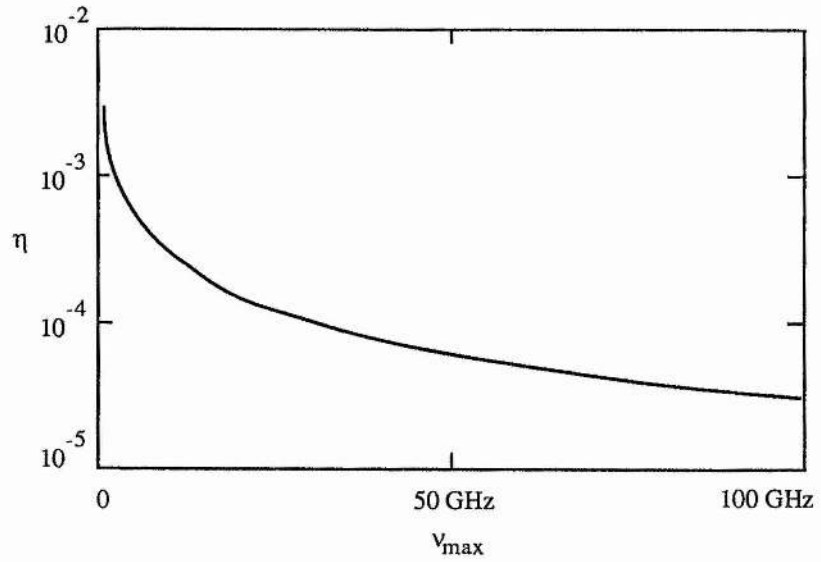

Figure 2.4. Graph of the diffraction efficiency per watt of rf power, η, against the maximum grating frequency, ν_{max}, for a $BaTiO_3$ TWEOD of dimension a = 2 mm illuminated by a collimated HeNe beam.

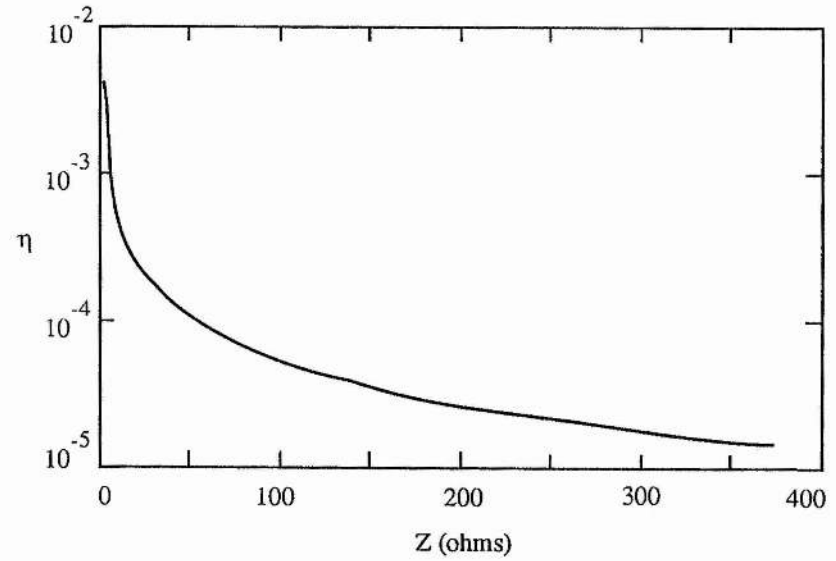

Figure 2.5. Diffraction efficiency per watt of rf power against stripline impedance for a $BaTiO_3$ TWEOD illuminated by a collimated HeNe beam.

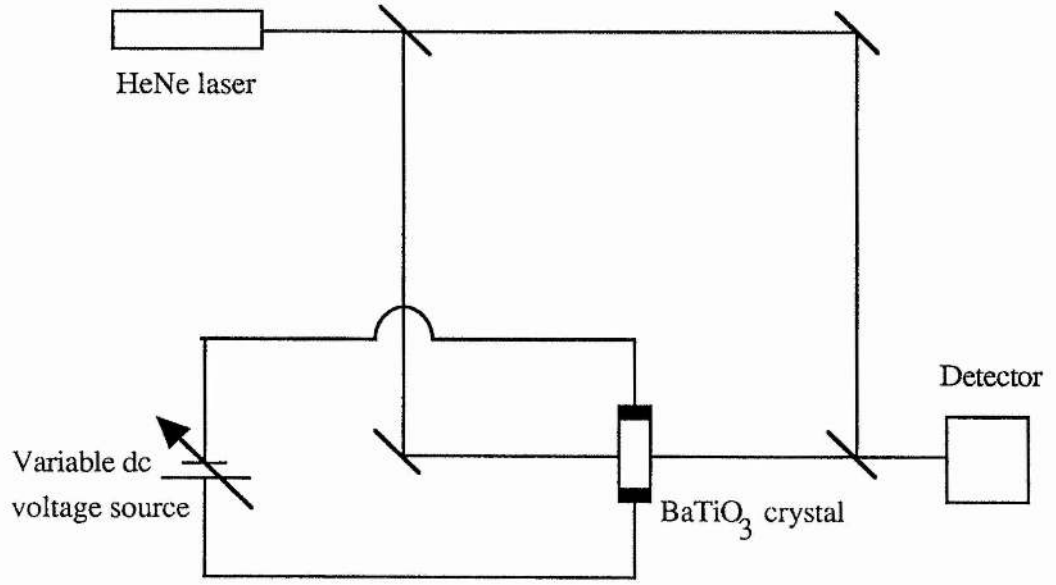

Figure 2.6. Schematic diagram of the Mach Zehnder interferometer used for measuring the electro-optic effect in a single crystal of $BaTiO_3$, where the crystal axis is taken to be into the page.

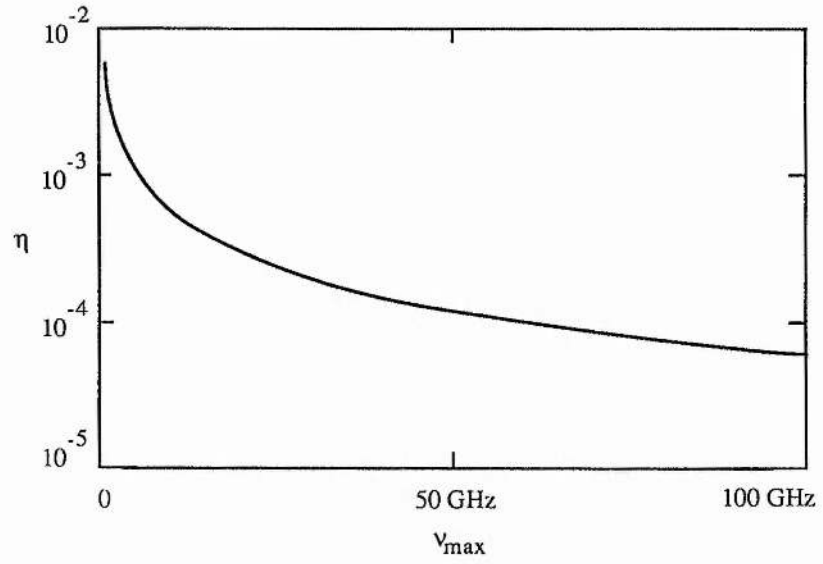

Figure 2.7a. Graph of the diffraction efficiency per watt of rf power, η, against the maximum grating frequency, ν_{max}, for a $BaTiO_3$ TWEOD, of dimension a = 2 mm, illuminated by a collimated HeNe beam, where we have used our value of 151×10^{-12} m/V for the electro-optic coefficient.

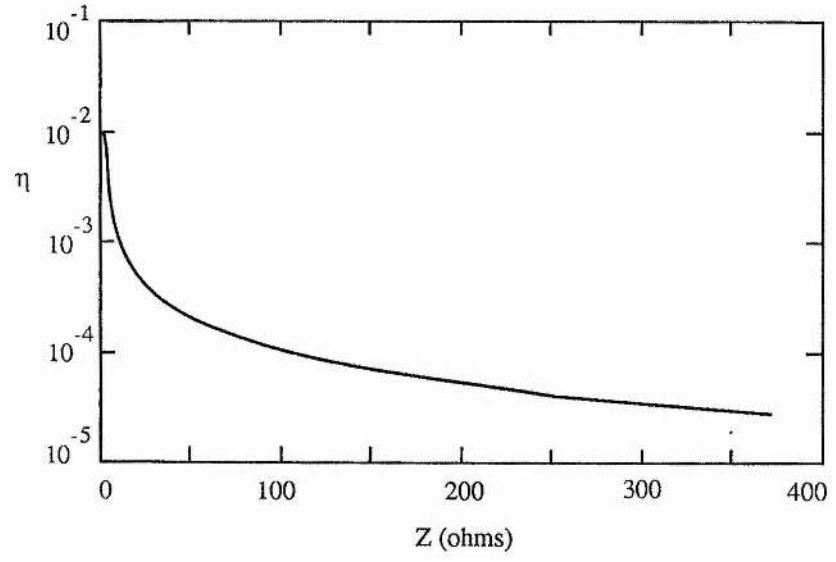

Figure 2.7b. Diffraction efficiency per watt of rf power, η, against stripline impedance for a $BaTiO_3$ TWEOD illuminated by a collimated HeNe beam, where we have used our value of 151×10^{-12} m/V for the electro-optic coefficient.

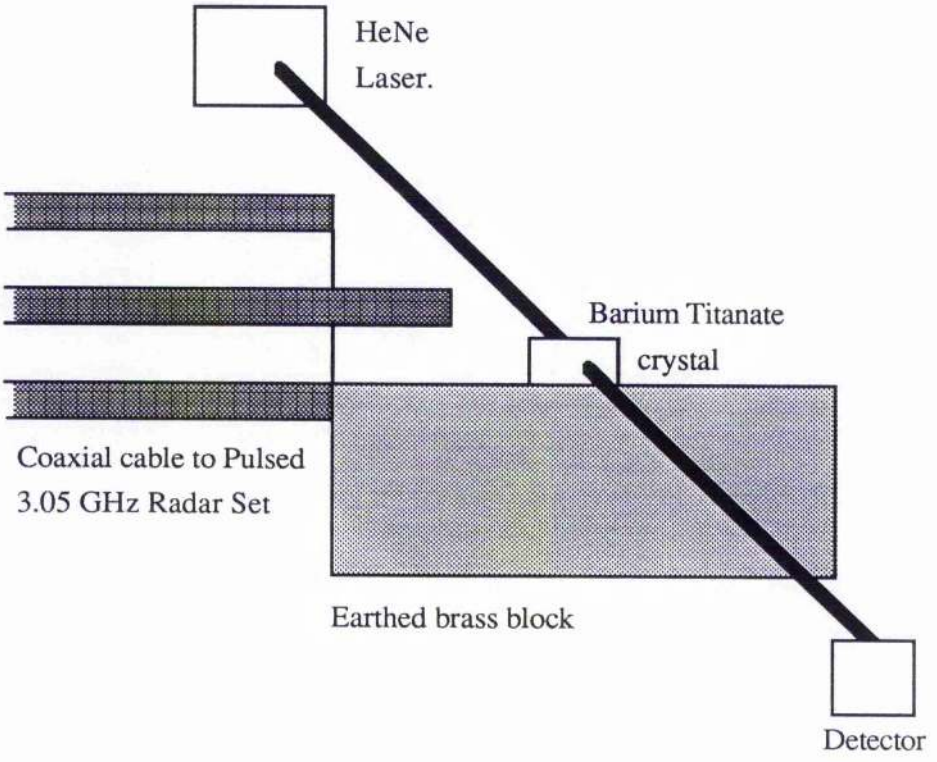

Figure 2.8. Schematic diagram of experimental set up for $BaTiO_3$ TWEOD operation with a 3.05 GHz pulsed radar set.

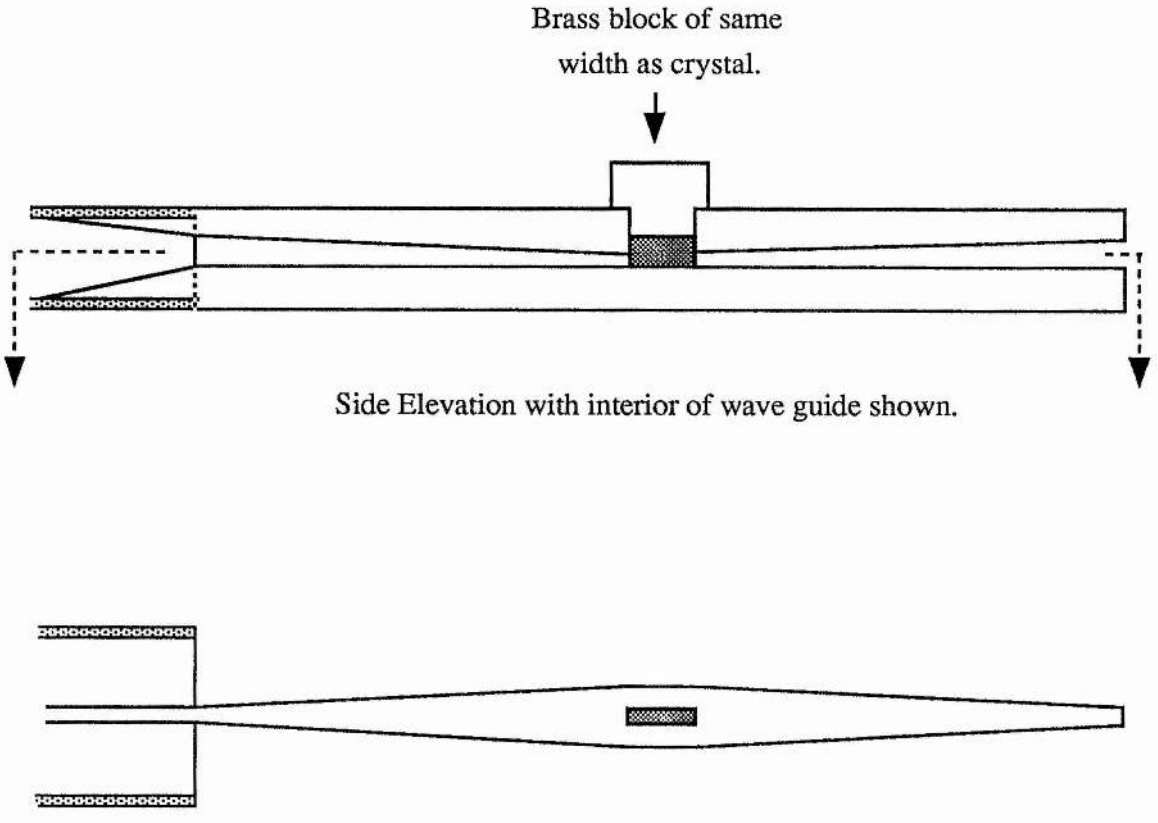

Figure 2.9. Diagram of waveguide to stripline transition and adiabatic stripline coupling for a 10 GHz $BaTiO_3$ TWEOD. The stripline and waveguide are brass. The brass block resting on top of the crystal holds a thin copper foil in place. The copper foil electrically connects the two halves of the upper stripline and is flush with the crystal's upper surface.

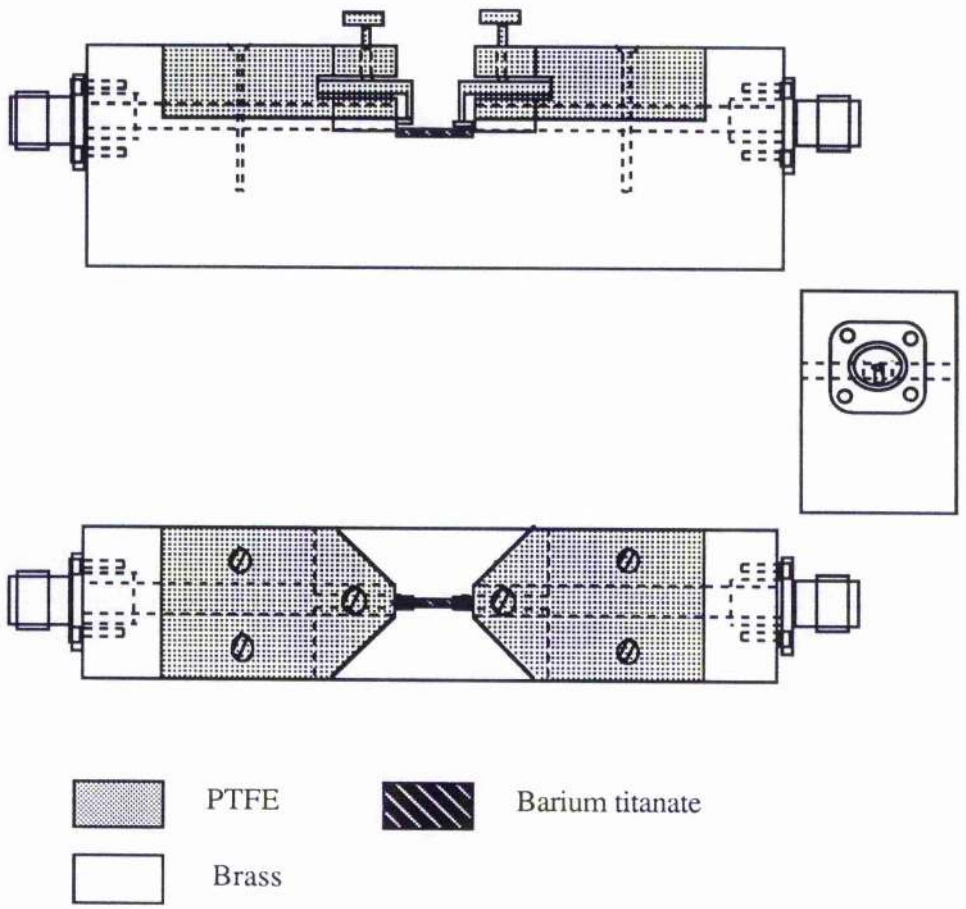

Figure 2.10. Diagram of the coaxial-stripline-coaxial transmission line mounting for a $BaTiO_3$ crystal, which was intended for use as a 50 GHz TWEOD.

§2.7 References.

[2.1] Acousto-Optic Signal Processing - Theory and Application. Ed: N J Berg and J N Lee. Marcel Dekker Inc. (New York) 1983.

[2.2] 3 GHz Bandwidth Bragg Cells. J C Poncot, P Nyeki, P H Defranould and J P Huiguard. Proc. IEEE Ultrasonics Symposium 1987. page 501-3. 1987.

[2.3] Quantum Electronics (3rd Ed.). A Yariv. John Wiley and Sons (Int). 1989.

[2.4] The Dielectric Behaviour of $BaTiO_3$ Single-Domain Crystal. W J Merz. Phys. Rev. **75** page 687. 1949.

[2.5] Radiofrequency Analysis Using Optical Signal Processing. Ph.D Thesis. W N Dawber. Uni. of St. Andrews, Fife, Scotland. 1991.

[2.6] Acousto-Optics. J Sapriel. John Wiley and Sons (Int.) 1979.

[2.7] Advanced Engineering Mathematics. 6Ed. E Kreyszig. John Wiley and Sons (Int.). 1989.

[2.8] The Physics of Transmission Lines at High and Very High Frequencies. P Grivet. Academic Press (London). 1970.

[2.9] Theoretical Model for Explaining the Ferroelectric Effect in Barium Titanate. W P Mason and B T Matthias. Phys. Rev. **74**(11) page 1622. 1948.

[2.10] Optics. E. Hecht and A. Zajac. Addison-Wesley Pub. Co. Inc. 1977.

[2.11] Lasers. A E Siegman.

University Science Books, Mill Valley, California, USA. (1986).

Chapter 3.

Transmission Diffraction Gratings based on Laser Media.

§3.1 Introduction.

The acoustic and electrical creation of ephemeral travelling and standing wave diffraction gratings is well documented [3.1, 3.2, 3.3, 3.4]. The nature of the dispersion in a laser medium, close to the laser transition frequency, on pumping the laser transition is also well documented [3.5, 3.6]. We wish to demonstrate that it is possible to use the anomalous dispersion round a pumped laser transition to form phase gratings.

The two methods of imposing rf information onto a grating based on the anomalous dispersion of a laser medium are; (a) frequency modulation of the pump radiation in the absence of cavity mirrors and (b) modulation of population inversion for a laser within a cavity. Both of these methods use a second laser to interrogate the grating at a frequency displaced from the centre frequency of the transition by half the transition bandwidth so as to achieve the maximum refractive index differential.

§3.2 Theory for Gratings based on Laser Media.

A well known feature of laser media is their anomalous dispersion around resonant transitions (see figure 3.1). The expression given by Yariv [3.5] for the refractive index round the transition is

$$n(\nu) = 1 + \frac{A_{21}c^3}{32\pi^3\nu^3} \frac{(\nu-\nu_{12})}{(\nu-\nu_{12})^2+(\Delta\nu/2)^2} \overline{N}, \qquad (3.1)$$

where; A_{21} is the spontaneous emission probability for the transition, $\Delta\nu$ is the transition bandwidth, ν_{12} is the resonant frequency of the transition and $\overline{N}$ is the population

inversion between the upper and lower laser states. The population inversion is given by the following expression;

$$\overline{N} = \overline{N}_o/(1+I_\nu/I_\nu^{(s)}), \tag{3.2}$$

where I_ν is the intensity at frequency ν and $I_\nu^{(s)}$ is the saturation intensity at that frequency.

The maximum inversion that can be obtained per unit volume of the laser medium is

$$\overline{N}_o = \left[1 + \frac{g_2 A_{21}}{g_1 \gamma_1}\right]\frac{\xi_2}{\gamma_2} - \frac{g_2 \xi_1}{g_1 \gamma_1}, \tag{3.3}$$

where: the quantities g_2 and g_1 are the degeneracies of the upper and lower laser states, respectively; the parameters ξ_2 and ξ_1 are the rates of photon absorption by the upper and lower laser states and the parameters γ_2 and γ_1 are the rates of population loss from the upper and lower laser states, respectively, excluding lasing and spontaneous emission from the upper level to the lower.

The above statement (3.3) can be simplified on assuming that the lower laser state is not pumped and that it decays faster than the spontaneous emission rate for the transition;

$$\overline{N}_o = \frac{\xi_2}{\gamma_2}. \tag{3.4}$$

On assuming no laser action in the medium, the equation (3.4) provides the upper limit to the modulation frequency for the device by way of the upper state decay rate. The rate of change of the refractive index with respect to time is thus given by the equation;

$$\frac{\partial n(\nu)}{\partial t} = \frac{A_{21} c^3}{32\pi^3 \nu^3} \frac{(\nu-\nu_{12})}{(\nu-\nu_{12})^2+(\Delta\nu/2)^2} \frac{1}{\gamma_2}\left[\frac{\partial \xi_2(t)}{\partial t}\right]. \tag{3.5}$$

The expression (3.5) is the rate of change of the refractive index at frequency ν due to the changes in the pump rate, $\xi_2(t)$, where the changes in the pump rate occur at rates slower than the rate of spontaneous emission, A_{21}. When the laser gain medium is placed in a resonant cavity, the fastest the medium can respond to pump rate modulation is the cavity decay time.

Thus the grating medium has grating frequency limitations related to the transition decay time or a cavity decay time depending on the implementation of the grating.

In all implementations, the grating is taken to have a spacing of a which, under the Bragg phase match condition [3.1, 3.2], deflects a portion of an incoming interrogating beam of wavelength λ_i by a diffraction angle of θ which is given by,

$$\sin\theta = \lambda_i/2a. \tag{3.6}$$

Equation (3.6) can be differentiated to obtain the variation in θ with respect to a

$$\frac{\partial\theta}{\partial a} = -\frac{\lambda_i/2a^2}{\left[1-(\lambda_i/2a)^2\right]^{1/2}}, \tag{3.7}$$

which, if we know the grating spacing function in terms of an imposed radio frequency, yields the variation in diffraction angle with radio frequency.

The gratings created by variations in the anomalous dispersion of a laser medium can be described in terms of the theory given in chapter 1. To adapt the theory given above to fit the formalism of chapter 1 the grating spacing is expressed as a wave number and the

refractive index change as a dielectric coupling coefficient:-

$$\frac{2\pi\alpha}{\Lambda} = |\mathbf{k}_g| = \frac{2\pi}{\boldsymbol{a}} \tag{3.8}$$

and

$$\chi_{12}^{(\alpha)} = \frac{\omega}{4} \langle 1|2n\varepsilon_o \Delta n^{(\alpha)}|2\rangle$$

$$= \frac{2\pi}{\lambda_o}\left[\frac{A_{21}c^3}{32\pi^3\nu^3}\,\frac{(\nu-\nu_{12})}{(\nu-\nu_{12})^2+(\Delta\nu/2)^2}\right]\left[\,\overline{N}(\boldsymbol{a}) - \overline{N}(\boldsymbol{a}/2)\right]. \tag{3.9}$$

In equation (3.9) the quantities $\overline{N}(\boldsymbol{a})$ and $\overline{N}(\boldsymbol{a}/2)$ are the population inversion at its lowest and highest points in the grating, respectively. The value of the dielectric coupling coefficient is thus related to the pump rate to, and the depletion rate from, the upper laser state. The diffraction efficiency (1.34),

$$\frac{I_{out}}{I_{in}} = \frac{|\chi_{12}^{(\alpha)}|^2}{\gamma^2}\,\sin^2\gamma z\,, \tag{3.10}$$

is therefore related to the coherence and intensity of the pump beam that forms the grating.

We require that the grating operates in the Bragg regime and therefore that the grating spacing is greater than the interrogating wavelength. The wavelength of the pump beam is generally shorter than that of the laser transition. Thus to comply with the Bragg condition (3.6) we require that our methods for grating creation are independent of the pump wavelength.

§3.3 Possible Implementations.

We now suggest two methods of creating a grating pattern in a laser gain medium due to the dispersion associated with the laser transition. There are at least two basic methods of creating such a grating. One is to pump with two mutually coherent beams at an angle to each other to create an angle-dependent grating. The other is to place the grating medium in a cavity to make it lase and use the cavity standing wave to form the grating. An rf modulation can be imposed on both these gratings by frequency modulation of the pump beam and modulation of the cavity length, respectively.

§3.3.1 Pump Field Modulation Implementations.

All pump field modulation implementations rely on the interference between two mutually coherent pump beams in the plane of the grating medium. The two beams are incident on the grating plane at angles of plus and minus ψ to the normal (see figure 3.2). This grating is then interrogated by a beam normal to the grating plane with frequency ν, which is in the vicinity of the laser transition frequency ν_{12}.

The grating created by this method has spacing

$$a = \frac{\lambda_p}{2\sin\psi}, \tag{3.11}$$

where λ_p is the wavelength of the pump radiation.

To impose the rf on the pump beam we propose to either modulate the pump laser cavity by way of an electro-optic cell in the pump beam. The imposed frequency will shift the frequency of the pump beam and thus the spacing of the grating.

When there is no modulation a first order diffraction pattern occurs at an angle of θ to the normal, which is related to the pump beam angle and frequency by

$$\sin\theta = \frac{\lambda_i \nu_p}{c} \sin\psi. \tag{3.12}$$

In equation (3.12) ν_p is the pump frequency and c is the speed of light at ν_p in the grating medium. The equation (3.12) provides a lower limit on the angle ψ for given ν_p and λ_i

$$\sin\psi \geq \frac{c}{\lambda_i \nu_p}. \tag{3.13}$$

The lower limit for the angle ψ (3.13) is equivalent to stating that the minimum grating separation is equal to half the incident wavelength. For our example, flourescien disodium dye, the maximum angle is $\psi_{max} = 33.6°$ from the normal.

The derivative of (3.7) with respect to the pump frequency is

$$\frac{\partial\theta}{\partial\nu_p} = \frac{\frac{\lambda_i}{c}\sin\psi}{\left[1 - \left[\frac{\lambda_i \nu_p}{c}\sin\psi\right]^2\right]^{1/2}}. \tag{3.14}$$

Given that the modulation on the pump frequency, $\delta\nu_p$, is far smaller than the pump frequency, $\delta\nu_p \ll \nu_p$, and that the change in diffraction angle due to the modulation, $\delta\theta(\delta\nu_p)$, is far smaller than the original diffraction angle, $\delta\theta(\delta\nu_p) \ll \theta$, the equation (3.14) yields an approximate expression for the diffraction angle due to the modulation frequency

$$\delta\theta(\psi,\delta\nu_p) = \frac{\frac{\lambda_i}{c}\sin\psi}{\left[1 - \left[\frac{\lambda_i \nu_p}{c}\sin\psi\right]^2\right]^{1/2}}\ \delta\nu_p. \tag{3.15}$$

It can be seen from figure 3.3 that the maximum diffraction angle per unit frequency occurs at the point where the angle ψ is maximised in compliance with equation (3.13). In figure 3.4 the modulation frequency required to obtain a one milli-radian change in the diffraction angle is plotted against the pump angle ψ. Both the angular response per gigahertz and the maximisation condition on the grating angle ψ are symmetrical about the point $\psi=\pi/2$, which means that the grating can be interrogated from either the pumped side or the other side of the medium.

The above describes one of the possible basic implementations of a phase grating in a non-linear medium that may be used for spectrum analysis. We now proceed to describe another basic implementation.

§3.3.2 Cavity Modulation Implementations.

All implementations based in a modulated cavity use the cavity standing-wave's interaction with a laser gain medium to form a phase grating. In all cases the interrogating beam shall be taken to illuminate the cavity transversely so different grating frequencies result in different diffraction angles (see figure 3.5).

The grating seen by the interrogating beam has a spacing given by

$$a = \frac{c}{2\nu_g} \tag{3.16}$$

where ν_g is the frequency of the cavity radiation responsible for the grating. The grating frequency ν_g need not be the frequency of the laser transition of the pump beam; it needs only to affect the population of the upper and lower states of the transition. Thus, the grating frequency can be a part of the pump system or part of the de-excitation system (see figure 3.6).

We now define the form of the variation in the grating spacing in terms of the rf signal. For convenience it is assumed that the rf signal has the form of a sine wave of single frequency ω_{rf} which on application to an intra-cavity modulator will result in a change in the cavity's optical length;

$$\Delta L(E_{rf},\omega_{rf}) = \Delta L_o(E_{rf})\sin(\omega_{rf}t). \tag{3.17}$$

The change in grating spacing results from the change in cavity length and is of the form

$$\Delta a = \frac{c}{2\nu_g}\frac{\Delta L}{L}, \tag{3.18}$$

where L is the unperturbed cavity length. The resulting change in diffraction angle is obtained on substituting (3.17) and (3.18) into equation (3.7) to obtain

$$\delta\theta = -\frac{\lambda_i\nu_g/2c}{\left[1-(\lambda_i\nu_g/c)^2\right]^{1/2}}\frac{\Delta L_o(E_{rf})\sin(\omega_{rf}t)}{L}. \tag{3.19}$$

Modulation of the cavity length causes a travelling wave grating to be superimposed on the cavity standing wave grating. Thus, we have a method for imposing frequency information as well as directional information on the emerging diffracted light.

There are various possible methods of imposing the frequency information on the cavity standing wave. These methods include (a) rf modulating the cavity length directly with an electro-optic cell to modulate the grating frequency; (b) rf modulating a seeding laser tuned to operate at a frequency between the grating laser's centre frequency and its half height frequency, thus creating a slow moving travelling wave which will affect the dispersion seen by the interrogating laser beam as it passes through the grating medium; (c) rf

modulation of a coherent microwave source in an external micro-wave cavity to switch an "inversionless" laser on and off [3.8, 3.9].

§3.4 Conclusions.

We conclude that transverse interrogation of a grating formed in a laser medium is possible. We also conclude that such a grating can be rf modulated in such a way as to create a frequency dependent grating or an amplitude dependent grating depending on whether a pump field or cavity modulation is being employed.

Both the pump field modulation and the cavity modulation implementations are capable of responding to the change in radio-frequency at a rate equal to the decay time of the upper laser state. Thus, the upper response time of such a device is equal to the stimulated emission time for the laser transition.

The response time of the grating is inversely proportional to the transition bandwidth which means that for an increase in speed there is a corresponding decrease in the variation in the dispersion over a given rf bandwidth.

Thus we have in the pump beam modulation implementation with a dye laser providing the laser medium, a possible ultra-fast (1-100 GHz) spectrum analyser and we have a possible high repetition rate beam scanner with a slower response time in the form of the cavity modulation implementation, using microwave de-excitation for the lower laser state.

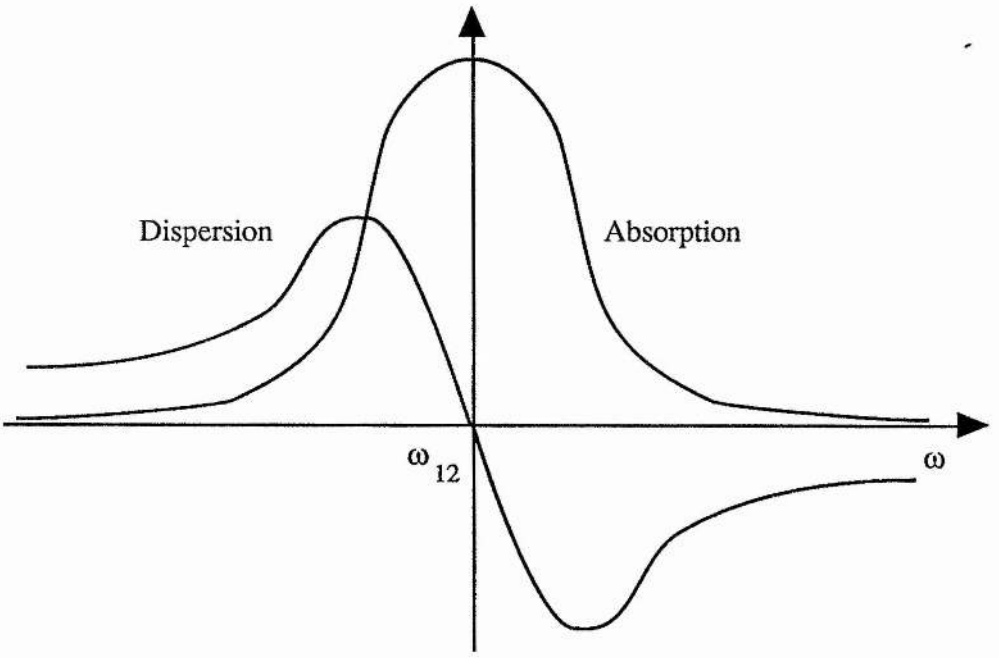

Figure 3.1. Graph of absorption and dispersion round a laser transition.

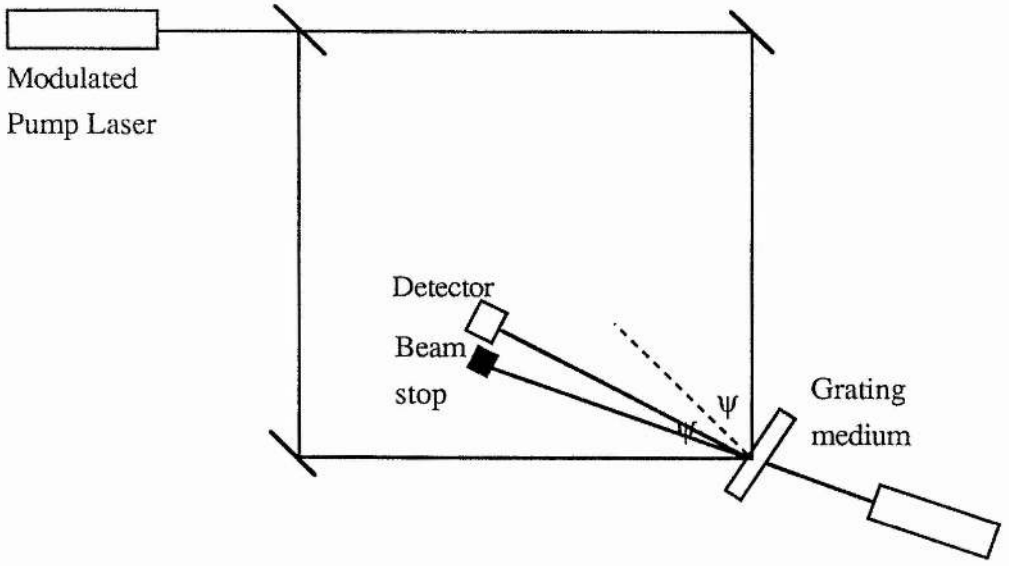

Figure 3.2. Diagram of pump beam modulation implementation of a diffraction grating in a non-linear medium.

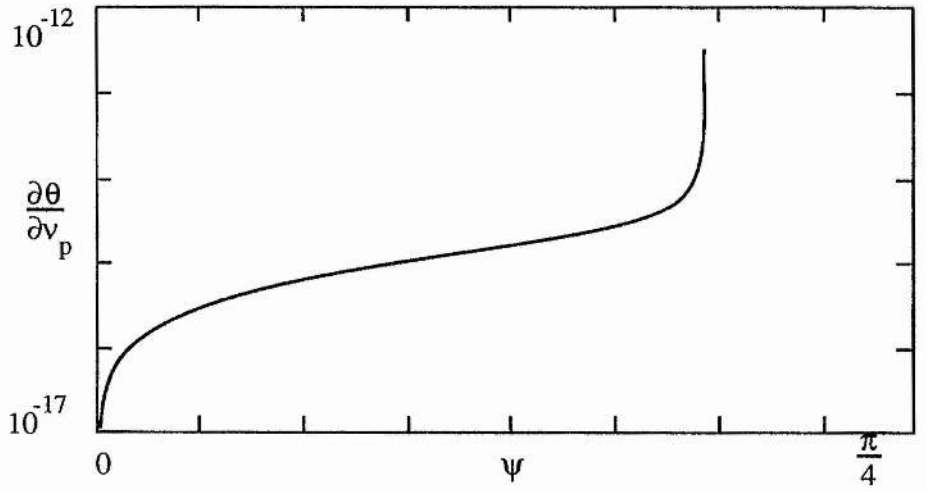

Figure 3.3. Graph of the variation in diffraction angle, θ, with respect to pump frequency, ν_p (i.e. rf pump modulation) against angle of pump beam incidence, ψ, for a fluorescien disodium grating medium.

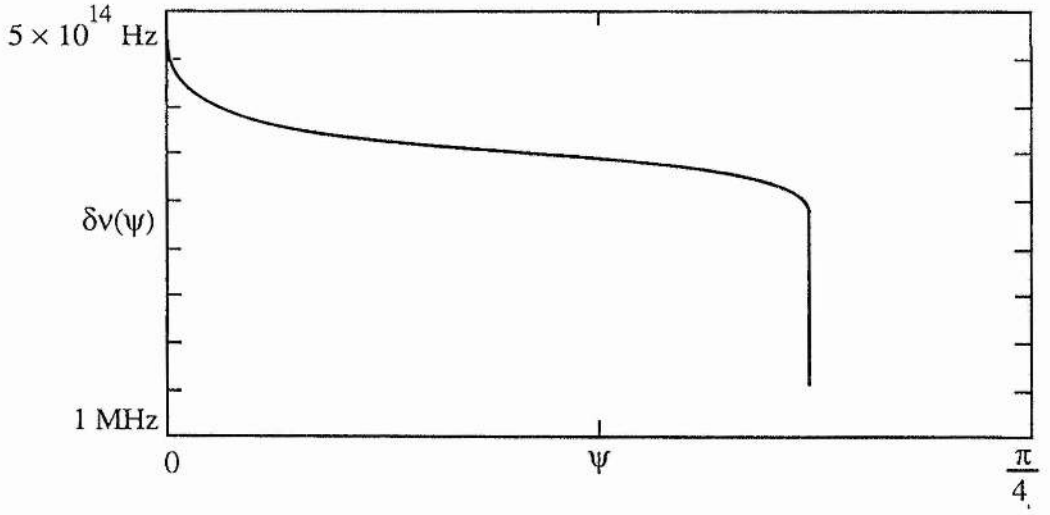

Figure 3.4. Graph of the modulation frequency required to diffract the interrogating beam by 1 milli-radian against angle of pump beam incidence, ψ, for a fluorescien disodium grating medium.

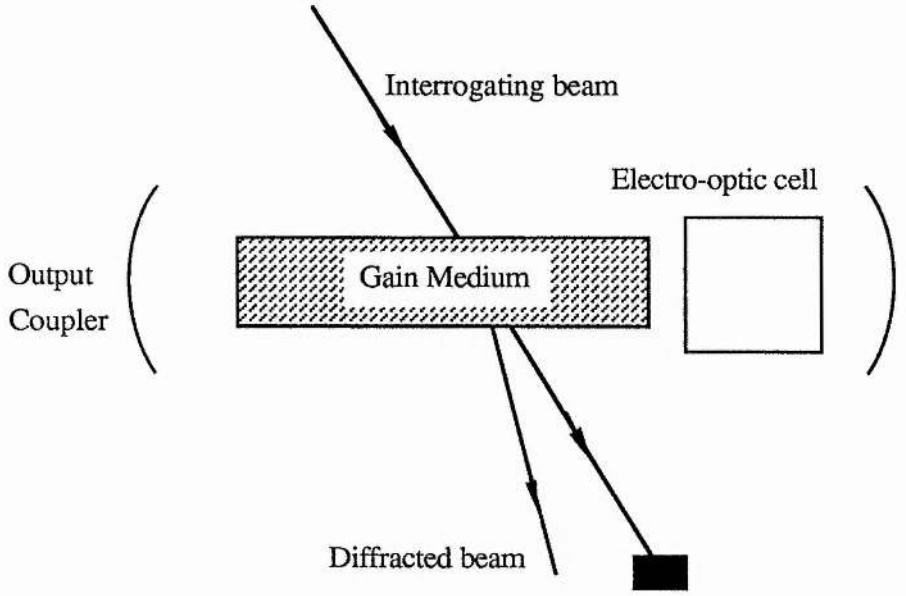

Figure 3.5. Diagram of a basic cavity modulation implementation.

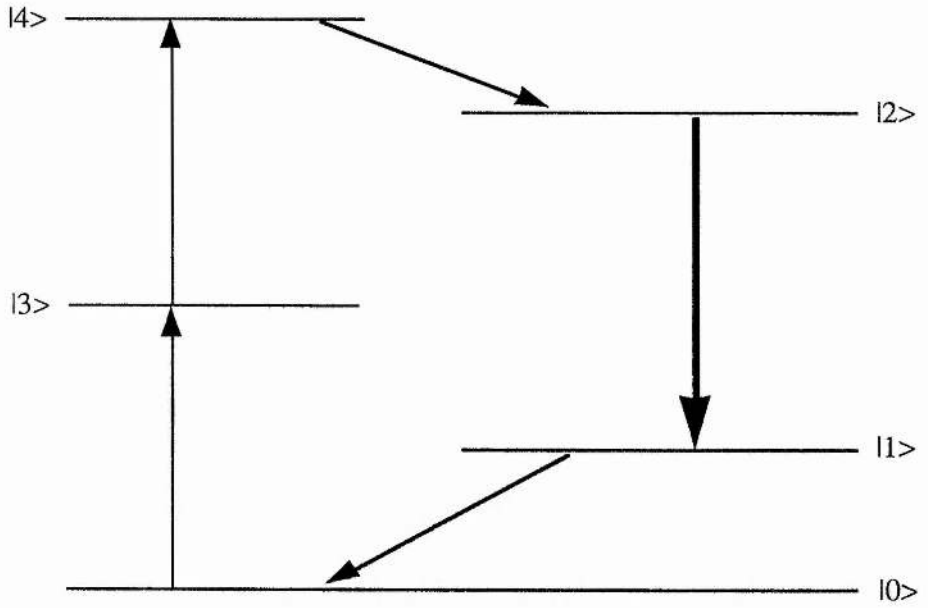

Figure 3.6. Energy level diagram showing possible points for microwave modulation. The pump system can be cavity modulated on either the 0-3 transition or the 3-4 transition. The decay transition 1-0 can also be modulated given that level 1 is metastable without a microwave perturbation to cause stimulated de-excitation.

§3.5 References.

[3.1] Acousto-Optic Signal Processing - Theory and Application. Ed: N J Berg and J N Lee. Marcel Dekker Inc. (New York) 1983.

[3.2] Acousto-Optic Signal Processing: Fundamentals and Application. P K Das and C M DeCusatis. Artech House (London). 1991.

[3.3] Handbook of Microwave and Optical Components (Vol. 4). K Chang (Ed.) Wiley Interscience, New York. (1991).

[3.4] Radiofrequency Analysis Using Optical Signal Processing (Ph.D. Thesis). W N Dawber. Uni. of St. Andrews, Scotland. 1991.

[3.5] Quantum Electronics (3rd Ed.). A Yariv. John Wiley and Sons (Int). 1989.

[3.6] Lasers. A E Siegman. University Science Books, Mill Valley, California, USA. (1986).

[3.7] Light. R W Ditchburn. Blackie and Sons Limited (Glasgow). 1963.

[3.8] Degenerate Quantum-Beat Laser: Lasing without Inversion without Lasing. M O Scully and Shi-Yao Zhu. Phys. Rev. Lett. **62**(24) 2813-6. 1989.

[3.9] Nonlinear theory of the degenerate quantum beat laser: Lasing without Inversion. Shi-Yao Zhu. Phys. Rev. **42**(9) 5537-43. 1990.

Chapter 4.

Optical Effects of Stress in Glass.

§4.1 Introduction.

The fact that glass becomes birefringent under stress has been known since the manufacture of optical components began. Most uses of glass to date have demanded optical uniformity to a greater or lesser degree and thus work has been directed primarily towards annealing techniques capable of removing stress-induced birefringences [4.1, 4.2]. Recently, however, interest in the stress induced birefringences themselves has grown. The main areas of interest being acousto-optics, stress induced birefringence in optical fibres and birefringence due to heat induced stresses in laser glasses [4.3, 4.4].

The use of uniformly stressed birefringent glass for the acousto-optic interaction presents itself as a viable alternative to the current acousto-optic technology. The main limitations of the current acousto-optic technology is the size and acoustic attenuation of birefringent crystals available [4.5] along with the steep increase in their price with size. The use of glasses in acousto-optics is minimal because they are currently only thought of as a group of optically isotropic materials and therefore as low Q materials. Glasses have two advantage over crystals, which are that large optically uniform blocks of glass are easier to produce, larger and cheaper than optically uniform single crystals (lithium niobate; for example), and that the coefficient of acoustic attenuation for some glasses is lower than in the crystals they would replace.

In this chapter we shall give an outline of the acousto-optic effect in an isotropic medium and a treatment of the acousto-optic effect in uniformly stressed birefringent glass.

§4.2 The Acousto-Optic Effect in an Isotropic Medium.

The acousto-optic effect in the Bragg regime [4.6, 4.7] is described by the general theory given in chapter 1.

To apply the general theory of chapter 1 to the special case of the acousto-optic interaction an expression for the dielectric coupling constant (1.23) in terms of the acoustic strain tensor is required. The strain tensor associated with an acoustic wave of amplitude vector, **u**, is $\partial u_k/\partial x_l$. The change in the refractive index due to the strain is related to the strain tensor by way of the elasto-optic tensor p_{ijkl} [4.8]:

$$\Delta\left[\frac{1}{\varepsilon_{ij}}\right] = p_{ijkl}\frac{\partial u_k}{\partial x_l}. \tag{4.1}$$

If the perturbation given by equation (4.1) is assumed to be small in comparison with the refractive index, then the perturbation tensor can be expressed as,

$$\Delta\varepsilon_{ij}^{(\alpha)} = -\varepsilon_o|\varepsilon_r|^2 p_{ijkl}.u_{kll}^{(\alpha)}, \tag{4.2}$$

where $|\varepsilon_r|^2$ is the contraction of the dielectric tensor with itself over the polarisation of the incident light and the superscript α denotes the order in the amplitude Fourier series, as in chapter 1.†

Thus, the coupling constant between the incident and diffracted optical radiation $\chi_{12}^{(\alpha)}$ has the form

$$\chi_{12}^{(\alpha)} = -\frac{\omega\varepsilon_o|\varepsilon_r|^2}{4}\langle 1|\, p_{ijkl}.u_{kll}^{(\alpha)}\,|2\rangle, \tag{4.3}$$

† Note that in (4.2) we have employed the bar notation for partial differentiation.

which on reference to equation (1.18) can be written as follows

$$\chi_{12}^{(\alpha)} = -\frac{\omega}{2}\sqrt{\mu_o \varepsilon_o |\varepsilon_r|^3}\left[p_{ijkl}\, u_{kll}^{(\alpha)}\right]_c . \tag{4.4}$$

The subscript c denotes that the tensor has been contracted over the polarisations of the incident and diffracted radiations.

The equation (4.4) can be written in the more accessible form

$$\chi_{12}^{(\alpha)} = -\frac{\pi}{\lambda_o} n^3\, p_c S\,, \tag{4.5}$$

where the elasto-optic tensor and the strain, S, are contracted over each other and the optical polarisations of the input and output optical beams.

The expression for the diffraction efficiency in the Bragg regime is obtained by substituting from equation (4.5) into equation (1.34):

$$\frac{I_{out}}{I_{in}} = \frac{\left[\frac{1}{\cos\theta}\frac{\pi}{\lambda_o} n^3\, p_c S\right]^2}{\left[\frac{\Delta\beta}{2}\right]^2 + \left[\frac{1}{\cos\theta}\frac{\pi}{\lambda_o} n^3\, p_c S\right]^2} \times \sin^2\left[\left[\left[\frac{\Delta\beta}{2}\right]^2 + \left[\frac{1}{\cos\theta}\frac{\pi}{\lambda_o} n^3\, p_c S\right]^2\right]^{1/2} z\right] \tag{4.6}$$

where z is the thickness of the acousto-optic interaction region.

When the phase factor, $\Delta\beta$, is zero the diffraction efficiency is

$$\frac{I_{out}}{I_{in}} = \sin^2\left[\frac{1}{\cos\theta}\frac{\pi}{\lambda_o} n^3 p_c S\ z\right], \tag{4.7}$$

which, on taking the first term of the MacLaurin series [4.9] to be approximate to the sine function in (4.7), can be expressed as a diffraction efficiency per watt of acoustic power :

$$\eta = \frac{I_{out}}{I_{in}}\frac{1}{P_{ac}} = \left[\frac{\pi}{\lambda_o} n^3 p_c\right]^2 \frac{2}{\rho v_a^3}\frac{z^2}{A\cos\theta^2}. \tag{4.8}$$

In (4.8) the strain term S has been replaced with the acoustic power:

$$P = \frac{1}{2}\rho v_a^3 A S^2, \tag{4.9}$$

where ρ is the density of the acoustic medium, v_a is the speed of sound in that medium and A is the cross-sectional area of the acoustic beam.

The other parameters of an acousto-optic Bragg diffractor follow the same pattern as that for travelling wave electro-optic diffractors. The Q (1.1) for an acousto-optic Bragg cell is

$$Q = 2\pi\lambda_o L\left[\frac{\nu_{rf}}{v_a}\right]^2 \tag{4.10}$$

and the time-bandwidth product (1.2) is

$$\tau B = \frac{D}{v_a}\Delta f. \tag{4.11}$$

In the acousto-optic case, τB does not necessarily approximate to the number of lines in the grating because the bandwidth of an acousto-optic device is not an indication of the upper operating frequency, but rather the device's operating frequency range around some centre frequency. Thus, acousto-optic diffractors are unlike the electro-optic diffractor, where the bandwidth is taken to be the upper frequency limit of the device since its lowest operating frequency is comparatively small.

In this section a brief outline of the theory behind the acousto-optic interaction in an isotropic medium has been given. It will provide a basis for the description of the device examined in the rest of this chapter and for the devices described in the following two chapters.

§4.3 Theory for Acoustic Waves in Birefringent Glass.

So far we have only dealt with the acousto-optic effect in isotropic media, which for our purposes is an annealed glass. The advantages of using glass as opposed to crystals for Bragg cell manufacture are size and cost (i.e. one can produce a piece of optical quality glass many times the size of an optical quality $LiNbO_3$ crystal with a fraction of the acoustic loss for a fraction of the cost).

The main advantage that crystal Bragg cells (normally $LiNbO_3$) have over glass ones is their large birefringence. The effect of the birefringence is to give the crystal Bragg cell a larger single orientation bandwidth and a larger change in diffraction angle per unit frequency than their glass counterparts. The effect of the birefringence on the performance of acousto-optic Bragg cells can be explained in terms of the phase matching condition (1.3)

$$\mathbf{k}_{out} - \mathbf{k}_{in} \pm \mathbf{k}_g = 0, \tag{4.12}$$

which can be split into its parallel and perpendicular components (see figure 4.1) to give the simultaneous equations

$$\nu n_2 \sin\theta_2 - \nu n_1 \sin\theta_1 = \frac{c\nu_{rf}}{v_a} \tag{4.13a}$$

and

$$n_2 \cos\theta_2 - n_1 \cos\theta_1 = 0. \tag{4.13b}$$

On solving the equation (4.13), the following expressions for the angle of incidence and diffraction are derived [4.8]:

$$\sin\theta_1 = -\frac{\nu_{rf}\lambda_o}{2n_1 v_a}\left[1 + \left[\frac{v_a}{\nu_{rf}\lambda_o}\right]^2 \left[n_1^2 - n_2^2\right]\right], \tag{4.14a}$$

and

$$\sin\theta_2 = \frac{\nu_{rf}\lambda_o}{2n_2 v_a}\left[1 - \left[\frac{v_a}{\nu_{rf}\lambda_o}\right]^2 \left[n_1^2 - n_2^2\right]\right]. \tag{4.14b}$$

The values for the angle of incidence and the corresponding diffraction angles are plotted against the normalised acoustic grating wavelength for a $LiNbO_3$ Bragg cell alongside the angles for a Bragg cell of isotropic material with the average refractive index in figure 4.2.

One solution to the problem of size and cost of crystals for Bragg cell manufacture is to improve the crystal growth techniques. The other is to produce glass of optical quality with a uniform birefringence built in.

To produce birefringent glass a piece of previously annealed glass has an external strain imposed upon it and is then heated to the glass' transformation point [4.10], which is a lower temperature than the annealing point [4.10]. At the transformation point the imposed

stresses become permanent to the glass structure and can thus be held indefinitely as a strain pattern.

The applied stress results in a strain , $S_{33}^{(0)}$, in the glass which is held in the glass after cooling past its transformation point. Thus the strain is "frozen in" and the glass will have a refractive index given by

$$\frac{1}{n^2(\zeta)} = \left[\frac{1}{n^2}+p_{1133}S_{33}^{(0)}\right]\sin^2\zeta + \left[\frac{1}{n^2}+p_{2233}S_{33}^{(0)}\right]\sin^2\zeta + \left[\frac{1}{n^2} + p_{3333}S_{33}^{(0)}\right]\cos^2\zeta \qquad (4.15)$$

where ζ is the angle of the incident radiation's polarisation to the optical axis as defined by the strain and n is the refractive index of the unstressed glass. The above expression can be rewritten in the familiar form of the polarisation dependent refractive index of a uniaxial crystal:

$$\frac{1}{n^2(\zeta)} = \frac{\cos^2\zeta}{n_e^2} + \frac{\sin^2\zeta}{n_o^2}, \qquad (4.16)$$

where $1/n_e^2 = 1/n^2 + p_{3333}S_{33}^{(0)}$ and $1/n_o^2 = 1/n^2+p_{1133}S_{33}^{(0)} = 1/n^2+p_{2233}S_{33}^{(0)}$.

The index ellipsoid for such a medium is shown in figure 4.3. For a general strain the index ellipsoid in an isotropic material can be written in matrix form as

$$\begin{bmatrix}D_1D_1\\D_2D_2\\D_3D_3\end{bmatrix}\cdot\begin{bmatrix}p_{1111} & p_{1122} & p_{1122}\\ p_{1122} & p_{1111} & p_{1122}\\ p_{1122} & p_{1122} & p_{1111}\end{bmatrix}\cdot\begin{bmatrix}S_{11}\\S_{22}\\S_{33}\end{bmatrix} + \frac{1}{n_o^2}\left[D_1^2+D_2^2+D_3^2\right]$$

$$+\begin{bmatrix}D_2D_3\\D_1D_3\\D_1D_2\end{bmatrix}\cdot\begin{bmatrix}\frac{1}{2}(p_{1111}-p_{1122}) & 0 & 0\\ 0 & \frac{1}{2}(p_{1111}-p_{1122}) & 0\\ 0 & 0 & \frac{1}{2}(p_{1111}-p_{1122})\end{bmatrix}\cdot\begin{bmatrix}S_{23}\\S_{13}\\S_{12}\end{bmatrix} = 1, \qquad (4.17)$$

where D_i is the normalised vector $D_i/\sqrt{(2\omega\varepsilon_o)}$.

We wish to impose a perturbation in the form of an acoustic wave on the uniaxially stressed glass. The waves have stresses associated with them, which we denote by $S_{ij}^{(\alpha)}$. These affect the polarisation and direction of propagation of radiation within the glass, which results in a relative change in the polarisation of the light on undergoing acousto-optic diffraction.

There are two distinct types of acoustic waves; (a) longitudinal acoustic wave and (b) transverse acoustic wave.

(a) Longitudinal Acoustic Waves.

In the case of longitudinal acoustic waves the maximum relative perturbation of the refractive index is achieved when the direction of propagation is along the axis corresponding to the lowest refractive index. For the sake of clarity, this direction is taken to be perpendicular to the optical axis.

On applying the acoustic strain $S_{22}^{(\alpha)}$ to the prestressed glass, the index ellipsoid becomes

$$\left[\frac{1}{n_o^2}+p_{1122}S_{22}^{(\alpha)}\right]D_1^2+\left[\frac{1}{n_o^2}+p_{1111}S_{22}^{(\alpha)}\right]D_2^2+\left[\frac{1}{n_e^2}+p_{1122}S_{22}^{(\alpha)}\right]D_3^2=1 \qquad (4.18)$$

Assuming that $p_{ijkl}S_{kl} \ll 1/n_o^2$ for all ijkl, the equation (4.18) yields a difference in phase between the diffracted and undiffracted beams of

$$\begin{aligned}\Phi &= (\phi_2-\phi_3)_{diff}-(\phi_2-\phi_3)_{undiff}\\ &= 2\pi\left[p_{1111}-p_{1122}\right]S_{22}^{(\alpha)}.n_o^3L/\lambda_o,\end{aligned} \qquad (4.19)$$

where L is the interaction length for the optical and acoustic waves.

The phase difference is the direct result of the change in the shape of the index ellipsoid (see figure 4.4). The change in the index ellipsoid need not change the output polarisation for all possible input polarisations, but the phase match condition (4.12) does apply in all cases and dictates the allowed input and output polarisations (see figure 4.5).

(b) Transverse Acoustic Waves.

Transverse acoustic waves are normally generated on the surface of an acousto-optic material and only penetrate for short distances into the material. The use of transverse surface acoustic waves (SAW) technology is becoming more prevalent in acousto-optic signal processing because of its coverage of the rf range 1-3 GHz, which in turn is due to the confinement of the acoustic wave to the surface and to the lower velocity of surface waves in comparison with bulk acoustic waves. Transverse acoustic waves produce a shearing strain in the transmission medium, which has the effect of rotating the index ellipsoid about an axis perpendicular to the shearing action (see figure 4.6).

For example, we wish to engender the largest possible change in refractive index; thus the strain which engenders a cross term between the optical axes and the xy-plane is chosen. This can be represented by the strain tensor element $S_{23}^{(\alpha)}$, which leads to the index ellipsoid having the form

$$\frac{D_1^2}{n_o^2}+\frac{D_2^2}{n_o^2}+\frac{D_3^2}{n_e^2}+D_2D_3(p_{1111}-p_{1122})S_{23}^{(\alpha)}=1. \qquad (4.20)$$

The rotated ellipsoid described by equation (4.20) can be written as

$$\frac{D_1^{\dagger 2}}{n_o^2}+D_2^{\dagger 2}\cdot\left[\frac{1}{n_o^2}+\frac{\Delta}{2}\cdot\left[1+\sqrt{1+\frac{4\delta^2}{\Delta^2}}\right]\right]+D_3^{\dagger 2}\cdot\left[\frac{1}{n_o^2}+\frac{\Delta}{2}\cdot\left[1-\sqrt{1+\frac{4\delta^2}{\Delta^2}}\right]\right]=1, \qquad (4.21)$$

where δ and Δ are defined as:

$$\delta = \frac{1}{2}(p_{1111}-p_{1122})S_{23}^{(\alpha)}; \qquad \Delta = \frac{1}{n_e^2} - \frac{1}{n_o^2}.$$

The difference in phase between the diffracted and undiffracted beams for any input polarisation is

$$\Phi = \Delta\left[1-\sqrt{1+\frac{4\delta^2}{\Delta^2}}\right]\frac{2\pi n_o^3 L}{\lambda_o}. \tag{4.22}$$

Thus for certain orientations a larger shift in the deflection angle per unit frequency can be achieved because of the combined effects of the shift in the index ellipsoid and the change in direction of propagation.

§4.4 Concluding Remarks.

Permanent strains in glass can be generated whilst cooling of the glass from the molten state whilst under tension. Such strains in the glass result in birefringence, which means that if the applied stress on a glass can be controlled then the generated birefringence in the glass can be controlled. The unstressed refractive index is also controllable by way of the the chemical composition of the glass.

We have shown that glasses can be used as acousto-optic media in much the same situations as birefringent crystals. We have also demonstrated that the production of both surface and bulk acousto-optic (transverse and longitudinal acoustic wave) devices incorporating media such as prestressed glass is possible. Surface wave devices provide the better of the two options since the acoustic wave rotates the index ellipsoid and, as such, come closer to the effects seen within non-centrosymmetric crystals.

A good figure of merit for prestressed glasses is the eccentricity of the index ellipsoid,

$$e = \frac{1}{n_o}\sqrt{|n_e^2 - n_o^2|}\ . \qquad (4.23)$$

The values of the eccentricity, e, are plotted for three different commercial glasses [4.11] in figure 4.7. The value of eccentricity for $LiNbO_3$ is e = 0.289.

If values for e similar to those for birefringent crystals can be obtained by prestressing glass, then a practical alternative to the crystal Bragg cells could be developed. The major difference between glass and crystal cells would then be in the diffraction efficiency per-Watt of acoustic power introduced to the cell.

The possible loss of power efficiency on moving from crystal cells to birefringent glass cells is far outweighed by the other possible advantages. These include; the possibility of tailor made birefringences, the production of Bragg cells with any desired acoustic path length and the reduction in production cost per cubic centimetre of acousto-optic medium.

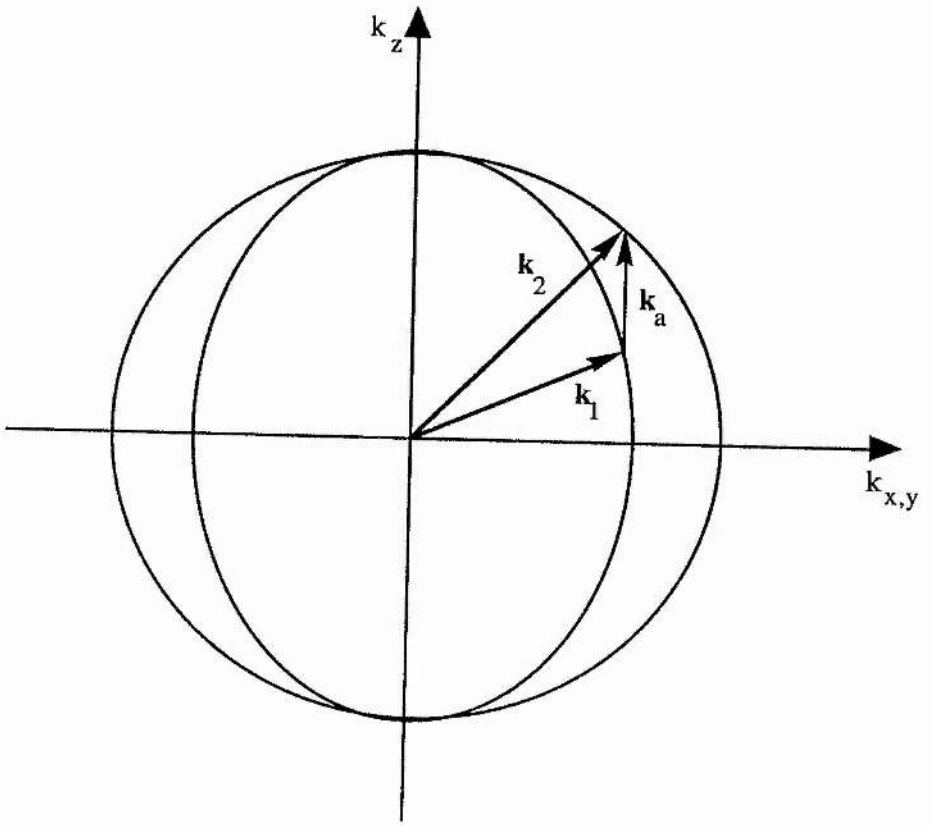

Figure 4.1. A possible phase match condition in an anisotropic acousto-optic interaction medium.

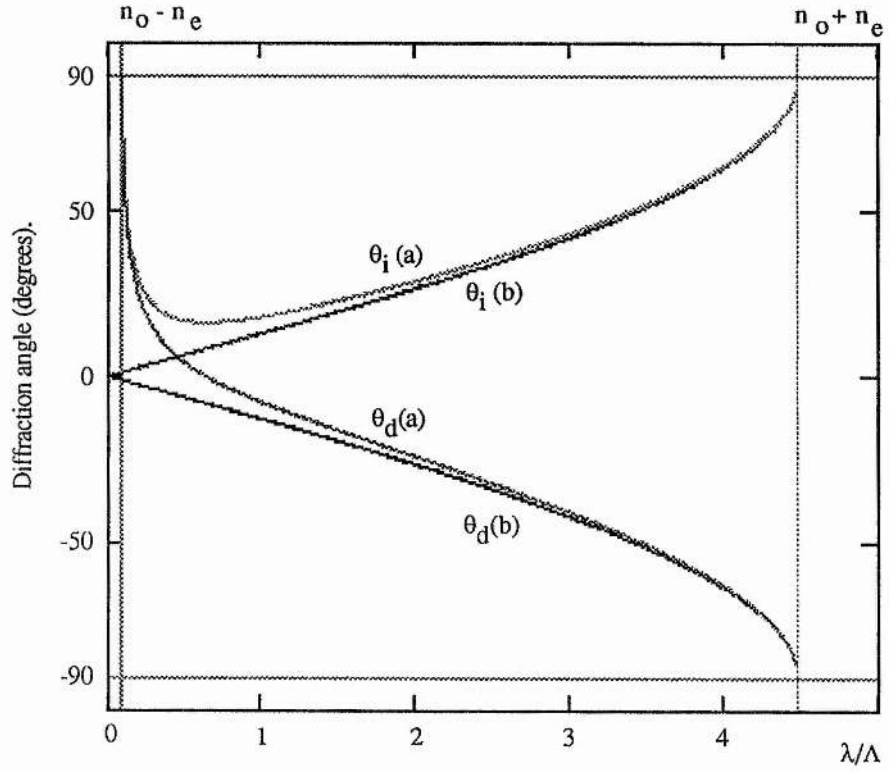

Figure 4.2. Graphs of the angle of incidence, θ_i, and diffraction, θ_d, against the normalised grating frequency λ/Λ for (a) a lithium niobate crystal and (b) an isotropic medium of the same average refractive index.

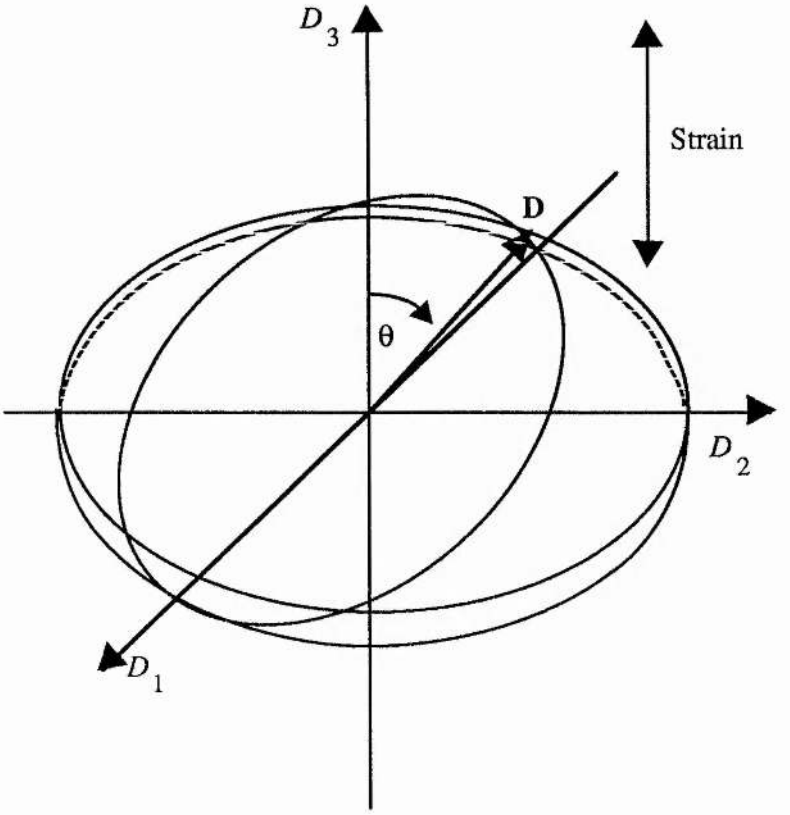

Figure 4.3. Diagram of a possible index ellipsoid for a stressed glass as seen in **D**-space. The angle θ is the angle between the optical axis of the glass and the polarisation of the incident radiation.

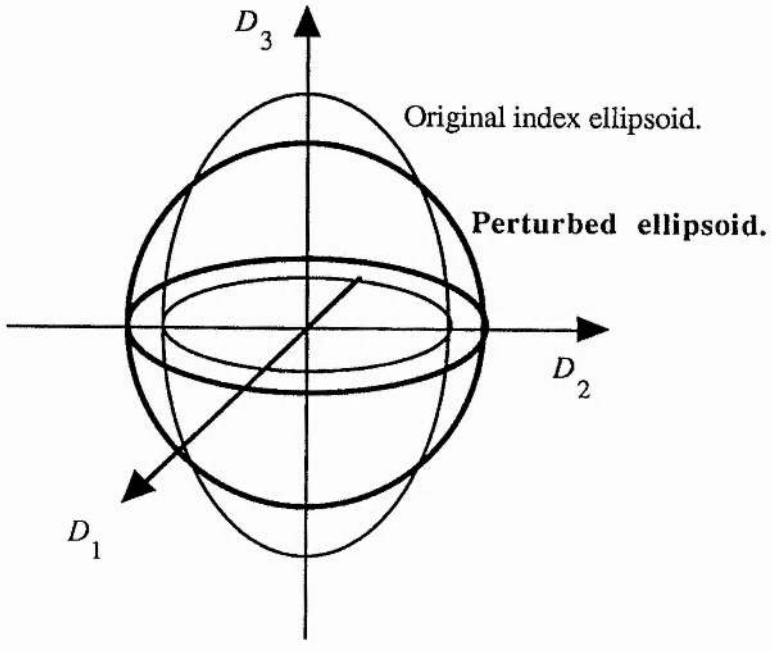

Figure 4.4. Diagram of a perturbation to the index ellipsoid.

Figure 4.5a.

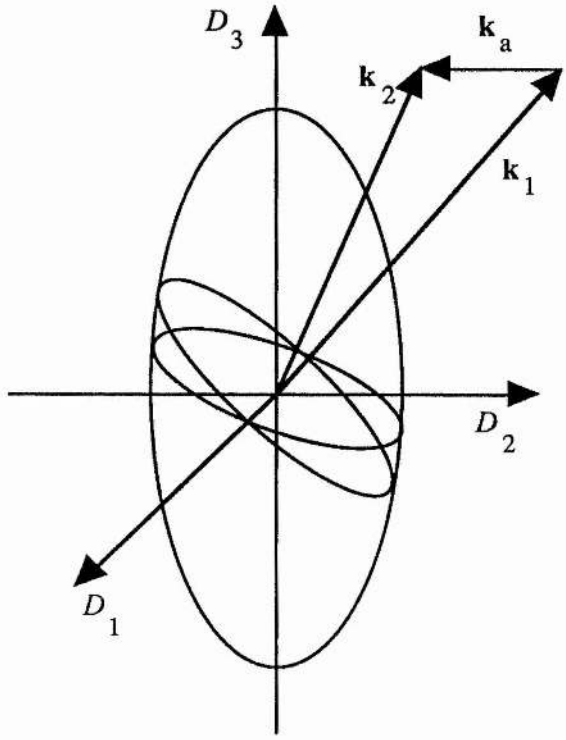

Figure 4.5b.

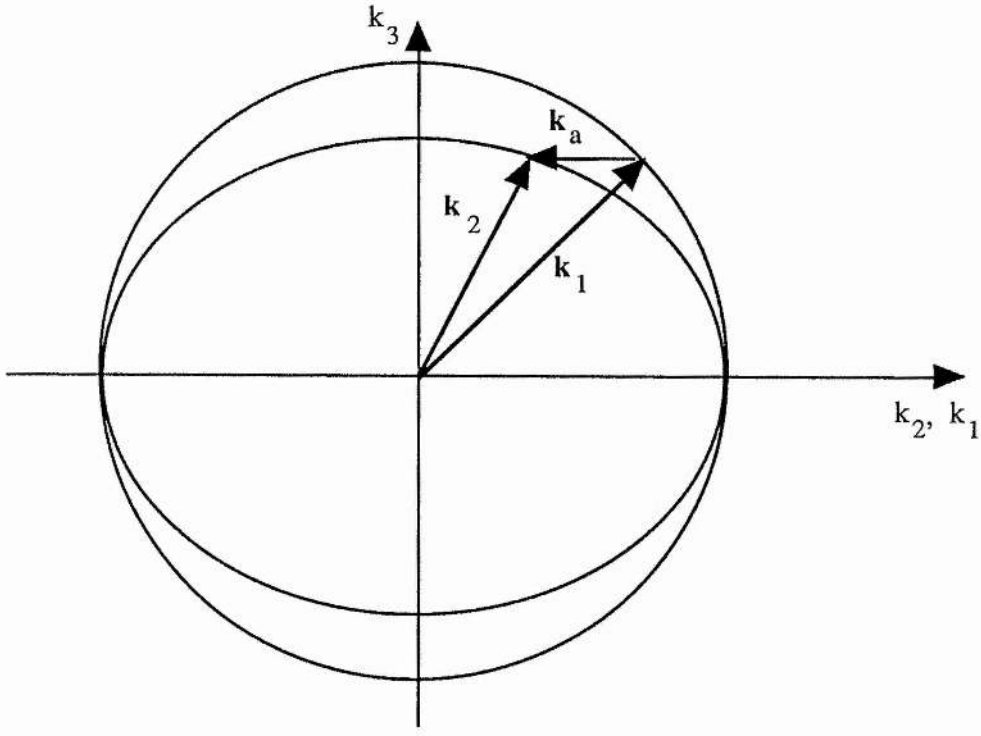

Figure 4.5. (a) Diagram of the change in index ellipsoid cross-section, as seen by the photon, on diffraction. (b) Diagram of the **k**-space equivalent of (a).

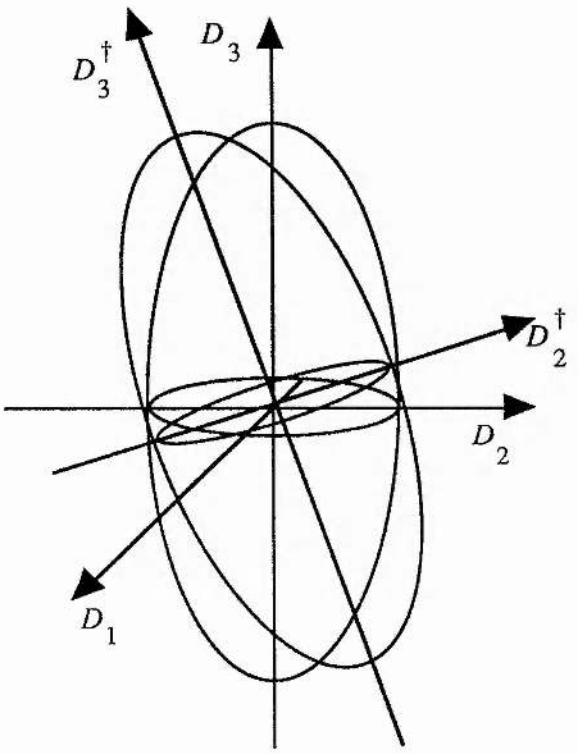

Figure 4.6. Rotation of the index ellipsoid in **D**-space at the strain maxima of a transverse applied acoustic wave.

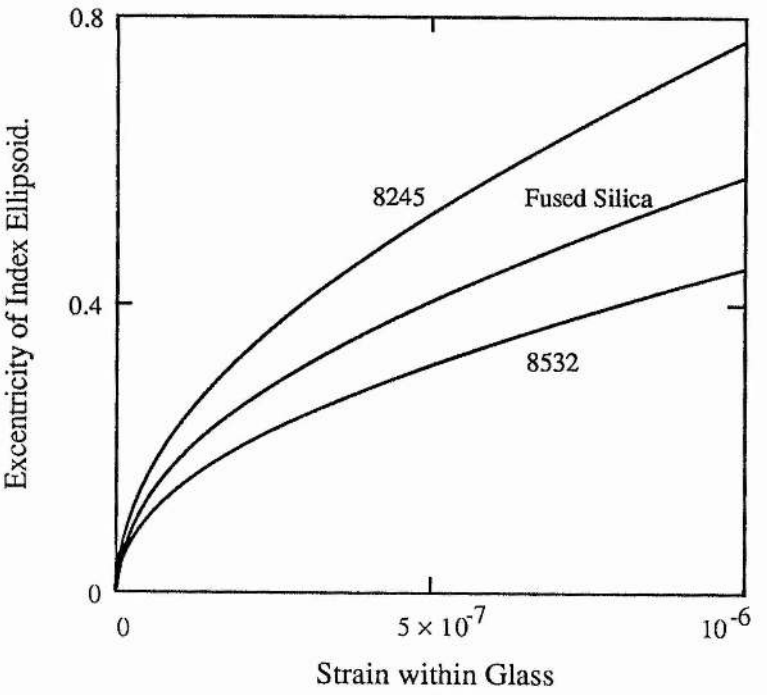

Figure 4.7. Graphs of the eccentricity of the index ellipsoid against internal strain for three different glasses: (i) fused silica (ii) Schott glass no. 8245; (iii) Schott glass no. 8532. To generate a strain of 10^{-6} in a glass a stress equivalent to a directional pressure of the order of 3/4 atmospheres pressure is required.

§4.5 References.

[4.1] Glass. G O Jones. Methuen & Co. London. 1956.

[4.2] Optics. E Hecht and A Zajac. Addison-Wesley Pub. Co. Inc. 1977.

[4.3] Measurement on the residual birefringence distribution in glass laser disk by transverse Zeeman laser. N Umeda and H Kohwa. Trans. Ins. Electronics, Information and Communication Engineers C-I. **J73C-I** no.10 page 652-7. 1990.

[4.4] Birefringent glass rods. T Lukaszewics and M Bozyk. Optica Applicata. vol.**17** no.3 page 265-8. 1987.

[4.5] Handbook of Microwave and Optical Components (Volume 4. Fibre and Electro-Optical Components). K Chang (Ed.) Wiley Interscience (New York) 1991.

[4.6] Acousto-optic Signal Processing (Theory and Implementation). N J Berg and J N Lee. Marcel Dekker Inc. New York, USA. 1983.

[4.7] Acousto-optic Signal Processing: Fundamentals and Applications. P K Das and C M DeCusatis. Artech House Inc. Norwood, USA. 1991.

[4.8] Acousto-Optics. J Sapriel. John Wiley and Sons (Int.) 1979.

[4.9] Advanced Engineering Mathematics. 6Ed. E Kreyszig. John Wiley and Sons (Int.) 1989.

[4.10] Schott Technical Glasses. Schott Glaswerke, Central Research and Development Division, Hattenbergstraße 10, 6500 Mainz, Germany. 1990.

[4.11] Handbook of Material Science (vol 2). C T Lynch (Ed.). Chemical Rubber Company Press (1974).

Chapter 5.

A Possible Method for the Creation of Permanent Diffraction Gratings and Volume Holograms using Acoustic Waves.

§5.1 Introduction.

In chapter 4 we gave an outline of the acousto-optic effect [5.1, 5.2] and an account of stress induced birefringence in glass. In this chapter we wish to marry the two effects to obtain a method for the creation of permanent acousto-optic gratings (see Appendix 3).

Currently no such method exists, the means for creating permanent diffraction gratings and holograms being based on photographic and etching procedures. The level of sophistication of the current grating production techniques is high, but does not present a direct method for recording rf information from an acousto-optic Bragg diffractor such that the resulting diffraction pattern may be reproduced at some unspecified time in the future. Indirect methods for rf signal recording do exist, but these involve either digital signal recording techniques [5.1] or taking photographs of the resultant diffraction pattern from Bragg cells [5.3, 5.4].

All the grating and hologram production techniques we examine in this chapter are in principle capable of preserving information from an acousto-optic Bragg cell. Here we discuss two general methods for producing permanent acousto-optic gratings. One is to "freeze" the stress associated with an acoustic standing wave into the grating medium. The other is to use optics to recreate the diffraction in a conventional photographic holographic medium [5.3].

Some potential applications of permanent acousto-optic gratings and holograms are as follows: single frequency phase and absorption transmission gratings for simple spectroscopy [5.5]; single frequency surface transmission and reflection gratings for simple

spectroscopy; phase and absorption volume holograms for use as masks in acousto-optic signal processing [5.1]; and distributive feedback mirrors for use in integrated optics (see chapter 6).

The treatment for stress induced birefringence and the acousto-optic effect in glass given in chapter 4 will form the basis of our theory for permanent acousto-optic gratings. Additions to the theory given in chapter 4 will be presented alongside the general treatment of permanent gratings in glass before we proceed to describe those produced in other materials. These materials include gels and polymers for volume grating production and gels, polymers and metals for surface grating production.

§5.2 Methods for Creating Volume Holograms and Surface Holograms Using Acoustic Waves.

§5.2.1 Permanent Volume Holograms in Glass Produced by Acoustic Waves.

The method for creating a permanent volume hologram in glass may be applied to all types of glass [5.6], silica and non-silica based, and is similar to the method for creating uniformly stressed glass in that the glass is passed through its transformation point [5.6] whilst an external stress is imposed on it.

The piece of the glass that is going to hold the hologram is cut so that two faces form an acoustic cavity (figure 5.1). It is then heated to a temperature above its transformation temperature and a longitudinal acoustic wave is introduced through one end of the acoustic cavity. The glass is then cooled and the acoustic wave with-drawn. The residual strain from the acoustic wave in the glass forms a phase grating.

The frequencies within the acoustic field must be multiples of the cavity's fundamental frequency,

$$\nu_f = \frac{v_a}{2L}, \tag{5.1}$$

which is the acoustic velocity in the glass, v_a, divided by twice the acoustic cavity length, L. The fundamental frequency (5.1) is akin to the transit time for travelling wave gratings in that it gives the frequency resolution for the device [5.1].

Within the resolution limit provided by ν_f any strain distribution can be represented as a Fourier series [5.7] with fundamental frequency ν_f. The distribution of strains in the x-direction, F(x), can be expressed as

$$F(x) = \sum_{m=1}^{\infty} a_m \sin\left[\frac{2\pi\nu_f m}{v_a} x\right], \tag{5.2a}$$

where the amplitude terms are given by

$$a_m = \frac{1}{L}\int_{-L}^{L} F(x) \sin\left[\frac{\pi m}{L} x\right] dx. \tag{5.2b}$$

When the distribution given in (5.2) is composed of a set of acoustic standing waves it will evolve in time, which results in the required strain pattern F(x) only being observed once every period of the fundamental standing wave. The process we wish to employ for freezing the pattern into the glass results in the glass being able to take up imposed strains for longer than the period of the fundamental standing wave and thus we cannot record a strain pattern as described by equation (5.2). The inability of our proposed technique to freeze in an instantaneous strain pattern is due to the length of time required to uniformly

heat the glass to, and cool it from, a temperature where all imposed stress are taken up by the glass.

The nature of glass is such that at a temperature greater than its transformation temperature, T_T, and lower than its annealing temperature, T_A, it will hold any stress imposed on it. The range between the two temperatures T_T and T_A is known as the transformation range and is of the order of 10 °C. In Pyrex [5.8], for example, the transformation range is between 525 °C and 560 °C.

If a glass at or just below its transformation temperature is compressed, it will undergo adiabatic heating [5.9], which will raise the local temperature into the transformation range. The imposed compression is therefore held within the structure of the glass. If the same piece of glass is then stretched, as it would be by the rarefaction of a longitudinal acoustic standing wave, the stresses imposed by the compression will not be removed because the glass is adiabatically cooled by the rarefaction and therefore taken outside the transformation range.

Thus the stress pattern formed by an acoustic standing wave, instead of being sinusoidal, will be the magnitude of the sine function. A direct result of the freezing process is that equation (5.2) does not apply and any strain distribution required will have to be constructed from a combination of the functions

$$f_n(x) = \left| \sin\left[\frac{\pi \nu_n}{v_a} x\right] \right|. \tag{5.3}$$

Using the superposition of the functions given by (5.3) it will be possible to produce simple strain patterns within glass permanent acoustic volume holograms. To freeze more complex acoustic strain patterns than those composed of the set of functions described by

(5.3) an indirect method of storage will be required. Such complex strain patterns will not be dealt with until section 5.3.

To find the appropriate acoustic frequency for the construction of a hologram in glass we take into account the variations in the acoustic cavity length and the speed of sound with respect to temperature. The effects of these variations on the fundamental frequency and the stress distribution will be as follows:

$$dv_f = \frac{1}{2L}\left[\frac{\partial v_a}{\partial T} - \frac{v_a}{L}\frac{\partial L}{\partial T}\right] dT. \tag{5.4}$$

The change in the fundamental frequency is the only important change to occur in the system on raising the temperature. The spatial variations in the strain pattern with temperature are directly proportional to the changes in acoustic cavity length. Therefore if a grating with a room temperature fundamental grating frequency of $v_f(RT)$ is required then a fundamental frequency of

$$v_f(T_t) = v_f(RT) + \frac{1}{2L}\left[\frac{\partial v_a}{\partial T} - \frac{v_a}{L}\frac{\partial L}{\partial T}\right](T_T - RT) \tag{5.5}$$

is used for grating production at the transformation temperature, T_T.

Thus we have a method for creating a phase grating of unknown diffraction efficiency within a block of glass. To find the diffraction efficiency the results obtained from the coupled mode equations in chapter 4 can be applied. All the equations that apply to acousto-optic diffraction in an isotropic medium also apply to permanent acoustic gratings, except the interaction length condition (2.10) which does not apply since the permanent grating is

stationary. The diffraction efficiency for a strain grating is given by equation (4.7);

$$\frac{I_{out}}{I_{in}} = \sin^2\left[\frac{\pi}{\lambda_o} n^3 p_c S\, L\right]. \qquad (5.6)$$

The diffraction efficiency for a range of prestressed glass gratings is plotted for three glasses [5.8, 5.10] in figure 5.2. The theoretical curves plotted in figure 5.2 are in agreement with the value for the diffraction efficiency given by Das and DeCusatis [5.11]. Das and DeCusatis give a value of 1% for the diffraction efficiency of a fused silica Bragg cell of thickness 2.2 mm, operating at a strain amplitude of 10^{-5} and a frequency of 100 MHz. They also state that strains greater than 10^{-4} can be generated within solid acousto-optic media but are seldom used since they shorten the life time of the media and present coupling problems at material boundaries.

We do not require strains of the order of 10^{-4} to be held within the glass on cooling, but they may be needed at the transformation temperature to generate the smaller strains required at room temperature. There is no need for high strains within the glass grating structure at room temperature since the diffraction efficiency is a function of the product of strain and interaction length. The upper limit on the interaction length, L, (2.10) that applies to travelling wave gratings does not apply to stationary gratings, therefore a long interaction length can be used to compensate for low grating strains. The strain required in a 10 mm interaction length fused silica phase grating to diffract 1% of the incoming light is approximately 5×10^{-6}, which is easily obtainable even allowing for a low uptake of the imposed strain by the glass.

Thus we have a possible method for the generation of permanent phase gratings in glass from acoustic standing waves.

In this section we have dealt with longitudinal, bulk, acoustic standing waves only but it should be noted that transverse acoustic standing waves [5.1, 5.12] should be capable of producing permanent strain patterns in glass at its transformation temperature.

§5.2.2 Production of Permanent Acoustic Gratings in Gels.

There are three methods for creating permanent acoustic gratings in a gel. Two are destructive methods where the gel matrix is shaken apart and the other is a constructive method where the gel is shaken as it sets to inhibit setting at particular points.

In the destructive process the gel is placed in an acoustic cavity and allowed to set. The set gel is then acoustically excited to produce small fissures at the anti-nodes of the acoustic standing waves (figure 5.3). The fissures will themselves present a diffraction grating, but the effect can be enhanced by the injection of other material into the spaces they provide.

Scattering of light from the fissures is, as all the other gratings discused in this chapter are, governed by the Bragg condition (1.26);

$$\sin\theta_B = \frac{\lambda_o}{2n_o d}, \tag{5.7}$$

where θ_B is the angle of diffraction of incoming light of wavelength λ_o on hitting a grating of spacing d in a medium with refractive index n_o.

If the fissures at the acoustic anti-nodes lie in the same plane, all the light scattered from the fissure walls will effectively undergo Bragg Diffraction (see figure 5.4). In the ideal case all the fissures will occur exactly at the anti-nodes and form a series of continuous planar discontinuities across the space occupied by the acoustic column. In reality the fissures will be disjointed and will spread for some distance on either side of the anti-node. The effect of

the spread will be to give a range of distances d over which the Bragg condition (5.7) holds. For a spread of δ round every anti-node there is a corresponding spread in diffraction angle $\Delta\theta$ given by

$$\Delta\theta = \frac{\lambda_o}{2n_o}\,\frac{\delta}{d^2}\,\frac{1}{\left[1 - \dfrac{\lambda_o}{2n_o d}\right]^{1/2}}, \tag{5.8}$$

which for a grating of spacing d = 50 μm and a fissure spread of δ = 5 μm illuminated with a HeNe laser has the value $\Delta\theta$ = 0.422 mrad. This gives an uncertainty of $\sqrt{2}.\Delta\theta$ = 0.597 which is 7% of the actual diffraction angle, $2 \times \theta_B$ = 8.44 mrad.

The spread of fissures may also give rise to non-parallel fissures which will scatter light in directions other than that given by the Bragg condition (5.7). Such effects are unwanted and if they do occur require a remedy. We now propose an alternative to using the fissure walls as scattering surfaces. Instead of using the fissures to introduce a foreign material to aid the scattering process (figure 5.3), they are used to introduce more gel with an added dopant at a temperature that will dissolve the fissure walls to give a gradual transition from the original gel to the doped gel. The result of this gradual transition is to give a phase grating as opposed to the reflection grating obtained from the fissure walls.

For the constructive method the gel is also placed in an acoustic cavity. The gel is insonified as it sets, thus inhibiting the formation of the gel matrix at the acoustic anti-nodes. If we can change the chemical make-up of the gel solvent as it sets, then we can cause a difference in refractive index between the sites of the acoustic nodes and anti-nodes. Through-out this process the acoustic length of the cavity must not change, thus a gel solution which has the same acoustic properties as the solid gel is required. The effect on the system of having a solid gel of different acoustic properties to its solution would be to remove the standing wave condition and therefore to disturb the solid gel.

Thus we have three methods for producing permanent acousto-optic diffraction gratings within gels: two destructive methods where fissures are formed in a set gel acoustically and one constructive method where the setting of a gel is acoustically impeded.

§5.2.3 The Production of Permanent Surface Gratings using Acoustic Waves.

To produce a high quality surface grating on glass, metal or other substrates, etching and photoresist [5.13, 5.14] techniques are usually employed. We suggest an alternative method of etching based on acoustics, which is a viable alternative to photoresists.

To produce a surface grating by etching, without the use of a resist, the grating substrate material is placed in a tank containing a fluid etching agent. An acoustic standing wave, of appropriate wavelength, is then set up in the etching agent or on the substrate material's surface (figure 5.5). The effect of the standing wave is to increase the rate of reaction on the surface of the grating substrate at the standing wave anti-nodes. The increase in the rate of reaction is due to the increased rate of transport of reaction product into the liquid, which increases the amount of etching agent in contact with the substrate at the site of the anti-nodes. Thus there is a differential rate of etching between the nodes and anti-nodes of the acoustic standing wave and therefore, after a given period of etching, a grating will be produced.

The factors affecting the production of such a grating are; the reaction rate between the grating substrate and the etching agent and the relative speeds of sound, in the substrate and in the etching agent. The three factors are interdependent. If the rate of reaction between the substrate and the etching agent is faster than the rate of transport due to the acoustic wave, then the effect of the acoustically induced transport will be negligible. If the rate of reaction

is comparable to, or slower than, the rate of transport at the anti-nodes then the transport of reaction product away from the reaction surface will become significant.

In the case where the acoustic standing wave is set up in the etching agent the wave is longitudinal, with the wave vector parallel to the grating substrate's surface. The acoustic waves need only form a standing wave pattern at the surface of the grating substrate's surface so as to provide the required differential in reaction rate between node and anti-node sites.

In the case where the acoustic standing wave is set up in the grating substrate the wave can be either longitudinal or transverse in nature. The use of either longitudinal or transverse acoustic standing waves within the grating substrate will aid grating formation by way of transmission into the etching liquid. The anti-nodes of the acoustic standing wave act as radiators of travelling waves into the etching liquid. The nodes of the acoustic standing wave do not oscillate and therefore are associated with areas of 'calm' in the etching liquid.

For longitudinal acoustic standing waves in the grating substrate transmission into the etching liquid can take one of two forms; (i) 'evanescent transmission' or (ii) 'percentage transmission'.

Evanescently transmitted waves will decay exponentially from their point of entry into the etching fluid. Thus the evanescent transmission of longitudinal acoustic standing waves from the grating substrate into the etching liquid does not present a viable method for grating production.

Percentage transmission of longitudinal acoustic waves into the etching liquid, on the other hand, is a linear process and therefore will provide good mixing at the sites of the acoustic anti-nodes. The percentage of the acoustic wave's amplitude transmitted through a surface perpendicular to the wave's motion is dependent on the mechanical impedances of the

grating substrate and the etching liquid which are functions of their respective densities, ρ_l, ρ_s and their respective velocities of sound v_l, v_s:

$$\text{Amplitude trans.\%} = \frac{2\rho_s v_s^2}{v_l(\rho_l v_l + \rho_s v_s)} \times \frac{100}{1}\,\%. \tag{5.9}$$

For the purposes of permanent surface grating creation, where a standing wave is required at the grating substrate's surface and transmission of the acoustic wave, a triangular acoustic resonant cavity can be set up using the surface of the grating substrate as the apex mirror as shown in figure 5.6. The angles of the triangle are such that the angle of incidence θ_i, and therefore of reflection θ_r, comply with the transmission condition

$$\theta_i < \sin^{-1}\left[\frac{v_s}{v_l}\right]. \tag{5.10}$$

The angle of incidence, θ_i, of the acoustic waves to the surface of the grating substrate also dictates the grating separation, d, produced by a given acoustic frequency, v_a;

$$d = \frac{v_s}{2v_a}\,\frac{1}{\sin\theta_i}. \tag{5.11}$$

The grating creation process, when using percentage transmission of longitudinal acoustic waves, is a compromise between the acoustic frequency used and the amount of disturbance within the etching liquid.

For transverse surface standing waves in the grating substrate the propagation of ultrasound from the anti-nodes of the standing wave in the grating substrate into the etching fluid is relied on to aid the transport of reaction products away from the reaction site (figure 5.7). The anti-nodes of the transverse acoustic standing wave in the grating substrate

oscillate perpendicularly to the surface of the substrate and therefore will create travelling longitudinal waves within the etching liquid. The travelling longitudinal waves so created will carry reaction products away from the anti-nodes of the standing wave, which will have the effect of creating a differential reaction rate between the acoustic nodes and anti-nodes. Thus a permanent surface diffraction grating can be created using transverse acoustic standing waves within the intended grating substrate.

In this section we have shown that it is possible to produce surface diffraction gratings and holograms with acoustic standing waves.

§5.3 Applications of Permanent Acoustic Gratings and Holograms.

§5.3.1 Permanent Uniform Acousto-Optic Diffraction Gratings.

The use of permanent gratings of single grating frequency for the differentiation of different wavelengths of light is well documented [5.5, 5.15].

For simple spectroscopy purposes surface and volume gratings can be used. Acoustically generated surface gratings will be limited in resolution by the rate of the chemical process used for etching and the stability of the acoustic cavity used to hold the acoustic standing wave. Another method for producing high definition surface gratings is that of etching after deposition of a photoresist [5.14]. Gratings produced by photoresist techniques are also limited in resolution by the rate of chemical etching. Thus if the process of permanent surface acoustic grating creation can be refined to the same degree as photoresist generated surface gratings then permanent acoustic surface gratings may provide a viable alternative to current surface grating creation techniques.

Where we envisage acoustic techniques for the generation of permanent optical grating generation to come into their own is in the field of volume phase grating creation, where the current photographic techniques are complicated and cumbersome [5.3].

The photographic alternatives to using acoustic waves for the production of permanent phase gratings include: optical damage of crystals to give variations in refractive index [5.20]; the formation of holograms in dichromated gelatin [5.3, 5.16, 5.17, 5.18]; the formation of holograms in photopolymers [5.3, 5.16, 5.19, 5.20]; and the formation of holograms in bleached photographic film [5.3, 5.16, 5.21]. All these alternative methods for producing phase gratings are complex and/or expensive. The use of acoustics may offer some advantages for the production of phase gratings and thus may be a preferable technique to photographic holography for the production of simple structures such as single frequency phase gratings.

§5.3.2 Permanent Acousto-Optic Holograms as Masks for Signal Processing.

The use of masks, both phase and absorption, in signal processing is also well documented [5.1, 5.11]. Masks in signal processing can be divided into two groups.

(i) Masks designed to operate in the Fourier transform plane. Fourier transform masks filter out unwanted spatial frequencies and perform image correlation tasks by containing the spatial Fourier transform of the desired image.

(ii) Object or image plane masks, which contain the same image as the desired image. We are primarily interested in the second group because of its potential applications in acousto-optic signal processing.

In acousto-optics, signal correlation can be carried out by time reversing the signal we wish to recognise by letting it propagate in a SAW Bragg cell [5.1] on which an acoustic column containing the unknown signal is counter propagating (Figure 5.8a). The acousto-optic correlator [5.1, 5.11] thus implemented is a very compact device for signal processing, but still contains a large amount of electronics to time reverse the reference signal. The use of permanent acousto-optic phase gratings in acousto-optic rf signal correlators will provide a further reduction in overall device size (see figure 5.8b).

Alternative techniques for generating phase images exist, which would lend themselves to producing devices of the same type as the acousto-optic correlator. These are all holographic [5.3, 5.16-22]. If an acoustic signal is recorded holographically, for use in an acousto-optic correlator, then the recording medium must propagate an acoustic wave at the same speed as the reference acousto-optic device (figure 5.9), otherwise there will be no correlation between the holographically recorded signal and the same signal propagating within the recording medium. A "velocity matched" permanent holographic mask can be achieved simply by optically damaging a crystal of the same substance as the original acousto-optic cell. The reference signal can thus be imposed on a crystal through which another signal can be propagated and therefore correlated with the reference signal.

Optically induced permanent refractive index changes in lithium niobate are well known [5.20]. Lithium Niobate is also the commonest material for constructing high Q acousto-optic Bragg cell from [5.1, 5.11], which would make it an ideal material for such an acousto-optic correlation device.

Thus we have two potential methods for the production of permanent phase holograms an acoustic signal for use in acousto-optic correlators.

§5.4 Concluding Remarks.

In this chapter we have outlined several methods for the creation of permanent diffraction gratings from acoustic standing waves. We have also outlined the two main uses that we envisage for acoustically produced permanent holograms.

The figures obtained theoretically for the diffraction efficiency of permanent acoustic gratings in glass are encouragingly high for the amount of stress imposed on the glass by the acoustic standing wave. A Fused silica permanent acousto-optic grating cell of thickness 50 mm would have a diffraction efficiency of 65% when its built in strain wave amplitude is 10^{-5}.

The motivation for the development of this technology comes from acousto-optic signal processing and the need for more compact rf correlators.

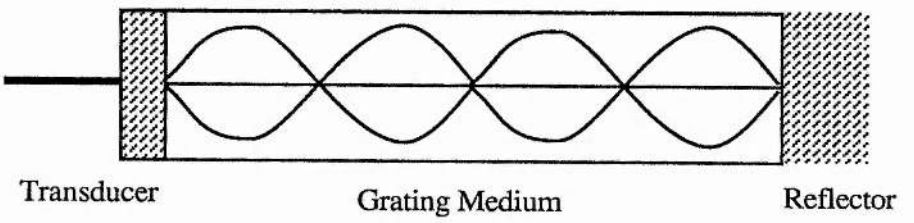

Figure 5.1 Schematic diagram of a simple one dimensional single frequency acoustic cavity for permanent acoustic grating generation running at a frequency which is four times its fundamental frequency.

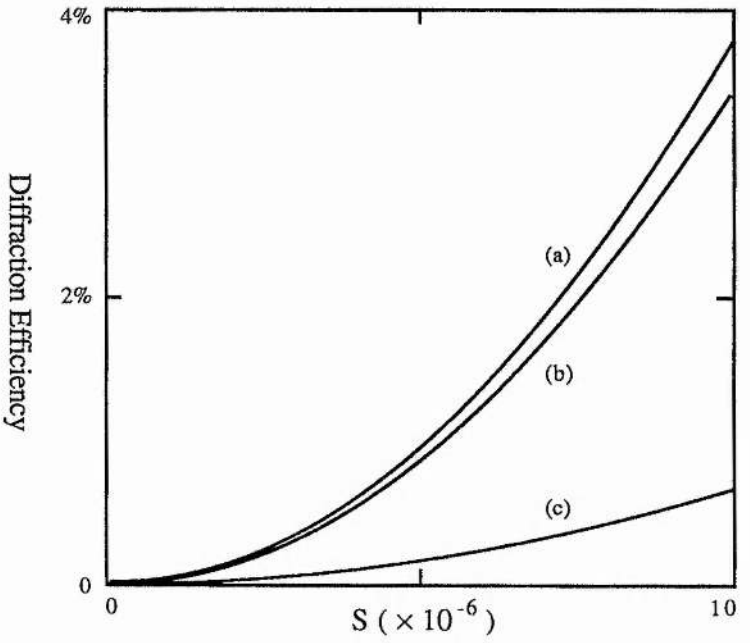

Figure 5.2a. Graph of diffraction efficiency against strain for an interaction length of L = 10 mm.

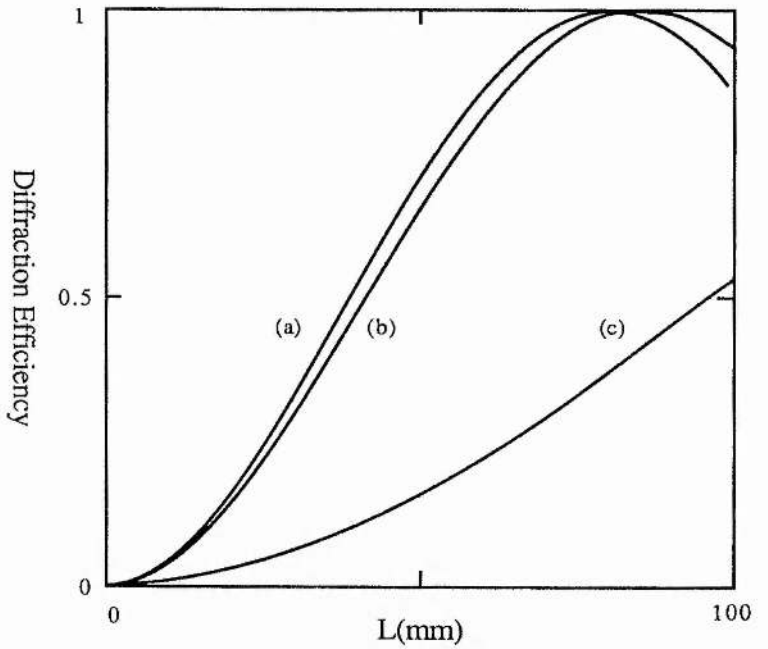

Figure 5.2b. Diffraction efficiency against interaction length for a constant strain of $S = 10^{-5}$.

Figure 5.2. Graphs of diffraction efficiency against (a) interaction length and (b) residual strain for three glasses; (a) Fused silica. (b) Schott glass No. 8532, which is used for encapsulating photodiodes. (c) Schott glass No. 8330, which is a Pyrex equivalent.

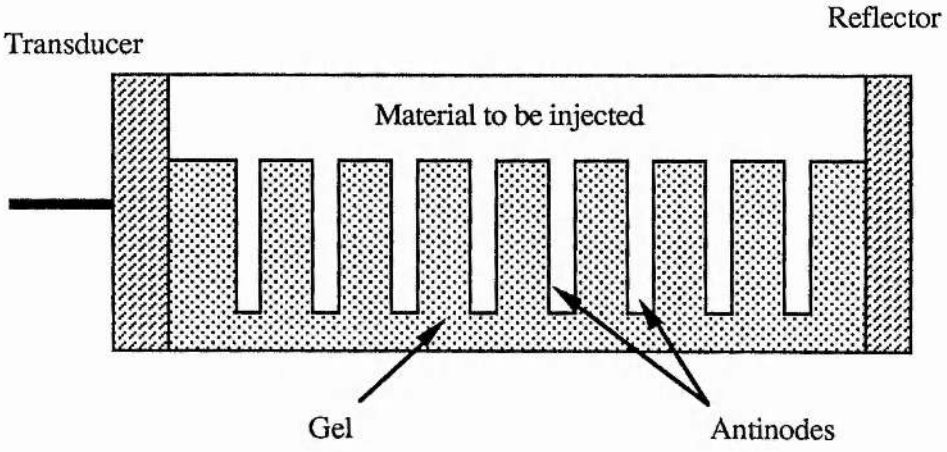

Figure 5.3. Schematic diagram of a simple matrix disruption method for creating a phase grating using a solid gel and a dopant. The dopant enters through the fissures in the areas of matrix disruption which coincide with the acoustic standing wave's anti-nodes.

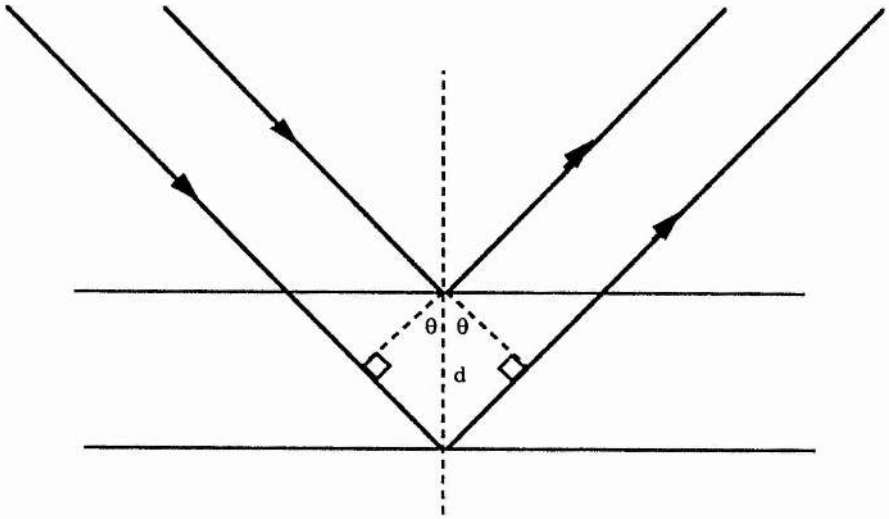

(a) Bragg diffraction from a series of single fissure boundaries at the anti-nodes of the acoustic standing wave.

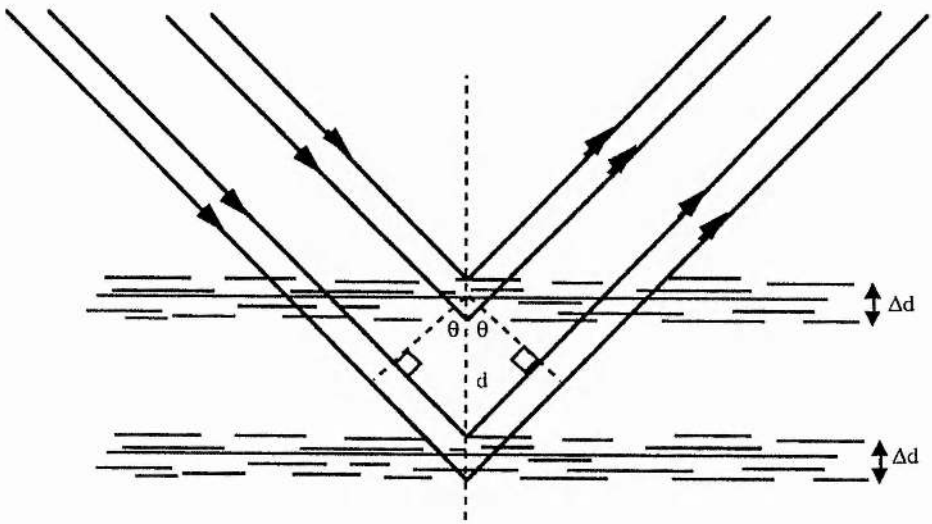

(b) Bragg diffraction from an acoustic anti-node where multiple parallel fissures have occurred. There will be a range of Bragg angles θ_B which corresponds to the range of fissure separations Δd within each layer.

Figure 5.4. Schematic diagrams of Bragg refraction from damage points coincident with acoustic anti-nodes in gelatin.

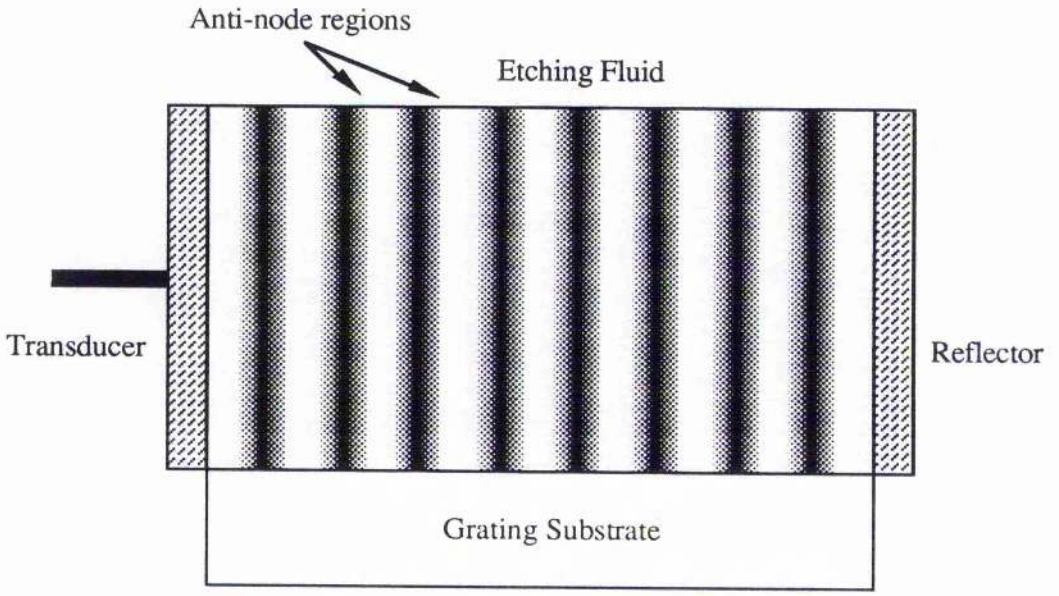

(a) Longitudinal standing wave in the etching fluid implementation for grating etching.

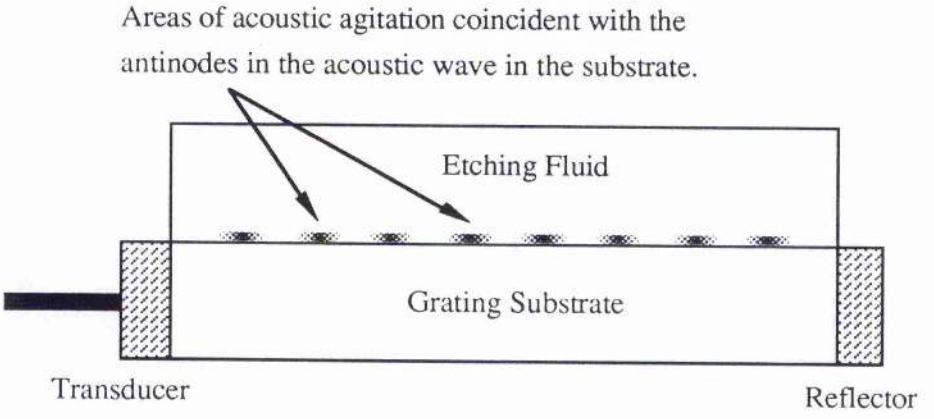

(b) Transverse standing wave in the grating substrate implementation for grating etching.

Figure 5.5. Diagrams of (a) the longitudinal and (b) the transverse acoustic standing wave implementations for etching diffraction gratings without the use of a resist.

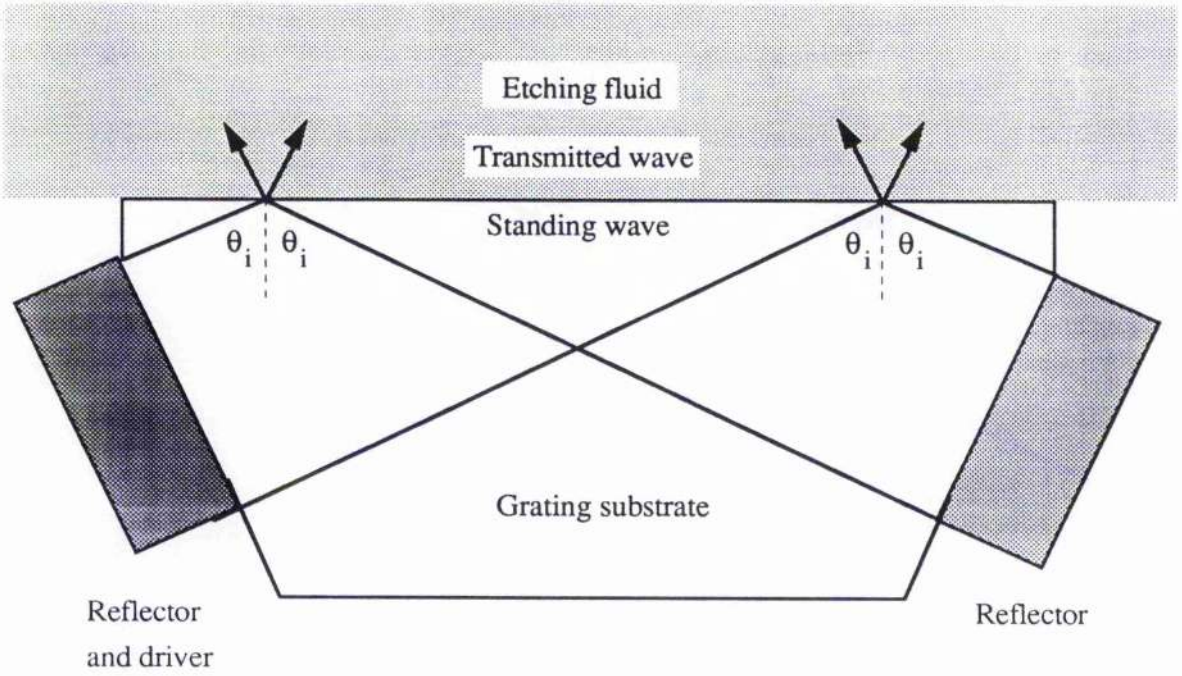

Figure 5.6. Schematic diagram of the standing wave cavity required to produce a permanent diffraction grating on a surface by using the transmission of longitudinal waves from the grating substrate into the etching fluid to provide a differential etching rate between the acoustic nodes and anti-nodes.

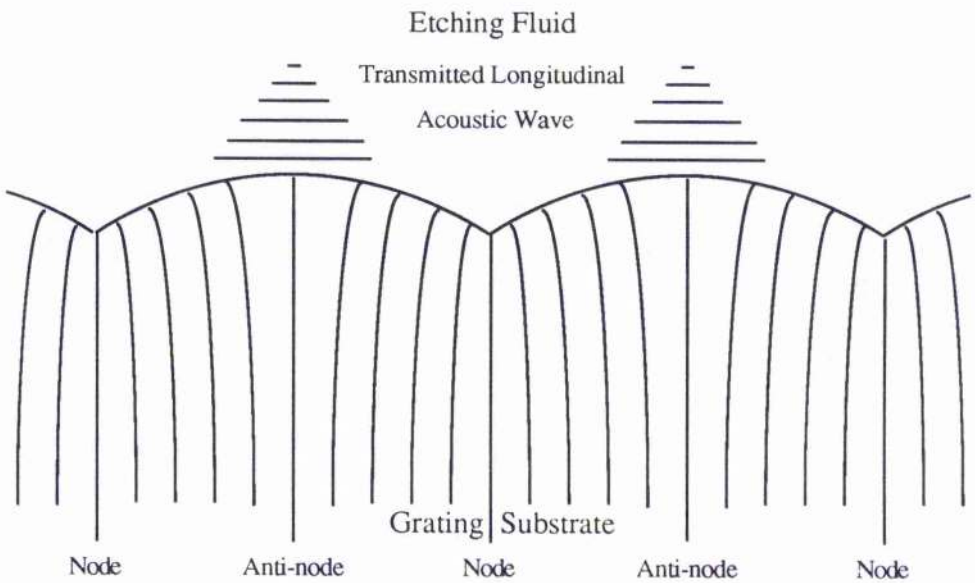

Figure 5.7. Schematic diagram showing acoustic compression waves in the etching fluid being generated by a transverse surface acoustic standing wave in the grating substrate. Note that all the anti-nodes are shown at their maxima to emphasise the effect and that in practice adjacent anti-nodes are 180° out of phase with each other at all times.

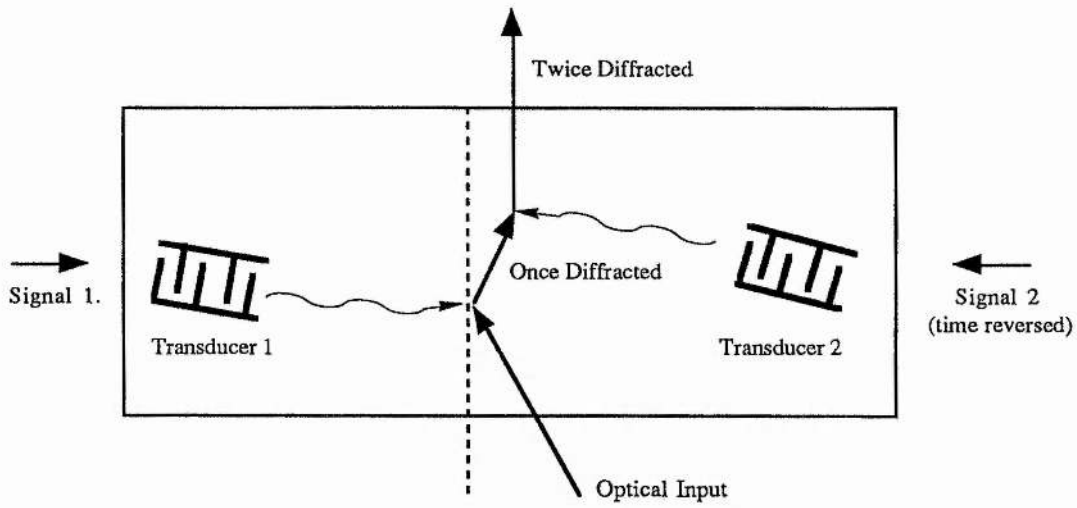

Figure 5.8a. Schematic diagram of an acousto-optic correlator where the difference in transducer attitude provides the difference between the angle of the doubly diffracted beam and the through-put beam. The double diffracted beam is the correlation between the two signals and beats with twice the signal frequency [5.1].

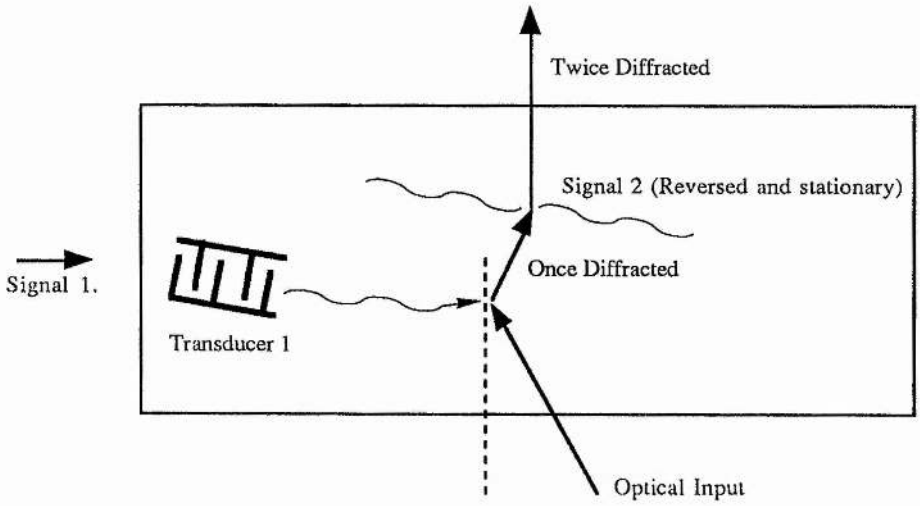

Figure 5.8b. Schematic diagram of an acousto-optic correlator where the difference between the tran: and the permanent stationary grating provides a difference in angle between the doubly diffracted beam and the through-put beam The double diffracted beam is the correlation between the two signals and has the signal frequency [5.1].

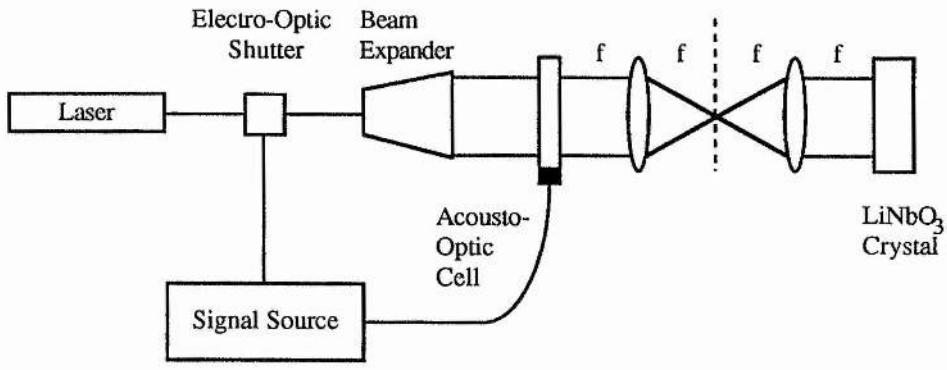

Schematic diagram of a possible set up for the photographic recording of a permanent acousto-optic damaging a lithium niobate crystal.

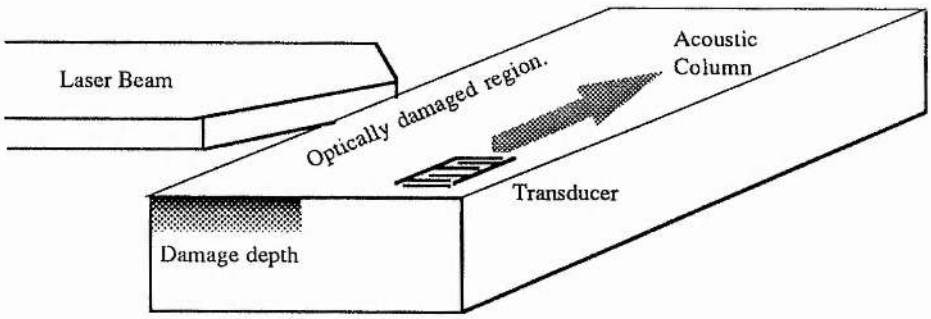

Diagram of the implementation of an acousto-optic correlator in a lithium niobate crystal, which stationary phase grating imposed on its surface by laser damage of the crystal structure as shown above.

Figure 5.9. Diagram of a photographic method for the implementation of permanent acousto-optic holograms for use in acousto-optic signal correlation.

§5.5 References.

[5.1] Acousto-optic Signal Processing (Theory and Implementation). N J Berg and J N Lee. Marcel Dekker Inc. New York, USA. 1983.

[5.2] The Diffraction of Light by Ultrasound. M V Berry. Academic Press (London) 1966.

[5.3] Volume Holography and Volume Gratings. L Solymar and D J Cooke. Academic Press (London). 1981.

[5.4] Holographic Storage in Lithium Niobate. F S Chen, J T LaMacchia and D B Fraser. Appl. Phys. Lett. **13** (7) page 223. 1968.

[5.5] Light, R W Ditchburn. Blackie & Son (Glasgow). 1963.

[5.6] Schott Guide to Glass. H G Pfaender. Van Nostrand Reinhold Co. (New York). 1983

[5.7] Advanced Engineering Mathematics. 6 Ed. E Kreyszig. John Wiley and Sons (Int.) 1989.

[5.8] Schott Technical Glasses Physical and Chemical Properties. Schott Glass Ltd, Stafford. (1989).

[5.9] Thermodynamics and an Introduction to Thermostatistics. H B Callen. John Wiley and Sons (Int.). 1985.

[5.10] Handbook of Physics. 3 Ed. American Institute of Physics. McGraw and Hill (New York). 1972.

[5.11] Acousto-optic Signal Processing: Fundamentals and Applications. P K Das and C M DeCusatis. Artech House Inc. Norwood, USA. 1991.

[5.12] Acoustics. A Wood. Blackie (London). 1940.

[5.13] Chemical Rubber Company Handbook of Material Science (Vol. 2). C T Lynch. CRC Press (New York) 1974.

[5.14] Photoresist resolution measurements during the exposure process. M S Sthel, C R A Lima and L Cescato. Appl. Optics **30** (35) page 5152. 1991.

[5.15] Optics. E. Hecht and A. Zajac. Addison-Wesley Pub. Co. Inc. 1977.

[5.16] Optical Recording Materials. G Savant and J Jannson. SPIE vol. **1461** Practical Holography V. page 79. 1991.

[5.17] Formation of the Holographic Structures of a Holographic Mirror by Post Exposure Treatment of a Dichromated Gelatin Layer. Yu. E Kuzilin, Yu. B Melnichenko and V V Shilov. Opt. Spectrosc. (USSR) **69** (1) page 106. 1990.

[5.18] Simplified Processing Method of Dichromated Gelatin Holographic Recording Materials. M H Jeong, J B Song and I W Lee. Appl. Optics **30** (29) page 4172. 1991.

[5.19] Self-Developing Materials for Holographic Recording.
D J Lougnot, C Carré, N Roumier and C Turck.
3rd International Conference on Holographic Systems, Components and Applications (IEE) **342** page 24. 1991.

[5.20] Theory of Holographic Recording on a Photopolymerised Material.
E S Gyulnazarov, V V Obukhovskii and T N Smirnov.
Optical Spectrosc. (USSR) **69** (1) page 109. 1990.

[5.21] Diffraction Efficiency of Bleached Photographically Recorded Interference Patterns. J Upatnieks and C Leonard. Appl. Optics **8** (1) page 85. 1969.

[5.22] Holographic Recording of Electrical Signals in Acousto-Optic Devices with a Nonsteady-State Reference Wave. A I Yeliseyev.
Sov. J. Commun. Technol. -Elect. **36** (14) page 99. 1991.

Chapter 6.

Potential Methods for the Creation of Distributive Feedback Mirrors and Other Phase Gratings in Optical Fibres.

§6.1 Introduction.

To date the only methods for obtaining optical feedback from a length of optical fibre have been stimulated Brillouin scattering [6.1], or cleaving the fibre so as to make mirror insertion possible.

A common method for creating high quality mirrors for narrow bandwidth reflection is thin film deposition to form what is known as a distributive feedback mirror, or DFB mirror [6.2]. A DFB mirror relies on a periodic change in refractive index to reflect incoming radiation of a specific frequency. The period of the refractive index perturbation must be half that of the wavelength of the light for maximum reflectivity [6.2].

We suggest that permanent DFB mirrors and other phase gratings can be created in optical fibres using acoustic waves (see Appendix 3).

The literature on acoustic waves in optical fibres concentrates on either using the acousto-optic effect to cause low frequency optical phase shifts [6.3 - 6.6], or using the acousto-optic effect to detect low frequency vibrations (< 100 MHz) [6.7], or stimulated Brillouin scattering [6.8 - 6.10], or acoustic soliton formation [6.11]. Stimulated Brillouin scattering (SBS) within optical fibres is a non-linear process whereby a high intensity optical wave causes electro-striction of the fibre and the resulting acoustic wave causes back-scatter of the incoming radiation. Most demonstrations of SBS in optical fibres have been achieved using light from argon ion lasers (λ = 5145 Å) [6.8, 6.9], but some work has been done at wavelengths commonly used for long distance optical links (λ = 1.5 μm) [6.10].

One of the disadvantages of using SBS for feedback within fibre optic systems lie in its being a non-linear optical effect that occurs at 'high' optical intensity [6.12]. An obvious case in point is where a mirror is required to complete a linear fibre laser cavity and the single pass gain of the laser does not take the intensity to a level where backward SBS becomes significant. Normally the fibre would be cleaved here and an external mirror system introduced to complete the cavity, but with a permanent fibre DFB mirror this would no longer be necessary and therefore the present practice would be improved on.

In this chapter we discuss methods for coupling high frequency acoustic waves into mono-mode optical fibres and suggest a method for "freezing" stress patterns generated by the acoustic waves into the fibres.

§6.2 Proposed Methods for Creating DFB Mirrors in Optical Fibres.

To create a DFB mirror in an optical fibre a mechanism is required for producing a periodic change in refractive index. Alongside this obvious requirement we impose the condition that the method of mirror creation does not require additional optical input to the fibre such as pump beams (see chapter 3), or any process that involves stripping the fibre of its cladding.

One method for creating DFB mirrors in optical fibres is to make use of acoustic waves to introduce a periodic change in refractive index. We now describe a method by which permanent DFB mirrors may be created acoustically in optical fibres.

§6.2.1 Methods for Introducing Acoustic Waves into Optical Fibres.

There are two methods for introducing acoustic waves into optical fibres. One is to use a piezo-electric block to stretch or squeeze the fibre to excite an acoustic wave [6.5, 6.6]. The other is to use SBS within the fibre to create the acoustic wave [6.8].

Single piezo-electric modulators tend to be used only at low frequencies (< 0.5 MHz). The frequency performance of piezo-electric transducers can be increased by an order of magnitude by employing phased array techniques [6.6] (figure 6.1). The acoustic frequencies at which optical back scattering occurs are of the order of 10 GHz, which at present cannot be generated in optical fibres by external piezo-electric drivers.

Stimulated Brillouin scattering on the other hand does occur at acoustic frequencies of the order of 10 GHz and is therefore a candidate for generating the strain pattern required for permanent DFB mirror creation. When SBS occurs the acoustic wave produced complies with the Bragg condition for diffraction (1.26),

$$\sin\theta_B = \frac{\lambda}{2\Lambda}, \tag{6.1}$$

and therefore has an acoustic wavelength, Λ, for a known input optical wavelength, λ. For backward SBS the Bragg angle, θ_B, is 90°. The acoustic wavelength is therefore half that of the incident light, which corresponds to the maximum reflection condition for the period of dielectric thin film DFB mirrors [6.2].

Thus we have two methods for generating acoustic waves in optical fibres, both of which have been demonstrated experimentally [6.4 - 6.6, 6.8 - 6.10]. At present SBS and low frequency (< 1 MHz) piezo-electric devices, respectively, are used to provide temporary

acoustic back-scattering and phase shifting of light within optical fibres. We suggest that acoustic waves may be used to create permanent diffraction gratings and DFB mirrors in optical fibres.

Before setting out the method for freezing acoustic waves into optical fibres we shall describe acousto-optic reflectors in terms of the coupled mode theory given in chapter 1.

§6.2.2 The Theory of Acousto-Optic Reflection in Optical Fibres.

On introducing an acoustic wave into an optical fibre it will be guided within the fibre by the difference in mechanical impedance between the fibre and its surroundings. In this treatment it is assumed that the acoustic wave is perfectly planar and propagates paraxially down the optical fibre. Assuming a planar acoustic wave which does not distort during transmission allows us to employ the coupled mode theory given in chapter 1 to describe acousto-optic reflection.

The interaction of a planar acoustic wave with propagating optical modes in a lossless optical fibre can be described by the coupled mode equations for the acousto-optic effect (1.27):

$$\frac{dA_1}{dz} = -i\frac{\beta_1}{|\beta_1|}\chi_{12}^{(\alpha)} A_2 \exp[-i\Delta\beta z] \tag{6.2a}$$

and

$$\frac{dA_2}{dz} = -i\frac{\beta_2}{|\beta_2|}\chi_{21}^{(-\alpha)} A_1 \exp[+i\Delta\beta z], \tag{6.2b}$$

where the phase term is given by

$$\Delta\beta = \beta_2 - \beta_1 - \frac{2\pi\alpha}{\Lambda} \tag{6.2c}$$

and the mode coupling constant $\chi_{12}^{(\alpha)}$ (4.5) is

$$\chi_{12}^{(\alpha)} = -\frac{\pi}{\lambda_o} n^3 p_c S^{(\alpha)} . \tag{6.3}$$

In equation (6.3), λ_o is the free space wavelength of the light, n is the refractive index of the interaction medium at that wavelength, p_c is the strain-optic constant and $S^{(\alpha)}$ is the α^{th} sinusoidal component's amplitude for the acoustically induced strain.

For direct optical reflection from the acoustic wave-fronts to occur the Bragg angle is $\pi/2$ and the phase match condition (6.2c) will have the form

$$k_{out} - k_{in} \pm k_g = 0. \tag{6.4}$$

The reflection efficiency within a fibre, ignoring the acoustic attenuation, obtained from coupled mode equations (6.2), is [6.13]

$$\frac{I_{out}}{I_{in}} = \frac{|\chi_{12}^{(\alpha)}|^2}{\gamma^2} \tanh^2 \gamma L, \tag{6.5a}$$

where γ is given by

$$\gamma = \left\{ \left[\frac{\Delta\beta}{2} \right]^2 + |\chi_{12}^{(\alpha)}|^2 \right\}^{1/2} \tag{6.5b}$$

and L is the length of the perturbation region.

The result quoted in (6.5) implies that, for an unattenuated acoustic wave which complies with the condition (6.4), the interaction length and the acoustic strain amplitude should both be as large as possible to maximise the mirror reflectivity.

Equation (6.5) does not apply to SBS, since SBS is a non-linear effect where the acoustic strains are generated by the optical input beam. We are only interested in SBS as a means for generating high frequency acoustic waves within an optical fibre, for subsequent freezing into the fibre, and thus do not require a theoretical treatment of the effect. In their "frozen" state the acoustic waves, initially generated by SBS, will comply with equation (6.5).

§6.2.3 A Possible Method for Producing Permanent Acousto-Optic DFB Mirrors in Optical Fibres.

So far permanent acousto-optic gratings have been dealt with on a theoretical level and the practicalities involved in their formation have not been considered. We now describe a possible method for their creation which employs the technique, already outlined in Chapter 5, for freezing acoustic standing waves into glass.

To create a permanent DFB mirror in an optical fibre an acoustic wave of half the frequency required by the Bragg condition (6.1) is introduced into the fibre. The acoustic wave then propagates along the fibre to a heated region which is at the fibre core's transition temperature (figure 6.2). The heated region is cooled at either end so as to give as high a temperature gradient as possible at its boundaries. The sharp changes in fibre temperature at the heated region boundaries will form an acoustic cavity in the heated region, which will support an acoustic standing wave (see figure 6.3). The strains associated with the acoustic standing wave are held within the fibre core, by the adiabatic heating process described in chapter 5, and form a periodic variation in the refractive index. The period of the refractive index variation, as in chapter 5, will be twice the acoustic input frequency. On cooling, the glass will hold the refractive index variation and a DFB mirror will be formed.

The frequency of the acoustic input is governed by three factors; (1) the change in the speed of sound, v_a, with respect to temperature, (2) the thermal expansion of the fibre and (3) the required grating period at the operating temperature. The acoustic frequency, $\nu_g(T_T)$, required at the transformation point, T_T, can be derived from the expression (5.5) to be

$$\nu_g(T_T) = \frac{1}{2}\left\{\nu_g(RT) + \frac{\nu_g(RT)}{v_a(RT)}\left[\frac{\partial v_a}{\partial T} - \frac{v_a}{L}\frac{\partial L}{\partial T}\right](T_T - RT)\right\}, \qquad (6.6)$$

where $\nu_g(RT)$ and $v_a(RT)$ are, respectively, the equivalent acoustic frequency and the speed of sound in the fibre at room temperature, RT. The frequency $\nu_g(RT)$ is that required to form a temporary acousto-optic DFB with the same characteristics as the permanent DFB mirror. If the variations in $\nu_g(RT)$ and $v_a(RT)$ with respect to temperature are small, then the value of $\nu_g(T_T)$ is approximately half that of $\nu_g(RT)$, due to the spatial frequency doubling effect, which occurs on freezing acoustic standing waves into glass (see section 5.2.1).

On replacing the grating frequency at room temperature with the $\theta_B = 90°$ Bragg condition (6.1) on grating spacing, a;

$$a = \frac{\lambda_o}{2n_o}, \qquad (6.7)$$

equation (6.6) can be put in the more applicable form;

$$\nu_g(T_T) = \frac{v_a(RT)n_o}{\lambda_o} + \frac{n_o}{\lambda_o}\left[\frac{\partial v_a}{\partial T} - \frac{v_a(RT)}{L}\frac{\partial L}{\partial T}\right](T_T - RT), \qquad (6.8)$$

where n_o is the refractive index of the fibre for light of wavelength λ_o at room temperature.

Figures for the variation in the speed of sound in fused silica, or associated qualities, with respect to temperature are not available. The coefficient of expansion with respect to temperature is $5 \times 10^{-7}\ ^{\circ}C^{-1}$. We therefore choose to ignore the temperature variation terms and thus obtain an approximate value of 5.75 GHz for the frequency required to create a permanent DFB mirror which will reflect a wavelength of 1.5 μm in a fused silica mono-mode optical fibre.

At present the most reliable method for introducing acoustic frequencies in the range 1 - 20 GHz into optical fibres is SBS. The equation (6.8) can be written in a form where the acoustic frequency at the transition temperature is replaced by the wavelength of the SBS pump radiation, $\lambda_p(T_T)$;

$$\lambda_p(T_T) = 2\lambda_o(RT)\frac{n_p(T_T)}{n_o(RT)}\left\{1 + \left[\frac{1}{L}\frac{\partial L}{\partial T}\right](T_T - RT)\right\}. \qquad (6.9)$$

If the expansion term is ignored again, a value of 2.9 μm is obtained for the pump wavelength required to create a permanent acousto-optic DFB mirror for 1.5 μm. As a 'rule of thumb' the pump wavelength for SBS will be approximately double that of the light to be reflected by the permanent DFB mirror.

The use of SBS and piezo-electric drivers will allow the construction of permanent acousto-optic DFB mirrors and other phase gratings in optical fibres.

§6.3 Concluding Remarks.

In this chapter we have suggested a possible method for creating DFB mirrors and other permanent gratings within optical fibres.

The use of such structures to create optical cavities [6.1, 6.14] and low loss optical coupling elements is well known in conventional discrete optics [6.14]. The advantages of having fibre integrated optics, over discrete optical components, including simple monolithic integrated optic devices, are those of low loss, high coupling efficiency and reduced production cost, all of which arise from the reduction in the number of joins between fibres and other components.

The use of ultrasound in optical fibres to produce phase gratings is well known and its application to the creation of permanent gratings is a logical step. We have suggested a method for freezing in the strains associated with an acoustic standing wave and have calculated the reflection efficiency of a DFB mirror constructed using this method.

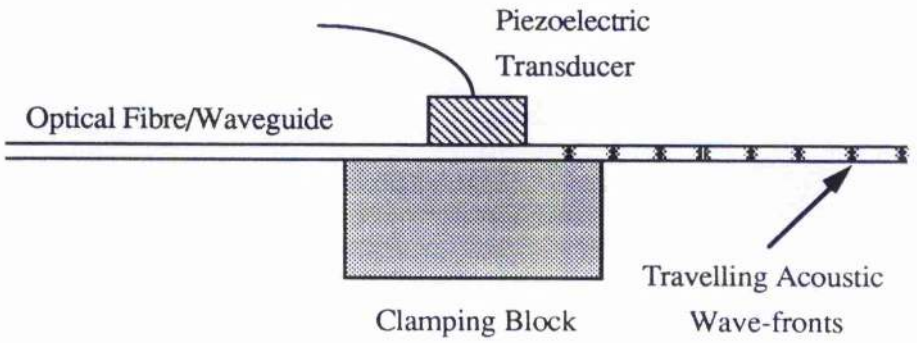

Schematic diagram of a standard single clamped piezo-electric driver system for the introduction of acoustic waves into an optical fibre or waveguide.

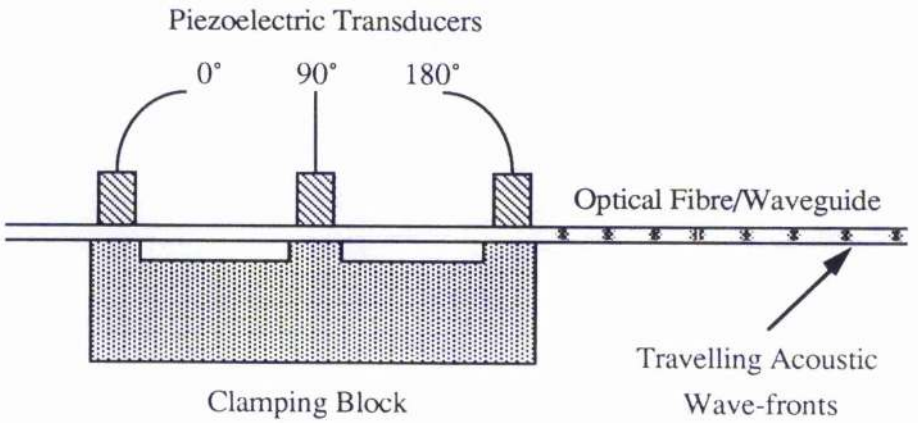

Schematic diagram of a three phase phased array clamped piezo-electric driver system for the introduction of acoustic waves into an optical fibre or waveguide [6.6].

Figure 6.1. Schematic diagrams of both single and phased array acoustic drive systems for the introduction of acoustic waves into optical fibres or waveguides.

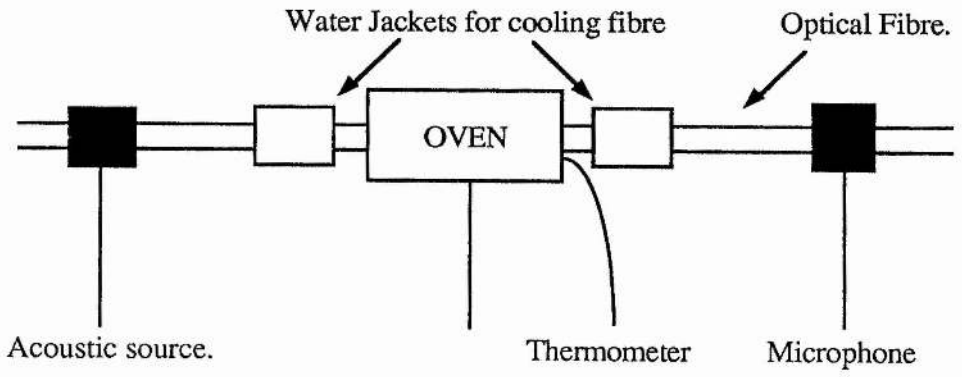

Figure 6.2. Schematic diagram of apparatus for constructing a permanent DFB mirror in an optical fibre using acoustic waves.

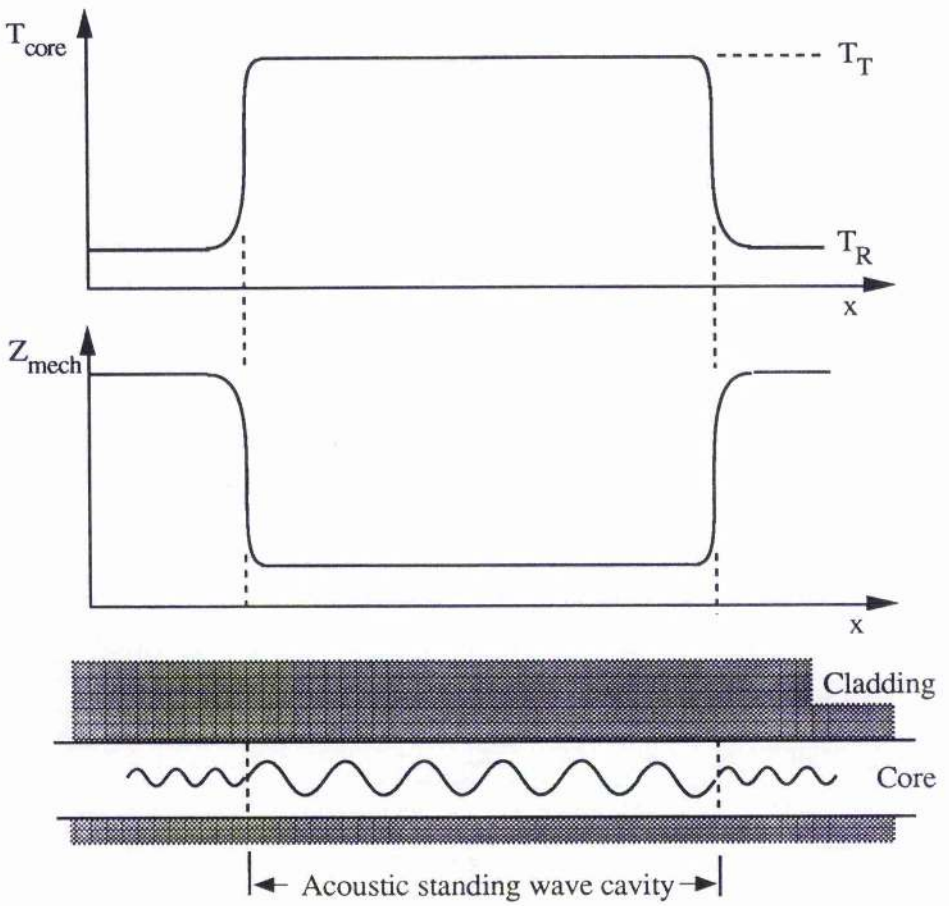

Figure 6.3. Diagram showing the process of formation for an acoustic standing wave cavity in an optical fibre due to the uniform heating of a section of the fibre.

§6.4 References.

[6.1] Quantum Electronics (3rd Ed.). A Yariv. John Wiley and Sons (Int). 1989.

[6.2] Thin-film Optical Filters. H A Macleod. Adam Hilger (London) 1969.

[6.3] Measurement of Sensitivity of Optical Fibres for Acoustic Detection.
J A Bucaro and T R Hickman. Appl. Optics. **18**(6) page 938. 1979.

[6.4] Acoustically Induced Birefringence in Optical Fibre.
L Flax, J H Cole, R P DePaula and J A Bucaro.
J. Opt. Soc. Am. **72**(9) page 1159. 1982.

[6.5] Acousto-Optic Frequency Shifting in Birefringent Fibre.
W P Risk, R C Youngquist, G S Kino and H J Shaw.
Opt. Lett. **9**(7) page 309. 1984.

[6.6] All Fibre Frequency Shifters Using Multiple Acoustic Transducers.
A P Ford, P A Greenhalgh and P A Davies.
Electronics Lett. **27**(13) page 1141. 1991.

[6.7] Single-Mode Fibre Ultrasonic Sensor.
R P De Paula, L Flax, J H Cole, and J A Bucaro.
IEEE J. of Quantum Electr. **QE-18**(4) page 680. 1982.

[6.8] Normal Acoustic Modes and Brillouin Scattering in Single Mode Optical Fibres.
P J Thomas, H M van Driel and G I Stegeman.
Phys. Rev. B. **19**(10) page 4986. 1979.

[6.9] Optical Frequency Shifter Techniques Based on Stimulated Brillouin Scattering in Birefringent Optical Fibre. C J Duffy and R P Tatam.
Appl. Optics **32**(30) page 5966. 1993.

[6.10] Identification of Longitudinal Acoustic Modes Guided in the Core Region of a Single Mode Optical Fibre by Brillouin Gain Spectra Measurements.
N Shibata, Y Azuma, T Horiguchi and M Tateda.
Opt. Lett. **13**(7) page 595. 1988.

[6.11] Nonlinear Behaviour of Sound and Its Application to Soliton Formation.
A Nakamura. Proc. IEEE 1988 Ultrasonics Symp. page 369. 1988.

[6.12] Role of Guided Acoustic Wave Properties in Single Mode Fibre Design.
C K Jen, J E B Oliveira, N Goto and K Abe.
Elect. Lett. **24**(23) page 1419. 1988.

[6.13] Coupled-Mode Theory for Guided Wave Optics. A Yariv.
IEEE J. Quantum Elect. **QE-9** (9) page 919. 1973.

[6.14] Handbook of Microwave and Optical Components (Vol. 4) K Chang (Ed.)
Wiley Interscience, New York. 1991.

Chapter 7.

Optical Frequency Division Multiplexing of Video Signals.

§7.1 Introduction.

A frequency division multiplexer, or 'optiplexer' has already been designed and built by W N Dawber et al [7.1, 7.2]. We have demonstrated the ability of such a system to deal with signals of high bandwidth like those in high speed data links or video transmission. For our demonstration we chose to multiplex a number of video signals because of their ready availability, simple visualisation and large bandwidth.

Dawber et al have estimated the total theoretical bandwidth of the optiplexer to be of the order of hundreds of gigahertz and have demonstrated an optiplexer with a single channel bandwidth of 1 MHz [7.1]. We demonstrate a working system carrying video signals, which have a single channel 3 dB bandwidth of 6 MHz. Dawber's figure for the total theoretical bandwidth of the optiplexer yields a number of the order of hundreds for the number of video channels that can be optically multiplexed. The true limitation of the bandwidth of a single device is that of the channelising Bragg cell (~2 GHz for a 2 GHz centre frequency cell), which limits the number of video channels that can be multiplexed to the order of a hundred.

The operating principles of the optiplexer apply in the case of two hundred channels to the same extent as they do in the case of two channels. For the sake of simplicity we chose to design and construct a two channel optiplexer.

§7.2 Principles of Operation.

Dawber's original device used one Bragg cell [7.3, 7.4] to create a number of equally spaced channels. This was done by modulating its 110 MHz rf source with 5 ns pulses at a rate of 5 MHz which has the effect of chirping the output before sending it to a Bragg cell. Viewed in the back focal plane of a lens at its focal length from the Bragg cell the light emerging from the cell is a spatial representation of the Fourier transform of the chirped signal. For the chirped signal this comprises a series of spots equally separated by a distance [7.1]

$$\Delta x = \frac{\nu_p f \lambda}{\nu_a}, \tag{7.1}$$

where: ν_p is the pulse frequency, f is the focal length of the lens and ν_a is the speed of sound in the Bragg cell. Such a series of spots would be contained within a sinc function round the centre frequency whose width depends on the pulse length. In Dawber's experiment the centre frequency was 110 MHz and the pulse length was 5 ns, which was the shortest pulse that could be obtained from the signal generator used [7.1].

The deflected beams contained frequency information as well as the spatial information, since on diffraction the light was frequency shifted by amounts equal to the acoustic frequency of the scattering phonons. Thus a series of separate channels was created each of which had a defined frequency and direction.

Onto these blank channels signals of bandwidth less than the channel separation were imposed by a set of Bragg cells operating as modulators. These modulated channels were then brought back together again along with a portion of the undiffracted beam to be detected (see figure 7.1).

The detector, a reverse biased BPX 65 photodiode, produced a current proportional to the incident radiation's intensity;

$$I = k \left| Ae^{i\omega_o t} + Be^{i(\omega_o+\omega_1)t} + Ce^{i(\omega_o+\omega_2)t} \right|^2, \tag{7.2}$$

where A,B,C are the amplitudes of the undiffracted beam and the two signal beams, respectively, and $\omega_o,\omega_1,\omega_2$ are the optical frequency and the two channel frequencies, respectively. On expanding equation (7.2) the two signal channel frequencies re-emerge along with the information encoded on them;

$$\begin{aligned} I = k\{ & ABcos(\omega_1 t) + ACcos(\omega_2 t) \\ & + A^2 + B^2 + C^2 \\ & + BCcos(\omega_1-\omega_2)t + BCcos(\omega_1+\omega_2)t\}. \end{aligned} \tag{7.3}$$

As well as the wanted terms there exist three dc terms and two cross terms representing the frequency sum and the frequency difference.

(In the multi-channel case it is interesting to note that, by taking the channels' amplitudes to be equal and unmodulated, the fraction of the ac current occupied by a single channel is the inverse of the square of the number of channels. For the general current expression

$$I = k\left|\sum_{n=0}^{N} A_n exp[i(\omega_o+\omega_n)t]\right|^2, \qquad \text{where } \omega_n=0 \text{ for } n=0,$$

the fraction of the ac current for channel n is $1/N^2$. The signal strength can be increased by increasing the reference beam amplitude, A_o, and decreasing the values for A_n, for all $n\neq0$, which increases the fraction of the ac current for each channel by the factor $M=A_o/A_n$. The only restriction on the value of M is the proximity to the background noise level of A_n.)

The detector current, given in equation (7.3), was buffered to remove the dc terms, amplified and then fed into a fourth Bragg cell interrogated by a second laser beam. The fourth cell was tuned to have maximum diffraction efficiency between ω_1 and ω_2, which automatically removed the sum and difference terms from the on-going signal. The information held on the two diffracted beams, represented by amplitudes B and C, was then recovered by way of two further detectors. Dawber has achieved a total system, modulation to detection, signal-to-noise ratio of 30 dB with a maximum modulation rate of 1 MHz and a modulation depth of 50%.

Starting from the operating principles for the optiplexer [7.1] we designed and built a two channel optiplexer (see figure 7.2). Our design does not include a channelising Bragg cell, as Dawber's did, since the modulating cells can be used to provide the different frequency shifts required for multiplexing. When using the modulating cells to produce the channel frequencies it is simpler to change the frequency separation of the two channels than when using a single channelising cell. Another advantage of the design in figure 7.2 over that in figure 7.1 for laboratory use is that it allows us to have greater intensities in each channel than is possible with a channelising Bragg cell configurations.

The ability to vary the frequency separation of the channels allows us to measure the cross-talk for different separations. There are two possible areas of cross-talk, XT_{12}, in an optiplexer system [7.1]. One is in the optiplexing interferometer and the other is in the receiving and deplexing stage (see figure 7.3). In the interferometer, the source of cross-talk is the imposed modulation of one channel intruding on the bandwidth of an adjacent channel's modulating signal when the channels are recombined. In the deplexing element, the cross-talk occurs due to the spatial proximity in the Fourier transform plane of the spectrum analyser [7.3]. The cross-talk between adjacent channels emerging from the deplexer is a function of the deplexing spectrum analyser's characteristics, assuming that the frequency separation in the interferometer stage is large enough to stop the channel side bands from over-lapping. The cross-talk relation for adjacent channels on re-emerging from

a spectrum analyser is [7.1];

$$XT_{12} = \frac{\int_{D-d/2}^{D+d/2} \text{sinc}(Lx/f)dx}{\int_{d/2}^{d/2} \sin(Lx/f)dx} \qquad (7.4)$$

where: d is the width of the channel in the Fourier transform plane;

D is the separation of the channels in the Fourier transform plane;

f is the focal length of the Fourier lens;

L is the Bragg cell aperture.

Equation 7.4 implies that the cross-talk between adjacent channels emerging from the deplexing spectrum analyser will tend to zero as the channel's frequency separation increases, given that the Bragg cell has a high Q and the Fourier transform lens has a focal length of the order of a metre. Thus, the only source of cross talk that needs investigation is that in the optiplexing interferometer.

§7.3 Experimental Results.

An optiplexer was built to the design shown in figure 7.2 with a couple of minor changes. The changes consisted of the use of a quarter-wave plate to bring the polarisation of the diffracted light round to that of the reference arm and the use of 10 cm lenses to focus the incident radiation into the Bragg cells and to recollimate the emerging radiation (see figure 7.4).

The Bragg cells used were of type AA.DTS.X which are produced by Automate et Automatismes of France. These cells have an operating frequency range of 100 MHz to

200 MHz. They can encode a video signal on the diffracted beam over a wide range of centre frequencies.

To shown that the A&A Bragg cells are capable of imposing a video signal on a laser beam a single video channel was set up. A single video channel was constructed using a modulated rf-source, a single Bragg cell and a photo-diode to receive the diffracted laser light (see figure 7.5).

We amplitude modulated a radio-frequency generator with a video signal, which was amplified by a $\times$ 2.5 amplifier (see appendix 2.2) to produce a signal with the video bandwidth and centre frequency 120 MHz. The signal produced by the rf generator was used to drive a Bragg cell which modulated a laser beam at the signal frequency. To obtain a diffracted spot that contained all the frequency information from the signal imposed on the Bragg cell it was necessary to focus the beam down into the cell in accordance with the expression;

$$\Delta\nu_{rf} = \frac{\pi w_1 v_a}{2\lambda f}, \tag{7.5}$$

where $\Delta\nu_{rf}$ is the bandwidth of the rf signal, λ is the beam's wavelength, f is the focal length of the lens and w_1 is the beam diameter at the front surface of the lens. The emerging light is recollimated by another lens and the diffracted light selected for transmission.

The transmitted light was focused down and detected by a BPX 65 photodiode which acts as a filter to remove all but the video signal. The detected signal was then amplified by a chain of video amplifiers (see appendices 2.3 and 2.4). The signal emerging from the video amplifiers was fed into an RGB monitor and the original picture was reproduced 'perfectly'. A section of the transmitted signal and the original signal were recorded to

show the lack of distortion (see figure 7.6). The rf spectra of the transmitted and received signals were also recorded and compare favourably with each other; i.e. there was no reduction of signal bandwidth. A delay of ~ 0.5 μs was recorded between the input signal and the received signal. This delay corresponds to the acoustic delay on transmission through the Bragg cell.

Using the information gained from constructing a single video channel we proceed to multiplexing two channels using the set-up depicted in figure 7.4. The multiplexed signal was received by a reverse biased BPX 65 photodiode in series with a 330 Ω resistor (see figure 7.7). The signal was then amplified by a chain of rf power amplifiers and fed into a second Bragg cell to be decoded and finally detected as two separate channels (see figure 7.3).

The section of the system that interests us most is the multiplexing interferometer. We wish to find out the minimum separation of adjacent channel's centre frequencies before cross-talk takes place and the channels cannot be separated by the deplexer.

The 3 dB bandwidth of a video signal is 6 MHz and thus the minimum frequency separation of the channels should be 6 MHz. The minimum separation can be tested experimentally by observing the change in an unmodulated channel due to the application of a signal to an adjacent channel over a range of frequency separations. The frequency separations used to test the cross-talk by the above method were 20, 10, 8 and 6 MHz. The observed change in frequency profiles around the unmodulated channels are shown in figure 7.8. The change in cross-talk is registered as a gradual encroachment of the signal onto a blank channel. The encroachment of the video signal onto the blank channel only becomes distinct from noise when the blank channel is separated from the video channel by 10 MHz or less. The cross-talk signal did not become significant until the video channel was within 6 MHz of the blank channel; i.e. it is of the same order of magnitude as the signal on the second channel at its 3 dB point.

To demonstrate the difference in cross-talk between a system operating with a channel separation of 6 MHz and one operating with a channel separation of 10 MHz a frequency profile of two received video channels was taken for the two frequency separations (see figure 7.8). The two graphs in figure 7.8 show clearly that for a separation of 10 MHz the signal drops to background noise between the two channels and that for a separation of 6 MHz the two signals run into each other.

§7.4 Improvements on the Current Implementation.

In our implementation, based on the design shown in figure 7.2, the scope for expanding the system to deal with a greater number of channels is limited due to the cost of Bragg cells, the efficiency of our beam splitting technique and the space it takes up.

To improve on the current design we would revert to the configuration shown in figure 7.1 and replace the modulating Bragg cells with integrated optical phase modulators. Recent developments in integrated optic have produced Mach Zehnder interferometric modulators with upper frequency limits exceeding 4.5 GHz and modulation depth of 12.7 dB for applied voltages of the order of 10 volts [7.5, 7.6, 7.7]. Thus the major limitation of the optiplexer is provided by the single orientation bandwidth of the channelising Bragg cell, which for acousto-optic Bragg technology is approximately 2 GHz.

The single orientation bandwidth of current Bragg cell technology is limited by acoustic absorption and other mechanical effects [7.3]. To improve on the total multiplexer bandwidth Dawber et al suggested the use of the TWEOD device described in chapter 2. An interim solution would involve using a primary channelising cell to split the beam into two separate beams with a frequency separation equivalent to the bandwidth limit of the secondary channelising cell. The secondary channelising cell would be placed at right angles to the primary channelising cell thus making it possible for the two beams produced

by the primary cell to use the secondary cell, at different points, to produce two separate arrays of channels which can be modulated and multiplexed (see figure 7.9). To deplex the channels the frequency range, over which the channels are spread, is split in two. Then the extra frequency, imposed on half the channels by the primary channelising Bragg cell, is removed electronically before the two halves of the channel array are fed into two separate deplexing Bragg cells.

§7.5 Conclusions.

We have designed and constructed a two channel optical frequency division multiplexer which was able to transmit two video signals simultaneously as optical information and a receiver for de-multiplexing the optically transmitted signals. The combination of the multiplexer and the receiver managed to pass two video signals simultaneously down one optical fibre without cross-talk occurring between the two channels. The transmission of video channels using an optical frequency division multiplexer constitutes an order of magnitude improvement on the single channel bandwidth demonstrated by Dawber [7.1].

The minimum channel separation from centre frequency to centre frequency, for which no cross-talk occurs, was found to be 10 MHz. The minimum channel separation that we found is greater than the expected separation given by the video 3 dB bandwidth of 6 MHz.

The two channel video optical multiplexer that was constructed in the laboratory is large (i.e. filled an area of two square metres) and sensitive to misalignment. We propose that a small integrated optic and optical fibre device can be constructed to deal with a large number of channels.

Thus we conclude that a multitude of high bandwidth (e.g. video signals with bandwidth 6 MHz) can be optically frequency-division multiplexed and be transmitted either though free space or down an optical fibre to be received and decoded by a second Bragg cell.

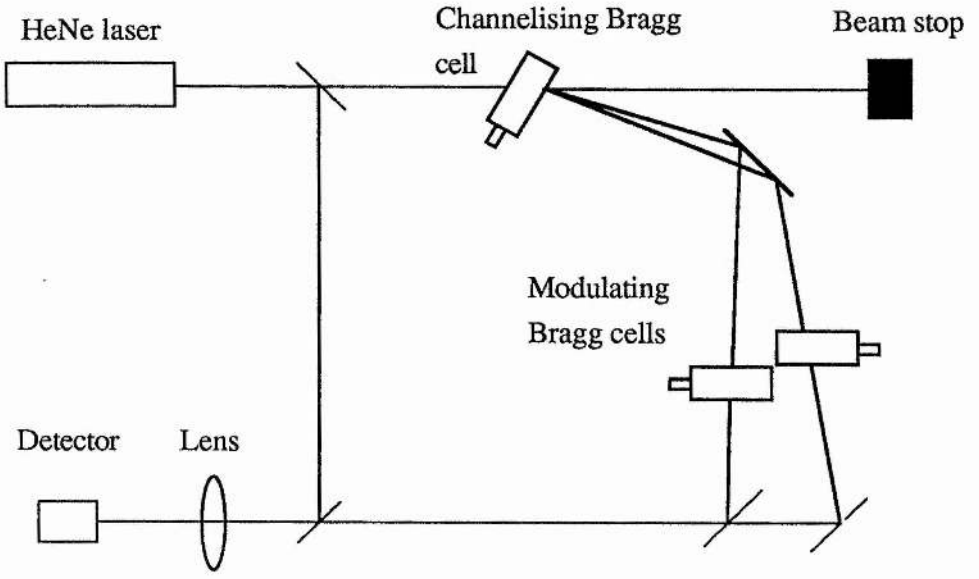

Figure 7.1. Diagram of original optical multiplexer or "optiplexer".

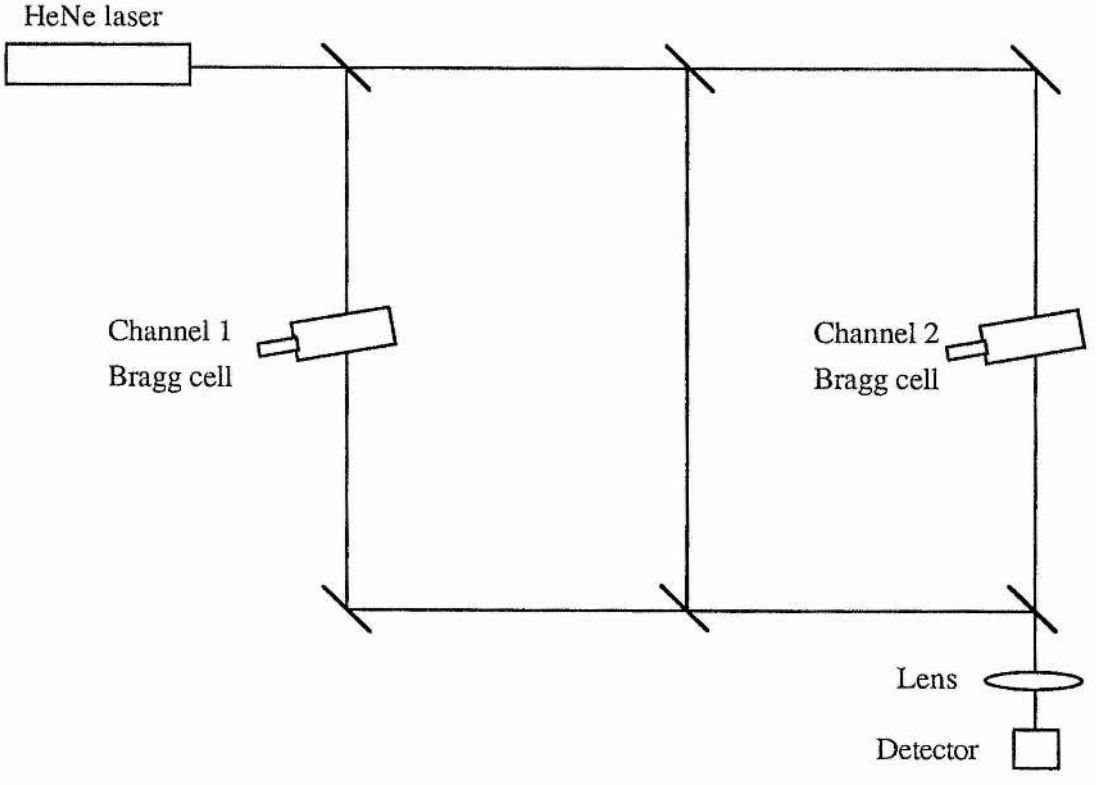

Figure 7.2. Amended design for optical multiplexer. Note that the beams shown as on-going from the Bragg cells are the diffracted beams.

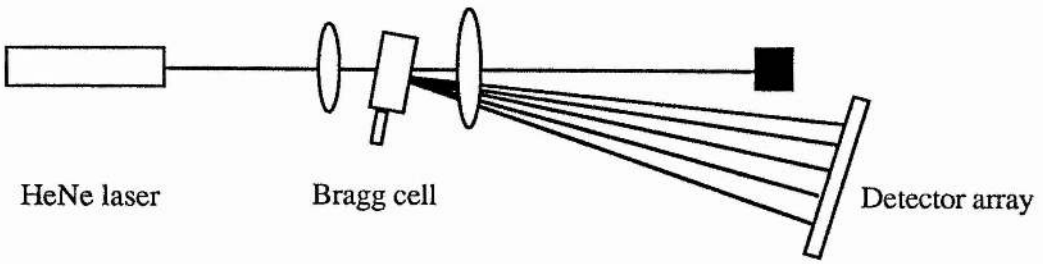

Figure 7.3. Optics for a multi-channel receiver and deplexer.

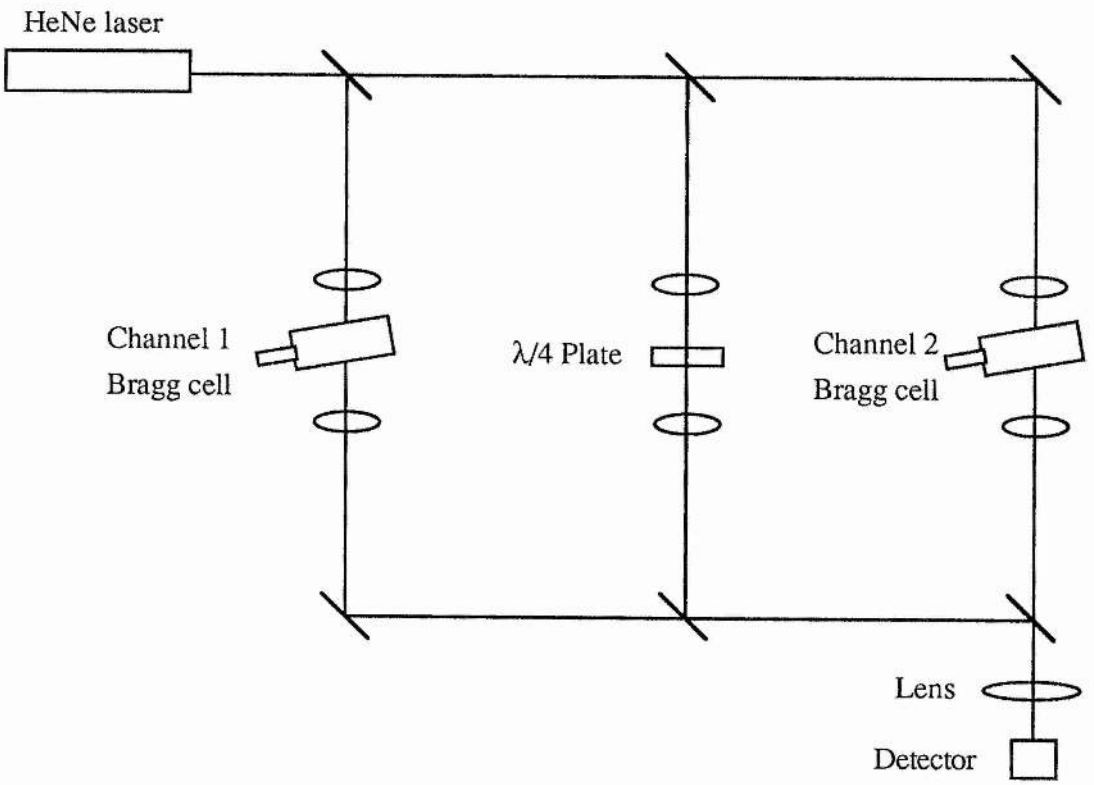

Figure 7.4. Amended design for optical multiplexer with additional optics to increase the quality of both beams and signals.

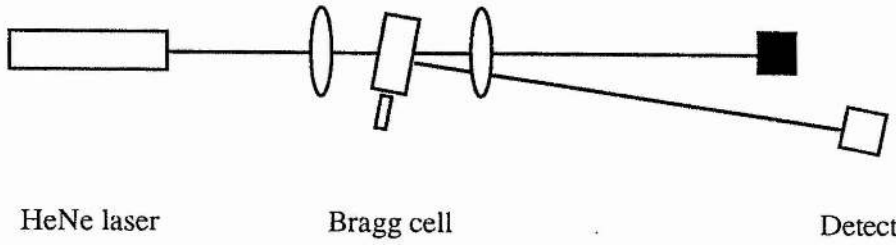

Figure 7.5 Optics for a single optical video channel where the Bragg cell is used as an amplitude modulator.

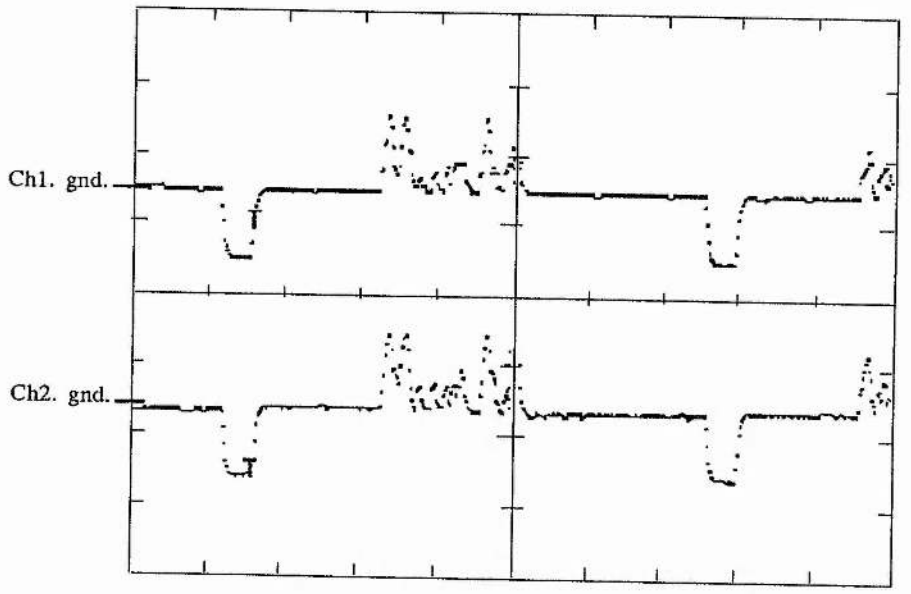

Figure 7.6a. Plots of a video signal entering (Ch1) and leaving (Ch2) a single optical video channel. The voltage per vertical division is 500 mV and the time base is 10 μs per division.

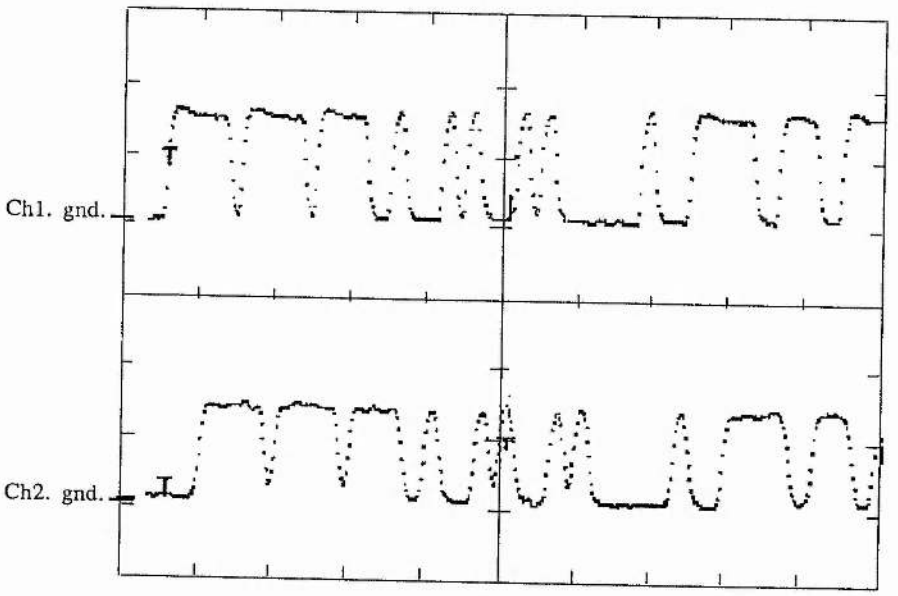

Figure 7.6b. Plots of a video signal entering (Ch1) and leaving (Ch2) a single optical video channel. The voltage per vertical division is 500 mV and the time base is 1 μs per division. Note the 0.5 μs delay between the input and output is due to the acoustic propagation delay in the Bragg cell.

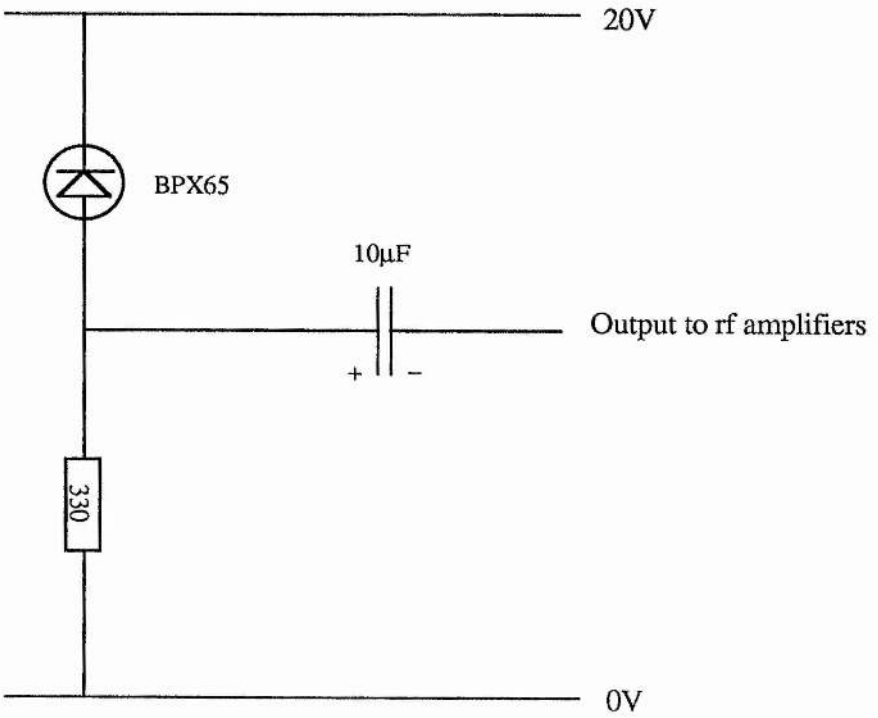

Figure 7.7. Electronics for the receiving detector.

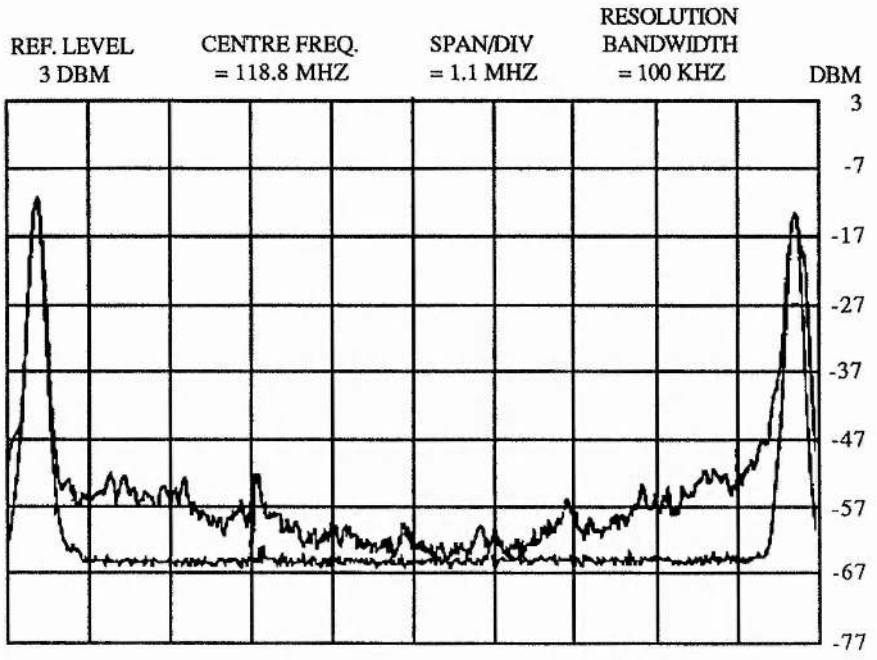

Figure 7.8a. Spectrum of two video channels with centre frequencies separated by 10 MHz and of two blank channels with the same frequencies.

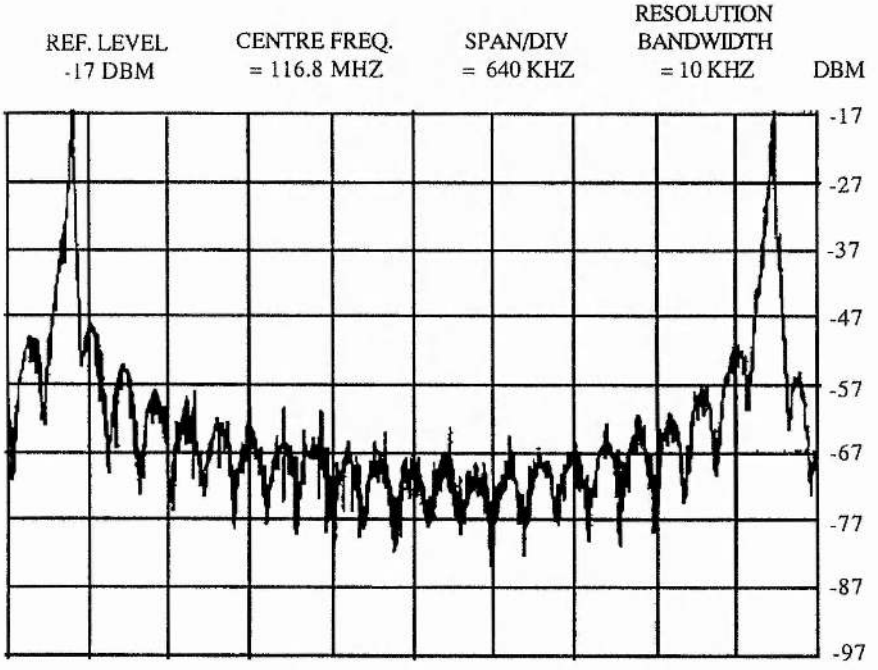

Figure 7.8b. Spectrum of two video channels with centre frequencies separated by 6 MHz.

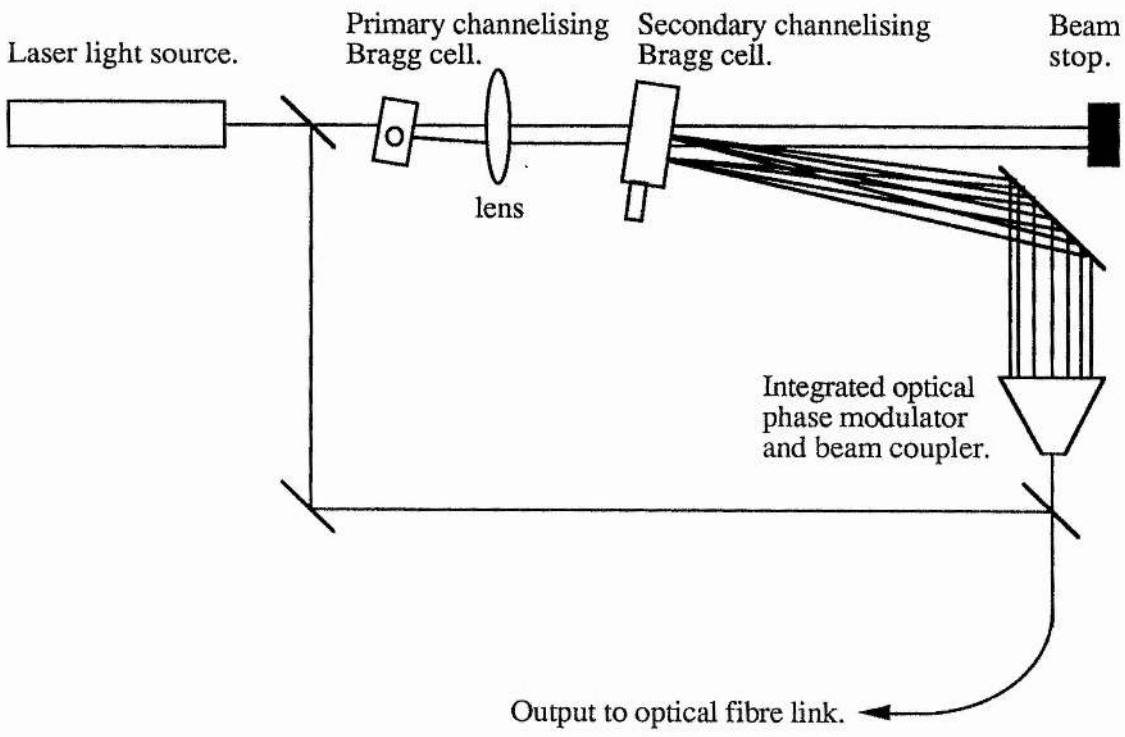

Figure 7.9. Diagram of an alternative implementation of the optiplexer where the signal array is split in two by a primary channelising Bragg cell so as to double the system bandwidth to twice that of the secondary channelising Bragg cell.

§7.6 References.

[7.1] Radio-frequency Analysis Using Optical Signal Processing. W N Dawber Ph.D. Thesis, Uni. of St. Andrews, Scotland. 1991.

[7.2] An Optical Multiplexer.
W N Dawber, B P Condon, P F Hirst, A Shaw and P Sutton.
U.K. Patent Application No. 9005647. 13 March 1990.

[7.3] Acousto-optic Signal Processing (Theory and Implementation).
N J Berg and J Lee. Marcel Dekker Inc. New York, USA. 1983.

[7.4] Acousto-optic Signal Processing: Fundamentals and Applications.
P K Das and C M DeCusatis. Artech House Inc. Norwood, USA. 1991.

[7.5] A High Frequency GaAs Optical Guided-Wave Interferometer.
J P Donnelly, N L DeMeo, G A Ferrante and K B Nichols.
IEEE J. of Quantum Electronics **QE21**(1) page 18. 1985.

[7.6] Broadband Y-Branch Electro-optic GaAs waveguide Interferometer for 1.3μm.
P. Buchmann, H Kaufmann, H Melchior and G Guekos.
Appl. Phys. Lett. **46**(5) page 462-4. 1985.

[7.7] GaAs PIN Electro-optic Travelling-wave Modulator at 1.3μm. S H Lin, S Y Wang and Y M Houng. Electronics Lett. **22**(18) page 934. 1986.

Chapter 8.

Conclusions.

In this work we have given descriptions of several new methods for the creation of optical diffraction gratings and their uses. The majority of the gratings that have been described are phase gratings. All phase gratings can be described in terms of the coupled mode theory [1.14] for the interaction of light with non-uniform transparent media given in chapter 1.

Of the gratings described only the TWEOD (Chapter 2) has been mentioned prior to this work; it having been conceived by Dawber et al [1.10, 1.11]. In section 2.2 the TWEOD was given a firm theoretical footing which was developed to the point where the interaction of the design parameters can be well understood. Several preliminary experiments were done on single crystal $BaTiO_3$ TWEOD, which point towards the embodiment of an actual device operating at a single frequency of 10 GHz.

An operating TWEOD would prove to be more than a novelty device, since it would stretch the range of real time rf spectrum analysis from its current acousto-optic limit of ~3 GHz towards 100 GHz.

Another device that promises a high speed response is the pump beam generated grating within a laser medium discussed in chapter 3. The speed of a grating in a laser medium is governed by the decay time of the optical cavity used, or in the absence of the optical cavity the decay time of the chosen laser transition [3.6]. Such a grating implementation lends itself to high frequency modulation and, given the correct pump angle, will lead to a modulation frequency angular response akin to that of current acousto-optic Bragg cells .

The use of ferroelectric crystals, mainly $LiNbO_3$, for the construction of acousto-optic Bragg diffraction cells is now common place [1.1]. The use of such crystals for Bragg cell construction has advantages and disadvantages attached to it. The advantages are: they are birefringent and therefore in the correct orientation will give large angular responses for

small acoustic frequency changes (i.e. high Q's are readily obtainable), they are piezo-electric and therefore require no external acoustic drive other than two electrodes, and they have high strain-optic constants, which allows high diffraction efficiencies for low acoustic input powers. The disadvantages are: optical quality ferroelectric crystals are expensive and the price rises exponentially with size, and they have high acoustic attenuation coefficients, which limits the effective acoustic column length. The advantages of using birefringent ferroelectric crystals for constructing high Q low τB Bragg cells far outweighs the disadvantages, but for the construction of high Q, high τB Bragg cells they do not.

In chapter 4 we propose a method for the creation of permanently, uniformly stressed glass which could be employed in Bragg cell manufacture. The advantage of using prestressed glass instead of unstressed glass is that it is birefringent. The advantages of using prestressed glass over birefringent ferroelectric crystals is that it has a low coefficient of acoustic attenuation and has a lower cost. The disadvantages are the loss of the internalised piezo-electric driver and the reduction in diffraction efficiency. Such prestressed birefringent glass could be used to construct high Q, high τB, low cost acousto-optic Bragg cells.

The use of uniformly stressed glass for Bragg cell construction leads us onto the use of periodically prestressed glass for phase grating creation. In chapter 5 we put forward a method for preserving the strains associated with acoustic standing waves in glass. The creation of permanent diffraction gratings using acoustic techniques is not confined to permanent phase gratings in glass and in chapter 5 a range of possible techniques for "freezing" acoustic standing waves was described for a range of different media. An acoustic technique for the etching of surface gratings onto suitable substrates was also discussed. The permanent acoustic gratings described in chapter 5 have uses ranging from simple single frequency diffraction gratings to masks for acousto-optic signal processing.

The techniques for "freezing" permanent acousto-optic gratings and masks into glass can also be applied to the production of permanent phase gratings in optical fibres. In chapter 6 we suggested that permanent DFB mirrors could be "frozen" into optical fibres. The obvious applications for such structures would be the creation of DFB lasers, laser mirrors and other phase gratings within continuous lengths of optical fibre, which could be used in optical communications for signal boosting and processing.

All the devices mentioned in chapters 2-6 have potential applications within the optical frequency division multiplexer (or optiplexer) described in chapter 7.

The optiplexer as envisaged by Dawber *et al* [1.10, 7.7] comprises four stages. In the first stage an array of frequency and spatially separated channels are created by an acousto-optic Bragg cell. The second stage comprises an array of electro-optic phase modulators which encode phase information on the separated channels which are then combined into a single beam. In the third stage the information carrying beam is recombined with the original optical beam on the surface of a photodiode. The resulting rf signal is then imposed on another Bragg cell which separates the channels again for reception by an array of photodetectors in the fourth stage to yield the transmitted information.

We foresee that the TWEOD devices, when developed, will be capable of replacing both the acousto-optic Bragg cells within the optiplexer and thus provide an order of magnitude increase in its total bandwidth. If a continuous rf spectrum is used with the TWEOD some method would be required to spatially differentiate the channels; the diffraction gratings produced by the methods described in chapter 5 could provide such a differentiation. Thus we see the TWEOD as an integral part of an optiplexer system as well as a useful tool for high frequency spectrum analysis.

The net effect of the potential technologies described within this work will be to increase the bandwidth for optical communications, to increase the resolution of current acousto-optic devices without loss of Q and to reduce the cost of some holographic components.

Appendix 1.

Dielectric Properties of Barium Titanate.

§ A1.1 Introduction.

Barium titanate has two qualities which makes it desirable for use in a TWEOD device. These are a high dielectric constant from dc to radio frequencies and a high electro-optic constant; which arise from $BaTiO_3$ belonging to a class of materials known as ferroelectrics.

Ferroelectrics are a section of a much larger set of substances called pyroelectrics. A pyroelectric has the property that a single crystal with no surface charge is polar; the polarity of the crystal is normally masked by twinning or by surface charges and is only revealed by heating the crystal, hence the name. A ferroelectric has the additional property that the polarisation can be reversed by applying a sufficiently strong electrical field; in a strong alternating field it shows hysteresis. [A1.1].

The property of ferroelectricity is in itself of no interest to us†, but the majority of the literature on $BaTiO_3$ is in connection with this property. Most of investigations into the ferroelectric effect in $BaTiO_3$ deal with the dielectric constant as a quantity and as such yield a large amount of information about it.

§ A1.2 The Dielectric Constant of $BaTiO_3$.

Since the 1940's many measurements of the dielectric tensor for single $BaTiO_3$ crystals have been made, the majority of them being with dc electric fields over a range of temperatures. We list a selection of the dc dielectric constants obtained to date in chronological order in table A1.

---

† Although the ferroelectric effect is of no interest, the class of materials is worth investigating further to identify other materials with high dielectric constants at radio frequencies.

Table A1

Reference	Year	Temperature	ε_c	$\varepsilon_{a,b}$
[A1.2]	1948	24°C	1000	2150
				1500
[A1.3]	1948	24°C	1250	1420
[A1.4]	1949	24°C	20	4300
[A1.5]	1955	24°C	------200------	

The selection in table A1 demonstrates the wide range of values given for the dc room temperature dielectric constant. Various factors may be used to explain this diversity:

(i) impurities in the crystal can act as dopants which change the crystal's bulk properties,

(ii) the uniformity of the polarisation within a single crystal can vary from sample to sample due to zoning effects outlined by Merz [A1.4],

(iii) crystal structure quality is a function of the different production techniques used (i.e. the number of discontinuities within the crystal lattice *et cetera*).

All the references quoted in table A1 do agree on one property of $BaTiO_3$; the existence of the Curie points for crystalline $BaTiO_3$ and their approximate temperatures. Devonshire [A1.6] states the four crystal states of $BaTiO_3$ and the position of the intervening Curie points, which are as follows: up to –100°C $BaTiO_3$ is rhombohedral; from –100°C to –5°C it is orthorhombic; from –5°C to 120°C it is tetragonal and above 120°C it is cubic in structure. To demonstrate the variation in dielectric constant with temperature we quote Merz's graph in figure A1.1 [A1.4].

The temperatures for the Curie points also vary according to author; the most restrictive Curie points for the tetragonal state are at 15°C and 90°C [A1.2] whereas the largest range for the state is from –5°C to 120°C [A1.4]. The operational regime for a poled tetragonal $BaTiO_3$ crystal is given as 15°C to 80°C by the crystal manufacturer JTT International Inc. [A1.7].

To explain the high values for the dielectric constant of $BaTiO_3$ and its variation with temperature several theoretical models have been proposed. These theories can be split into two distinct groups; the semi-classical models [A1.3, A1.8] and the phenomenological studies [A1.1, A1.5, A1.6, A1.9].

The value of the dielectric constant of $BaTiO_3$ at radio frequencies has also been investigated, but only at the bottom of the infra-red spectrum [A1.10, A1.11] or as a means of examining the nature of a Curie point [A1.9].

The two infra-red papers [A1.10, A1.11] confirm the Curie point temperatures. One of them, Ballantyne [A1.10], gives a graph of the reflectivity against frequency between dc and 120×10^{12} Hz for a selection of temperatures. In his graphs Ballantyne gives measured values for the reflectivity at 25 GHz from which we have calculated the dielectric constant to be as follows:

$$\varepsilon_a(25\ \text{GHz}, 24°\text{C}) = 576, \qquad \varepsilon_a(25\ \text{GHz}, 100°\text{C}) = 121.$$

The room temperature value for $\varepsilon_a(25\ \text{GHz})$ does not agree with the result of Deorani [A1.8] which gives a value of $\varepsilon_a(25\ \text{GHz}) \approx 2050$. Also Ballantyne's graph does not show the rapid drop in reflectivity between 10 GHz and 100 GHz one would expect from Deorani's results for the dielectric constant.

The diversity of values for the dielectric constant ε_a lead us to use and educated guess for its value. We choose to use the same value as Dawber [A1.12], $\varepsilon_a = 3000$, since he used it in the original $BaTiO_3$ calculations.

In the light of the range of values for the dielectric constant of $BaTiO_3$ at any frequency local measurements of ε_a at specified frequencies are advisable and should be made.

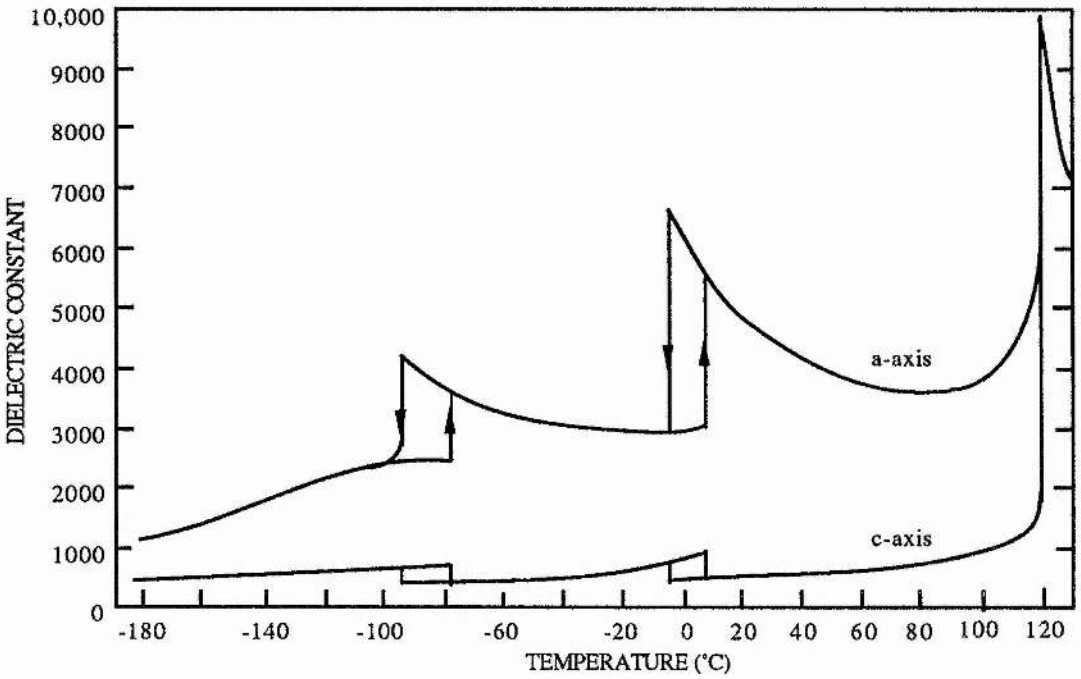

Figure A1.1. Graph of the dielectric constant against temperature for a single domain $BaTiO_3$ crystal [A1.4].

A1.3 References.

[A1.1] Theory of Ferroelectrics. A F Devonshire.
Advances in Phys. (Phil. Mag.) **3**(10) page 85. 1954.

[A1.2] Domain Structure and Dielectric Response in Barium Titanate Single Crystals.
B Matthias and A von Hippel. Phys. Rev. **73**(11) page 1378. 1948.

[A1.3] Theoretical Model for Explaining the Ferroelectric Effect in Barium Titanate.
W P Mason and B T Matthias. Phys. Rev. **74**(11) page 1622. 1948.

[A1.4] The Dielectric Behaviour of $BaTiO_3$ Single-Domain Crystal. W J Merz.
Phys. Rev. **75** page 687. 1949.

[A1.5] Dielectric Behaviour of Barium Titanate in the Paraelectric State.
M E Drougard et al. Phys.Rev. **98**(4) page 1010. 1955.

[A1.6] Theory of Barium Titanate. A F Devonshire. Phil. Mag. **40** page 1040. 1949.

[A1.7] JTT International Inc.
3403 Technological Ave., Suit 12, Orlando, FL 32817 USA.
Tel. (407) 382-2700.

[A1.8] Dielectric behaviour of ABO_3 type ferroelectric perovskite. S C Deorani.
Indian J. Pure & Appl. Phys. **29** page 526. 1991.

[A1.9] The Dielectric Properties of $BaTiO_3$ Single Crystal in the Paraelectric State
from 1 kc/sec to 2000 Mc/sec. E Stern and A Lurio.
Phys. Rev. **123**(1) page 117. 1961.

[A1.10] Frequency and Temperature Response of the polarization of Barium Titanate. J M Ballantyne. Phys. Rev. **136**(2A) page A429. 1964.

[A1.11] Radiofrequency Analysis Using Optical Signal Processing. W N Dawber. Ph.D. Thesis. University of St. Andrews, Scotland. 1991.

Appendix 2.

Electronic Amplification of Video Signals for use in the Optiplexer.

§ A2.1 Introduction.

In this appendix we describe the electronics circuits devised to increase the amplitude of the video signals in the optiplexer. Video amplification is required in two places within the system; firstly to increase the signal strength before it is used to modulate the rf source for introduction into the modulating Bragg cell and secondly to amplify the signal from the demultiplexer to a level sufficient to drive an RGB monitor. Section A2.2 deals with the amplifier which takes the video output from a video recorder / computer and takes it to the correct level for introduction into the rf generator as a modulation. Sections A2.3 and A2.4 deal with the amplifiers which take a deplexed channel from its received state to the required level for introduction into an RGB monitor.

§ A2.2 Input Amplifier.

The input amplifier raises a standard video output to the level were it can be used to modulate the rf-source which then drives the Bragg cell.

The input electronics for each channel consists of a two stage amplifier which converts the input signal from a 1 V dc bias with a 850 mV peak signal voltage and a –500 mV TTL marker to a 2 V dc bias with a 2 V peak signal voltage and a –1.25 V TTL marker. This amplification means that the modulation of the rf-signal results in the Bragg cell modulating the incoming laser beam with a maximum diffraction efficiency of about 50%. The circuit diagram for the input amplifier is shown in figure A2.1.

§ A2.3 Photodiode and Primary Output Amplifier.

The photodiode and primary output amplifier detects the diffracted light from a single channel of the deplexing spectrum analyser and amplifies the signal by a factor of 5.

The primary output amplifier is only a slight variation on the input amplifier. It takes the output from a reverse biased BPX 65 photodiode in series with a 1kΩ resistor and amplifies its ac component only. The amplifier consists of two stages each having a voltage gain of 5 which yields an overall gain of just under 23. The output resistance of 1 kΩ means that only 90% of the op-amp's output voltage is transmitted and thus the overall gain is reduced.

Note that the amplifier's bandwidth automatically excludes the rf carrier frequency from the incoming signal and leaves only the video signal to be amplified.

The circuit diagram for the photodiode and amplifier is shown in figure A2.2.

§ A2.4 Variable Video Amplifier.

The secondary output video amplifier has a variable gain which allows us to achieve the correct signal level for introduction into a standard RGB monitor.
The variable video amplifier is yet another version of the input amplifier. The amplifier consists of two stages; the first stage is a $\times 5$ inverting stage and the second stage is variable between a gain of zero and 5. It has an ac output coupling impedance of 75 Ω to a 5 volt dc level within the amplifier and a 175 Ω impedance to external ground. The circuit diagram for this amplifier is shown in figure A2.3.

§ A2.5 Electronic Component Details.

All the above amplifiers were built with Burr Brown OPA620-KP op-amps. These have a stated slew rate of 250 V/ms so that they can cope easily with amplifying video signals with signal bandwidth of 6 MHz. At peak outputs approaching the OPA620-KP op-amp's supply voltage of 5 volts the amplifier starts to oscillate at 10 MHz which we compensated for by putting in an extra resistance on the positive input to increase the stability.

The other electronic component of note is the BPX 65 photodiode which has a stated junction capacitance of 3.5 pF on applying 20 V, which allows us to detect frequencies up to 500 MHz with a 50 Ω load.

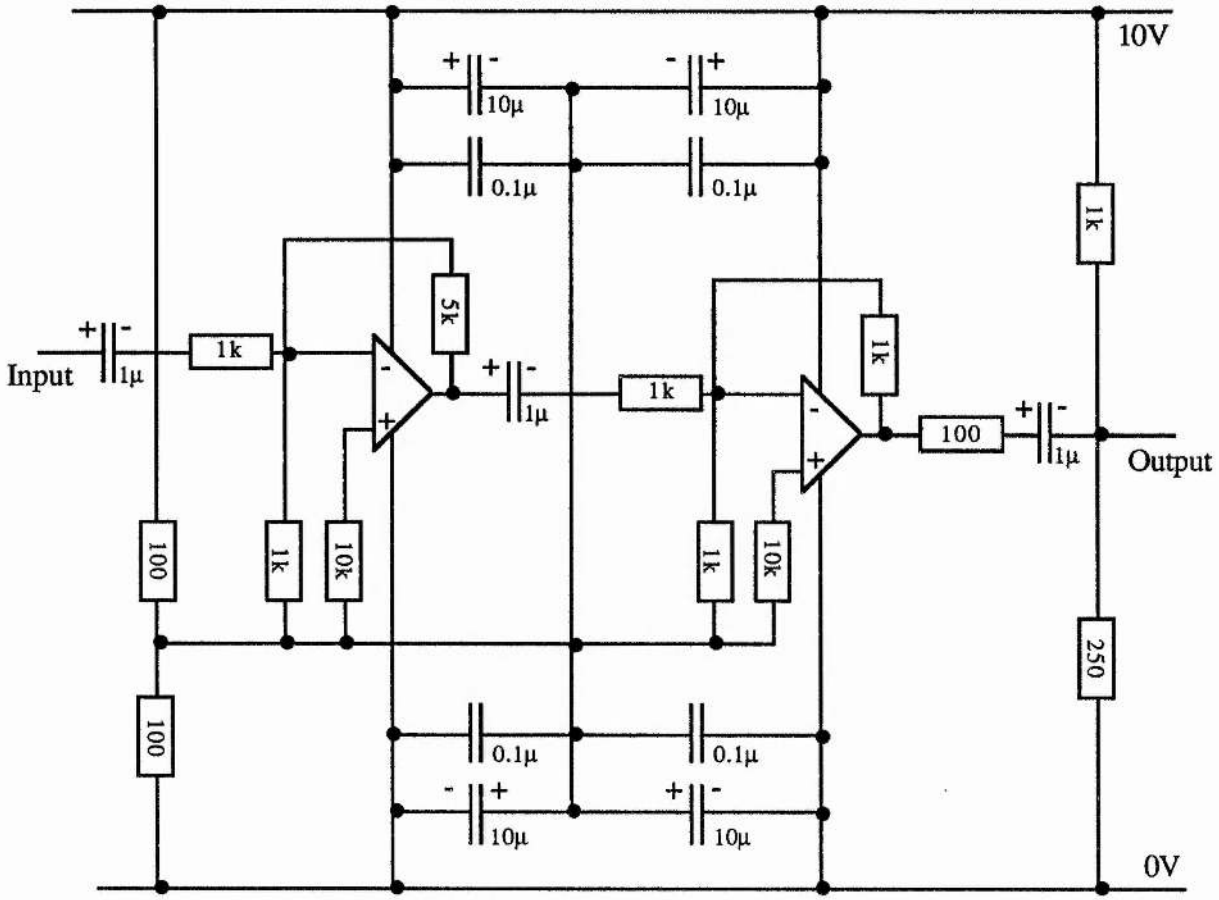

Figure A2.1. Circuit diagram of the video input amplifier.

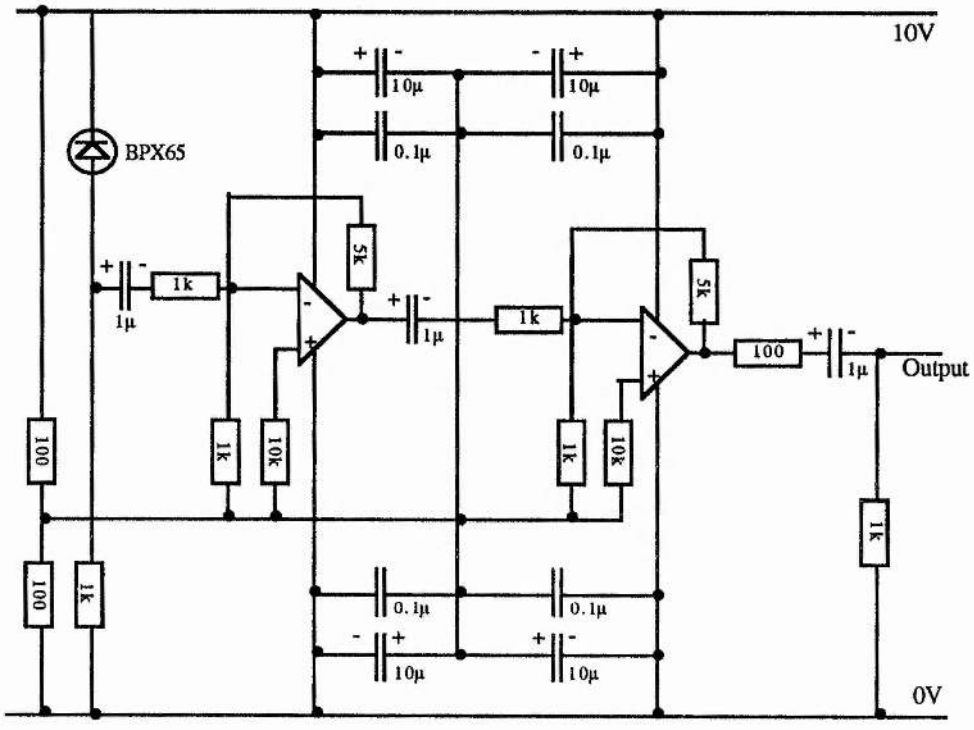

Figure A2.2. Circuit diagram of optical video receiver and amplifier.

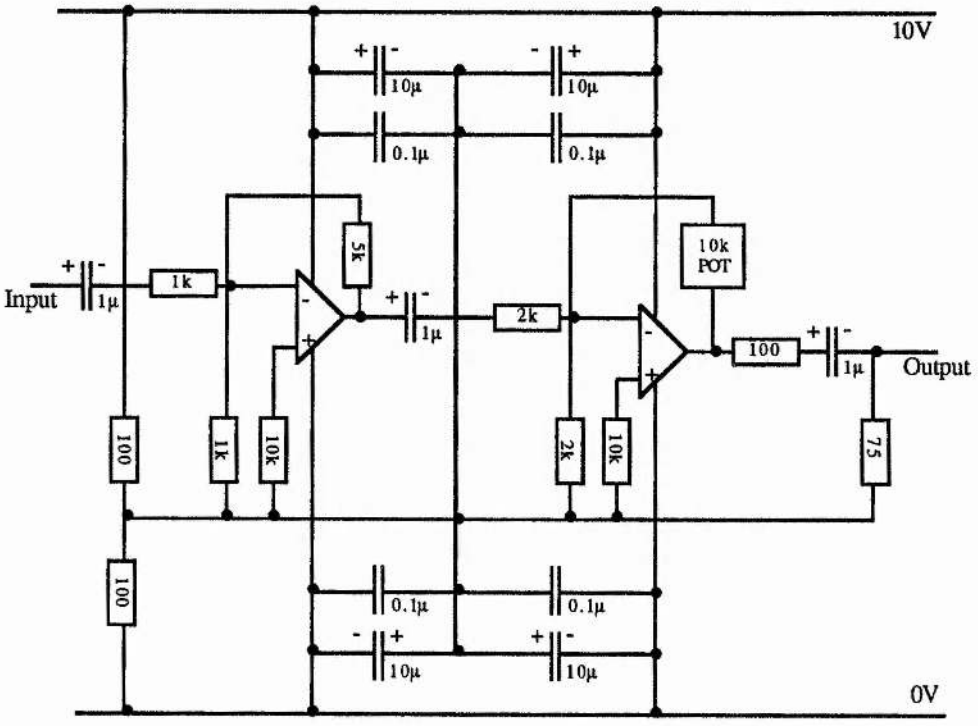

Figure A2.3. Circuit diagram of variable video amplifier.

Appendix 3.

Patent Applications Filed.

This appendix consists of copies of the text of the two patent applications made as a result of the work presented within this thesis.

The first patent application is in connection with the work outlined in chapter 5 which is titled "Apparatus and Method for Manufacturing Gratings and Volume Holograms." and has UK Patent Application No. 9305031.8.

The second patent application is in connection with the work outlined in chapter 5 which is titled "Distributive Feedback Mirrors." and has UK Patent Application No. 936002.6.

§ A3.1.

Apparatus and Method for Manufacturing Gratings and Volume Holograms.

E. D. Findlay, A. Maitland and P. Sutton.

UK Patent Application No. 9305031.8.

Apparatus and Method for Manufacturing Diffraction Gratings and Volume Holographs.

The invention relates to the creation of permanent diffraction gratings and volume holographs. The invention, in its various embodiments, can provide both phase gratings, amplitude gratings, phase holographs and amplitude holographs.

At present, permanent diffraction gratings and holographs are created using techniques which are based on machining, etching or photographic processes. In current practice, non-permanent, ephemeral diffraction gratings are generated in transparent media using acoustic waves to produce cycles of compression and rarefaction which are accompanied by changes in refractive index. Cells in which acousto-optic diffraction gratings are created are known as "Bragg cells". All Bragg cells require a constant acoustic input from a suitable transducer to maintain the diffraction grating within the acoustic-optic medium.

To form a diffraction grating using acoustic waves we use a suitable transducer to create an acoustic standing wave to a chosen medium. The medium is held within a resonant cavity of length L which conforms to the following condition:

$$L = nv/2f$$

where n is the number of grating lines in length L; v is the speed of sound in the medium; and f is the acoustic frequency.

The acousto-optic grating created within a Bragg cell may be the result of a standing wave system produced by the acoustic transducer according to the boundary conditions within the cell or the acousto-optic grating may be the result of a travelling wave system. In the one case the grating nodes and antinodes are spatially stationary while, in the other, their location is time-dependent.

The object of the present invention is to provide apparatus and methods for utilising the changes produced in media by acoustic waves and 'freezing' these changes such that gratings and volume holographs persist after removal of the acoustic waves.

The invention provides in one form a method for manufacturing diffraction gratings or volume holographs wherein:

a. a medium is insonified by means of a source of acoustic waves to produce acoustic waves in the medium; and
b. the medium is treated such that the structure of the medium is altered in regions stressed by the presence of antinodes of the acoustic waves and the altered structure is at least partially retained on removal of the acoustic waves.

In another form the invention provides a method for manufacturing diffraction gratings or volume holographs wherein:

a. a medium is selected such that it can be structurally altered in regions of high stress produced by an acoustic wave in the medium; and
a. the medium is insonified by means of a source of acoustic waves to produce acoustic waves in the medium such that the structure of the

medium is altered in regions of the medium stressed by the presence of antinodes of the acoustic waves and the altered structure is at least partially retained on removal of the acoustic waves.

The formation of an acoustic standing wave in or the passage of acoustic waves through a medium puts the medium under stress at the positions of the anti-modes of the acoustic wave. The inventors have realised that this variation in local stress, periodic in the case of a standing wave, can be utilised by careful processing of the medium such that the stress pattern is effectively remembered by the medium.

The method may make use of acoustic standing waves or travelling acoustic waves in the medium. Where the acoustic waves are such that the stress applied to the medium at the antinodes is sufficient to damage the material then no further processing of the medium may be needed to produce the required grating or holograph. In those media where the damage to the antinode areas is insufficient to produce a practical grating or holograph a second material can be injected into the medium such that it alters the optical properties of the medium at the positions of the antinodes. The second material may be such as to form a heterogeneous mixture/solution with the first medium in such a way as to produce concentration gradients resulting in spatial refractive index variations which follow the acoustic standing wave distributions.

The grating may be formed by an accumulation of light scattering particles in the regions of nodes of the acoustic standing wave pattern in a medium seeded with suitable particles. Changes are then induced in

the medium to ensure that the grating pattern of scattering particles is retained permanently by the medium when the acoustic transducer is switched off.

The grating may be formed in the medium by the refractive index variations which are due to, and follow, the pattern of nodes and antinodes of the distribution of acoustic standing waves. Changes are then induced in the medium to ensure that the grating pattern of refractive index changes is retained permanently by the medium when the acoustic transducer (source of acoustic waves) is switched off/removed. In one such arrangement, a reaction mixture is made of components of a matrix medium, an acoustic standing wave is then generated in the mixture while the matrix medium forms such that stress variations caused by the acoustic standing wave periodically aid and inhibit matrix formation and finally the acoustic wave is removed to leave a periodic grating structure.

A further step in the method is to add a further chemical component after application of the acoustic standing wave to promote setting of the matrix material.

In a further arrangement the grating material is selectively doped. This may be applied after setting up an acoustic standing wave in a setting gel and then applying the dopant material in contact with the gel such that the dopant diffuses selectively into (or away from) the high stressed regions of the antinodes of the acoustic standing wave.

In an arrangement for producing a phase grating in glass, the glass is

first heated above its annealing temperature and then an acoustic standing wave is applied while the glass is cooled below the annealing temperature such that the glass becomes birefringent at the locations of the antinodes of the acoustic standing wave. In order that the spacing between antinodes should be constant as the temperature of the glass varies the frequency of the acoustic wave may be varied in dependence on the glass temperature.

The above arrangements lead to permanent phase or amplitude gratings after removal of the acoustic standing wave. In another embodiment of the invention a semi-permanent grating is produced as follows:
an electro-viscous medium is used and a travelling acoustic wave is applied to this medium,
an electric field is then applied to the medium to cause a change of phase of the electro-viscous material from liquid to solid in such a way as to retain the essential features of the stress distribution and the associated refractive index distribution. This grating persists once the acoustic standing wave is removed but lasts only as long as the electric field is applied. This arrangement is suitable for matched filter applications where a portion of the travelling acoustic wave can be captured in the electro-viscous medium and then compared with a known wave using known electro-optic techniques.

All of the above arrangements can be applied using multiple acoustic sources and resonant cavities to establish complex two and three dimensional patterns.

By using more than one acoustic transducer and choosing the locations of

the individual transducers, gratings of great complexity can be formed. If the frequency at which each transducer is driven is also introduced as an option, gratings of almost any spatial design can be produced within the limitations of the boundary conditions which dictate the standing wave nature of the vibration pattern produced. Such gratings have the character of volume holograms.

The invention will now be described by way of example only with reference to the accompanying Drawings of which:

Figure 1 illustrates application of the invention to manufacture of a one dimensional single frequency diffraction grating;

Figure 2 is a diagram of a one-dimensional gel tank implementation of the invention;

Figure 3 illustrates a simple matrix disruption method for creating a phase grating using a solid gel and a dopant;

Figure 4 is a diagram of equipment for producing a grating in glass; and

Figure 5 is a schematic drawing of an arrangement for producing a two dimensional grating.

Figure 1 illustrates a means for making a one dimensional diffraction grating. A transducer (10) is coupled to one ind of a grating medium (11) and a reflector (12) is placed at the end of the medium opposed to the transducer. The transducer is driven at a constant frequency f and the spacing L between transducer (10) and reflector (12) is arranged such that an acoustic standing wave (13) is established in the medium (11) where the spacing between nodes is equal to the required line

spacing of the grating. Thus the length L is given by:

$$L = nv/2f$$

where:

v is the speed of sound in the medium (11); and

n is the number of grating lines (i.e. nodes) in the length L.

According to a first arrangement, the amplitude of the standing wave is chosen such that the stress applied to the medium at the antinodes exceeds the elastic limit of the medium whereby a structural periodicity remains after the acoustic wave is removed. Alternatively, in this arrangement a set gel could be selectively destroyed at positions of the antinodes of the acoustic wave.

In a second arrangement shown in Figure 2, colloidal dispersive particles are added to an unset gel to form a uniform suspension within the gel. The gel (20) is then put in a tank (21) having one end wall formed by a transducer (22) and the opposed end wall formed by a reflector (23). As in the first arrangement an acoustic standing wave is established in the gel. This results in a migration of the dispersive particles towards the nodes of the standing wave pattern. The standing wave is removed after the gel sets such that the dispersive particles do not diffuse away from the regions of higher concentration. The outer face (24) of the reflector (23) is slanted to prevent further standing waves being set up by reflection from the face (24).

The apparatus shown in Figure 2 may be used for a further arrangement of the invention. The tank (21) is filled with a reaction mixture of component parts of a pre-selected matrix medium. An acoustic standing wave is applied to this 'molecular soup' such that the variations in stress caused by the acoustic wave periodically aid and inhibit matrix formation. Some molecules require a high degree of mixing to form properly. Application of the acoustic wave creates a differential rate of molecular production and hence a diffraction grating when the mixture is set, for instance, by the addition of some other chemical.

Figure 3 shows an arrangement of selective doping of a solid medium insonified by means of a standing acoustic wave. In similar manner to the arrangements already described a standing acoustic wave is set up in a gel 30 in a resonant enclosure 31 by means of opposed transducer 32 and reflector 33. Above the gel 30 there is provided material 34 to be injected into the gel. Such material could be dispersive, it could have a higher or lower refractive index than the gel medium or it could act as a dopant to lower the refractive index on introduction, as for example water introduced into gelatine. Heat may be applied to promote injection of the material into the insonified gel. As shown, the material enters most easily at the antinodes 35 of the acoustic wave pattern. On removing the acoustic waves the periodic structure of the gel is retained.

Figure 4 shows the application of the method to glass. A rectangular slab of glass (40) has one end (41) polished to act as a reflector with a transducer (42) coupled to the remote end. An oven 43, through which the glass can pass, is arranged to heat the glass above its annealing

temperature to form a phase grating. The glass is then cooled while maintaining an acoustic standing wave. Once cooled below the annealing temperature, birefringence is induced into the glass at the antinode positions of high stress. A potential difficulty with this technique is the possible different rates of change with temperature of the velocity of sound and the length L of the acoustic cavity, ie

$$\frac{d}{dT} v_a(T) \neq \frac{d}{dT} L(T)$$

where v_a is the velocity of sound in the glass and L is the acoustic cavity length. The effect of the difference between these two rates of change with respect to temperature can be removed by changing the frequency of the acoustic signal so that it is constantly matched to produce the same number of antinodes over the length of the acoustic cavity.

The invention can also be applied to produce semi-permanent gratings by use of electro-viscous media. An electric field is applied to an electro-viscous medium through which an acoustic travelling wave is established. The electric field causes a change of phase of the medium from liquid to solid in regions of high stress and thus provides a semi-permanent grating representing a snap-shot of the travelling wave in the medium after removal of the acoustic wave. On removal of the electric field the diffraction grating disappears. This technique enables an acoustic wave to be held in the electro-viscous medium in a manner such that it can then be compared with another acoustic signal using standard electro-optic techniques.

In the arrangements thus far described single frequency gratings have been produced. The invention can also be applied using multiple acoustic sources to establish complex two and three dimensional interference patterns.

Figure 5 shows, for convenience, a simplified arrangement for producing a two dimensional grating making use of any of the one dimensional techniques described above for freezing the acoustic wave pattern in the grating medium 50. The medium 50 is elliptically shaped with surface mounted transducer and reflector pairs 51, 52 and 53,54 located respectively on the major and minor axes of the medium.

As described the invention has a number of possible uses including:

a) simple diffraction gratings for spectrum analysis

b) phase and absorption masks for use in Fourier optics

c) filters for rf signal processing by acousto-optic signal processing

d) creation of small polarisation dependent graded index lenses.

Claims

1. A method for manufacturing diffraction gratings or volume holographs wherein:

a. a medium is insonified by means of a source of acoustic waves to produce acoustic waves in the medium; and

b. the medium is treated such that the structure of the medium is altered in regions stressed by the presence of antinodes of the acoustic waves and the altered structure is at least partially retained on removal of the acoustic waves.

2. A method for manufacturing diffraction gratings or volume holographs wherein:

a. a medium is selected such that it can be structurally altered in regions of high stress produced by an acoustic wave in the medium; and

a. the medium is insonified by means of a source of acoustic waves to produce acoustic waves in the medium such that the structure of the medium is altered in regions of the medium stressed by the presence of antinodes of the acoustic waves and the altered structure is at least partially retained on removal of the acoustic waves.

3. A method for manufacturing diffraction gratings or volume holographs as claimed in claim 1 wherein a second material is injected into the medium such that it alters the optical properties of the medium at the positions of the antinodes of the acoustic waves.

4. A method for manufacturing diffraction gratings or volume holographs

as claimed in claim 3 wherein the second material forms a heterogeneous mixture/solution with the first medium so as to produce concentration gradients resulting in spatial refractive index variations which follow the acoustic standing wave distributions.

5. A method for manufacturing diffraction gratings or volume holographs as claimed in claim 3 or 4 wherein injection of the second material results in an accumulation of light scattering particles in the regions of nodes of the acoustic wave pattern in a medium seeded with suitable particles.

6. A method for manufacturing diffraction gratings or volume holographs as claimed in claim 1 or 2 wherein a reaction mixture is made of components of a matrix medium, an acoustic standing wave is then generated in the mixture while the matrix medium forms such that stress variations caused by the acoustic standing wave periodically aid and inhibit matrix formation and finally the acoustic wave is removed to leave a periodic grating structure.

7. A method for manufacturing diffraction gratings or volume holographs as claimed in claim 6 wherein there is included the further step of adding a further chemical component after application of the acoustic standing wave to promote setting of the matrix material.

8. A method for manufacturing diffraction gratings or volume holographs as claimed in claim 1 wherein the material is selectively treated by a dopant.

9. A method for manufacturing diffraction gratings or volume holographs as claimed in claim 8 wherein an acoustic standing wave is first set up in a setting gel and then the dopant material is applied in contact with the gel such that the dopant diffuses selectively into (or away from) the high stressed regions of the antinodes of the acoustic standing wave.

10. A method for manufacturing diffraction gratings or volume holographs as claimed in claim 9 wherin the material is selected to be glass, the glass is first heated above its annealing temperature and then an acoustic standing wave is applied while the glass is cooled below the annealing temperature such that the glass becomes birefringent at the locations of the antinodes of the acoustic standing wave.

11. A method for manufacturing diffraction gratings or volume holographs as claimed in claim 10 wherein the frequency of the acoustic wave is varied in dependence on the glass temperature in order that the spacing between antinodes should be constant as the temperature of the glass varies.

12. A method for manufacturing diffraction gratings or volume holographs as claimed in any one preceding claim wherein the acoustic waves are standing waves.

13. A method for manufacturing diffraction gratings or volume holographs as claimed in any one of claims 1 to 11 wherein the acoustic waves are travelling waves.

14. A method for manufacturing diffraction gratings or volume holographs as claimed in claim 13 wherein a semi-permanent grating or holograph is produced according to the following steps:
an electro-viscous medium is selected and a travelling acoustic wave is applied to this medium,
an electric field is then applied to the medium to cause a change of phase of the electro-viscous material from liquid to solid in such a way as to retain the essential features of the stress distribution and the associated refractive index distribution.

15. A method for manufacturing diffraction gratings or volume holographs as claimed in any one preceding claim wherein more than one acoustic source is used to establish complex two and three dimensional patterns.

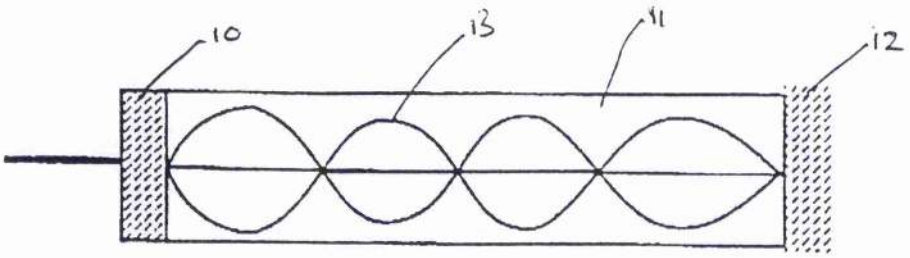

FIGURE 1

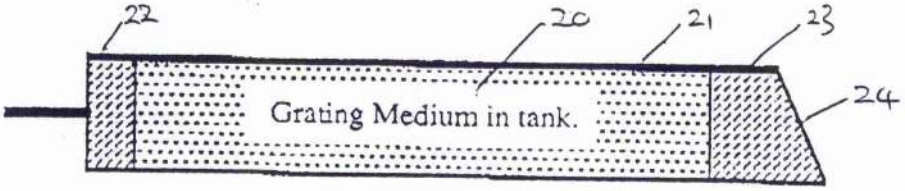

FIGURE 2

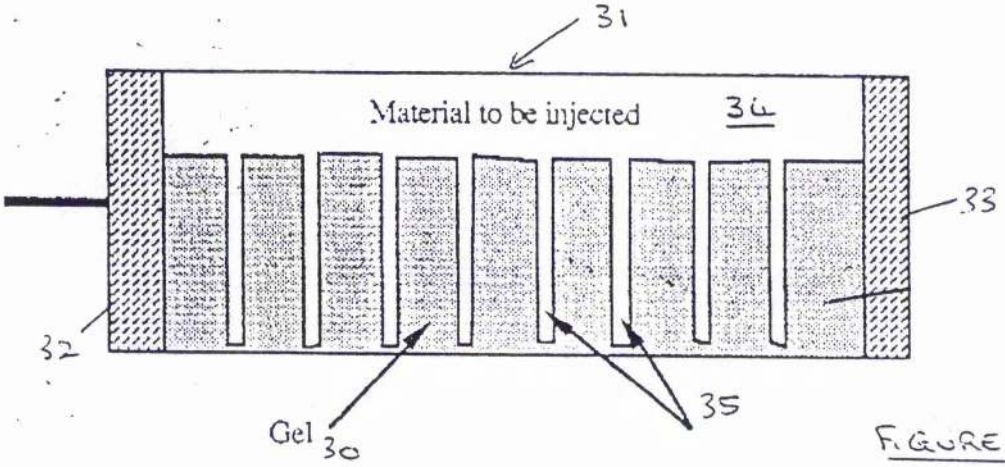

FIGURE 3

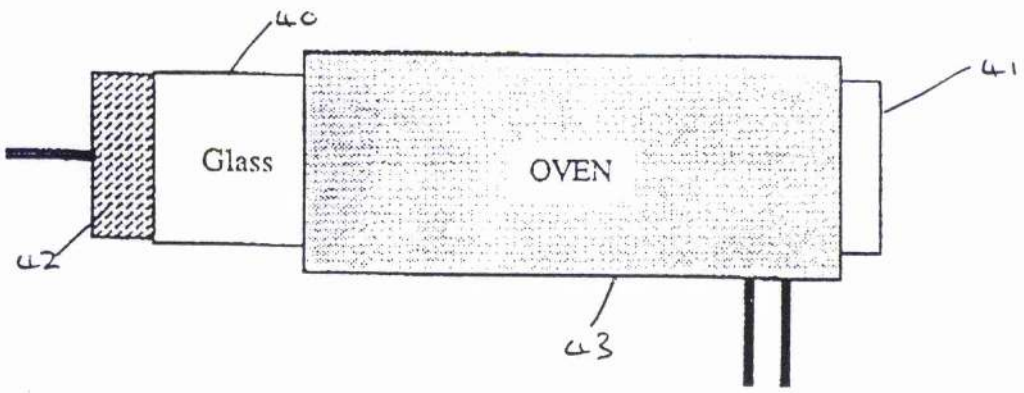

FIGURE 4

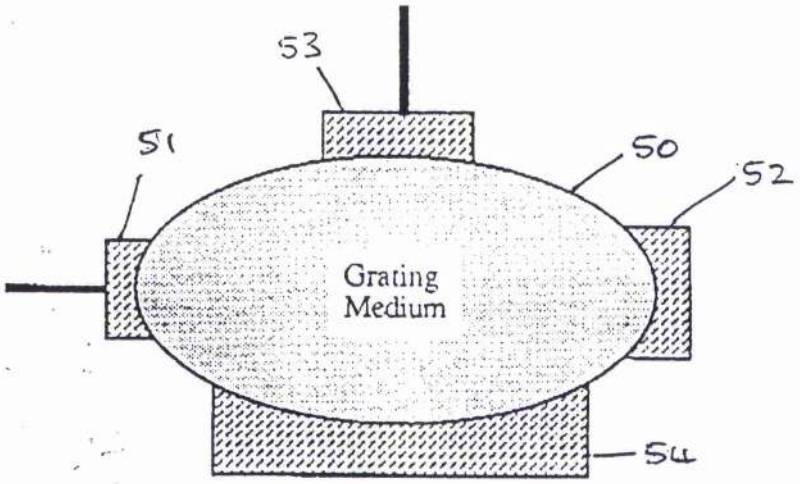

FIGURE 5

§ A3.2.

Distributive Feedback Mirrors.

E. D. Findlay and A. Maitland.

UK Patent Application No. 936002.6.

Distributed Feedback Mirrors

The present invention relates to distributed feedback (DFB) mirrors and in particular to such mirrors for use in optical fibres or waveguides.

Present methods for creating DFB mirrors are centred around semiconductor lasers [H Kogelnik and C V Shank, "Coupled-Wave Theory of Distributed Feedback Lasers", J. Appl. Phys. 43(5) 2327 (1972)], photodetectors [K Kishino et al. IEEE J. of Quantum Electronics, QE27(8) 2025 (1991)] and multilayer laser mirrors deposited on glass or a crystal substrate [E Hecht "Optics" (2nd Ed.) Wiley International (1987)]. There is no known method at present for creating a DFB mirror within a continuous length of optical waveguide or fibre.

GB Patent Application No 9305031 describes a method for manufacturing diffraction gratings or volume holographs by insonifying a medium with acoustic waves. Variations in stress in the medium produced by the sound waves are used as a means to vary the optical properties of the medium.

One object of the invention is to provide a DFB mirror within an optical fibre and methods for creating such a mirror by providing a permanent stationary grating within the fibre. A further object of the invention is to create a DFB mirror within an optical fibre by establishing a travelling wave grating in the fibre.

In one form the invention provides an optical fibre distributed feedback mirror comprising an optical fibre for transmission of laser light

wherein the refractive index has a periodic variation along a predetermined length of the fibre thereby providing a mirror integral with the fibre.

In an alternative arrangement an optical fibre distributed feedback mirror comprises an optical fibre and an acoustic source coupled thereto to generate a travelling wave along the optical fibre so as to physically perturb the optical transmission medium and thereby produce a periodic variation in refractive index thereby providing a mirror integral with the fibre.

In another form the invention provides a method for manufacture of a permanent distributed feedback mirror in an optical fibre comprising the steps of:

a) heating a section of an optical fibre above the annealing temperature of the fibre core at a location where a distributed mirror is required;
b) transmitting an acoustic wave along the optical fibre so as to generate an acoustic standing wave in the heated section of the fibre; and
c) cooling the heated section below the annealing temperature while maintaining the acoustic wave.

Advantageously a temperature controlled oven is provided for heating the optical fibre and the acoustic energy and the frequency thereof transmitted through the heated section of the optical fibre is monitored so as to stabilise the location of the acoustic standing wave in the heated section.

The DBF mirrors using travelling or standing waves are preferably created by injecting a high frequency acoustic wave in the frequency range of 1-10GHz into the optical fibre.

The travelling wave grating can be tuned over a range of frequencies and feedback efficiencies depending on the bandwidth and dynamic range of the acoustic source, but it cannot be localised in the optical propagation direction of the fibre.

The invention will now be described by way of example only with reference to the accompanying Figure which is a schematic drawing of an apparatus for producing a permanent distributed feedback mirror within an optical fibre.

A small oven 1 is placed around a section of optical fibre 2 at the point along the fibre where a mirror is required. An acoustic source 3 is coupled to the optical fibre 2 sufficiently distant from the oven to be unaffected by the oven heat and a microphone 4 (sensitive to acoustic energy transmitted along the fibre by the source 3) is coupled to the fibre on the side of the oven remote from the source. The oven temperature is then increased until the waveguide material is above its annealing point (or made molten), which automatically creates an acoustic cavity due to the change in acoustic velocity with temperature. The annealing (molten) region of the optical fibre must comply with the length condition (4) given below.

The acoustic source 3, of frequency f_{ac} (of order GHz) given by equation

(3) below, is then switched on and the intensity of the source is increased so as to achieve the maximum possible periodic perturbation of the dielectric without causing permanent damage outside the heated region. The acoustic standing wave established in the optical fibre produces a periodic variation with length in the refractive index of the optical fibre medium. Such variation of refractive index within the heated portion of the optical fibre is equivalent to a diffraction grating within the fibre. At this stage, further tuning of the length of the heated region can be effected by using the microphone 4 to detect when the resonance condition (4) is achieved when a minimum acoustic energy will be transmitted through the heated region of the fibre.

The oven 1 is then switched off and the optical fibre 2 cooled while maintaining the acoustic standing wave to 'freeze' the grating into the material of the heated region and then the acoustic source is turned off. Then when the acoustic standing wave is removed the grating remains permanently in the optical fibre.

The permanent grating in the optical fibre is generated using acoustic waves, which are frozen in place. To freeze the acoustic waves into the fibre core the appropriate section of the fibre is heated to a temperature above which stress patterns are annealed out (or doping ions are free to move). Then after imposing an acoustic standing wave this is frozen into place by dropping the temperature below the annealing point (or returning to the solid state).

The invention may also be used by employing a travelling acoustic wave within the optical fibre in a similar frequency range to create an

ephemeral grating, or distributed feedback mirror, within the fibre. The travelling wave grating can be tuned over a range of frequencies and feedback efficiencies depending on the bandwidth and dynamic range of the acoustic source, but it cannot be localised in the optical propagation direction of the fibre as in the case of the permanent mirror.

THEORY

Acoustic waves can be guided down an optical waveguide by the difference between the speed of sound in the optical waveguide and its surroundings. A guided acoustic wave can then be used to form a permanent diffraction grating under the conditions given in GB Patent Application No 9305031 which can be summarised as:

(i) a resonant acoustic cavity must be formed such that an acoustic standing wave can be set up;
(ii) a mechanism must be present for preserving the stress patterns engendered by the acoustic standing wave, so when the acoustic source is removed a diffraction grating remains.

Such a sinusoidal diffraction grating will have diffraction efficiency (E) given by:

$$E = \tanh^2\left[\frac{\pi n_1 d}{n_o \lambda \cos\theta_B}\right] \qquad (1a)$$

where n_1 is the amplitude of the perturbation to the refractive index, d

is the depth of the grating, n_o is the unperturbed refractive index, λ is the wavelength of the incident light in free space and θ_B is the Bragg angle, taken to be the angle between the wave vector of the incident radiation and the grating vector. In the case of distributive feedback mirrors within waveguides the Bragg angle is $-\overline{\pi}$ and thus the diffraction (reflection) efficiency is:

$$E = \tanh^2\left[\frac{\overline{\pi} n_1 d}{n_o \lambda}\right] \qquad (1b)$$

For an unperturbed refractive index n_o of 1.5 and an optical wave length λ = 1.5 μm, the refractive index perturbation that yields a 1% reflection efficiency is n_1 (approx equal to $10^{-7}m^{-1}$.

For the diffracted beam to have the opposite direction of propagation to the incoming beam the Bragg angle has a value of -pi and thus the Bragg condition ($\cos \theta_B = \lambda/2\Lambda$) becomes:

$$\Lambda = \lambda/2 \qquad (2)$$

where Λ is the acoustic wavelength (and therefore grating wavelength) in the medium. For the 'heating, imposition of acoustic field and freezing' method to attain the maximum reflectivity, the acoustic frequency must comply with the following conditions:

$$f_{ac} = \frac{2}{1+\alpha(T_2-T_1)} \cdot \frac{v(T_2)}{n_o \lambda} \qquad (3)$$

where α is the medium's coefficient of expansion, $v(T_2)$ is the speed of sound at the annealing temperature, T_2, of the optical fibre material and T_1 is the fibre's operating temperature. For cavity resonance, which increases the efficiency of grating creation, the cold cavity length condition is:

$$L(T_1) = \frac{N}{1+\alpha(T_2-T_1)} \cdot \frac{v(T_2)}{f_{ac}} \qquad (4)$$

where N is a positive integer.

The present invention thus provides a method for producing mirrors within active and non-active optic fibres of different reflectivities and at different wavelengths as desired. Mirrors thus produced are integral to the optical transmission lines and do not therefore incur coupling losses.

Although the invention has been described in relation to the use of acoustic waves it may also be possible to use electrical standing waves of the appropriate wavelength (given by equation 2) within a molten doped glass to redistribute the active ions and thus form a grating.

Claims

1. An optical fibre distributed feedback mirror comprising an optical fibre for transmission of laser light wherein the refractive index has a periodic variation along a predetermined length of the fibre thereby providing a mirror integral with the fibre.

2. An optical fibre distributed feedback mirror as claimed in claim 1 wherein an acoustic source is coupled to the optical fibre to generate a travelling wave along the optical fibre so as to physically perturb the optical transmission medium and thereby produce a periodic variation in refractive index thereby providing a mirror integral with the fibre.

3. An optical fibre distributed feedback mirror as claimed in claim 2 wherein the acoustic source has a frequency in the range of 1-10GHz.

4. An optical fibre distributed feedback mirror as claimed in claim 3 wherein the acoustic source is tunable over a predetermined range of frequencies.

5. A method for manufacture of a permanent distributed feedback mirror in an optical fibre comprising the steps of:

a) heating a section of an optical fibre above the annealing temperature of the fibre core at a location where a distributed mirror is required;
b) transmitting an acoustic wave along the optical fibre so as to generate an acoustic standing wave in the heated section of the fibre; and

c) cooling the heated section below the annealing temperature while maintaining the acoustic wave.

6. A method for manufacture of a permanent distributed feedback mirror in an optical fibre as claimed in claim 5 wherein a temperature controlled oven is provided for heating the optical fibre and the acoustic energy and the frequency thereof transmitted through the heated section of the optical fibre is monitored so as to stabilise the location of the acoustic standing wave in the heated section.

7. A method for manufacture of a permanent distributed feedback mirror in an optical fibre as claimed in claim 5 or 6 wherein the acoustic wave is selected to have a frequency in the range of 1-10GHz.

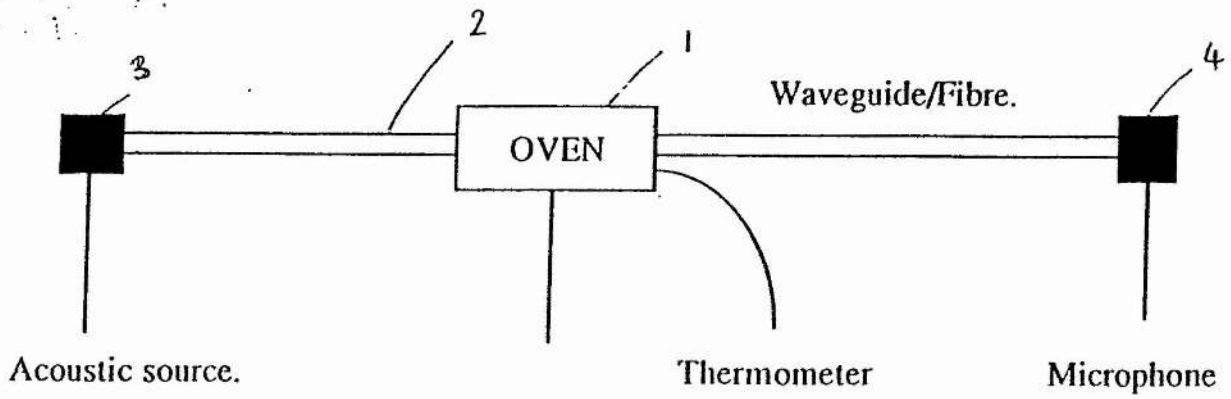

Figure 2, Schematic diagram of construction apparatus.